THE UNIVERSITY OF CALGARY

Response-Based Design Criteria

Including the Treatment of Model Uncertainty

by

Luc Huyse

A THESIS
SUBMITTED TO THE FACULTY OF GRADUATE STUDIES
IN PARTIAL FULFILLMENT OF THE REQUIREMENTS FOR THE
DEGREE OF MASTER OF SCIENCE

DEPARTMENT OF CIVIL ENGINEERING

CALGARY, ALBERTA

December, 1995

THE UNIVERSITY OF CALGARY

FACULTY OF GRADUATE STUDIES

The undersigned certify that they have read, and recommend to the Faculty of Graduate Studies for acceptance, a thesis entitled "Response-Based Design Criteria Including the Treatment of Model Uncertainty" submitted by Luc Huyse in partial fulfillment of the requirements for the degree of Master of Science.

Chairperson, Dr. M.A. Maes

Department of Civil Engineering

A. Ghali

Dr. A. Ghali

Department of Civil Engineering

Dr. M.C. Singh

Department of Mechanical Engineering

December 12 1995

Abstract

In structural reliability a new trend has developed to formulate design criteria directly for the response variable instead of specifying a high or low percentile for the load or resistance variables.

A new method to develop Response-Based Design Criteria is introduced and compared with existing methods and their ability to include model uncertainty is discussed. Their accuracy and efficiency is benchmarked by means of three applications, which are of gradually increasing computational complexity.

The first application is a moving load problem on a two-span continuous beam. The most likely joint occurrences for the two point loads are determined for different responses. Wave forecasting is the subject of the second application. The maximum extreme crest height of a wave for different return periods is studied. The last application deals with the drilling operability of marine risers. The design significant wave height and current profile are determined from the critical response angle.

Acknowledgements

This research was made possible through the financial support of the National Energy Board of Canada (PERD Program), Mobil Exploration and New Ventures, The University of Calgary (Conference Travel Grant), the Department of Civil Engineering at The University of Calgary, and the Bruce M. Irons Memorial Scholarship.

I am particularly indebted to my supervisor, Dr. Marc A. Maes for his continuous support and encouragement and extensive proofreading of the manuscript.

I also would like to thank my friend Dr. Philippe Geyskens who convinced me to come to Canada.

Table of Contents

List of Tables

List of Figures

List of Abbreviations

AIS	Asymptotic Importance Sampling
API	American Petroleum Institute
CDF	Cumulative Distribution Function
COV	Coefficient of Variation
FORM	First-Order Reliability Method
GBS	Gravity-Based Structure
GEVD	Generalized Extreme Value Distribution
LSF	Limit State Function
MCS	Monte Carlo Simulation
MLL	Maximum (Log-)Likelihood
PDF	Probability Density Function
PML	Point of Maximum Likelihood
RAO	Response Amplitude Operator
RBDC	Response Based Design Criteria
RNG	(Pseudo-)Random Number Generator
SORM	Second-Order Reliability Method
TLP	Tension-Leg Platform

List of Symbols

Lowercase Roman Letters

$f_{X_2\|X_1}(x_2, x_1)$	conditional PDF of X_2, given X_1
$f_{\mathbf{X}}(\mathbf{x})$	the probability density function of $\mathbf{X}$
$g(\cdot)$	limit state function in the original domain
$g_L(\mathbf{u})$	linearization of the LSF at $\mathbf{u}^*$ in the U-space
$g_u(\mathbf{u})$	limit state function in the standard normal space
$h(\cdot)$	response model
$h_u(\mathbf{u})$	response model in **U**-space
ℓ	log-likelihood function
m	number of samples
n	problem dimension or critical response return period
q	exceedance probability
t	transformation to the standard normal space
u	variable u (standard normal space)
$\mathbf{u}$	vector u (standard normal space)
u_i	component i of vector $\mathbf{u}$
$\mathbf{u}^*$	minimal distance point in the standard normal space
x	variable x (original space)
$\mathbf{x}$	vector x (original space)
x_i	component i of vector $\mathbf{x}$
$\mathbf{x}_q^*$	PML corresponding to exceedance probability q
y_q	critical response level of Y with exceedance probability q

Uppercase Roman Letters

$\mathbf{A}$	matrix A
$\mathbf{C}_X$	covariance matrix of the variable X
$\mathrm{COV}(\cdot)$	coefficient-of-variation operator
$\mathrm{Covar}(\cdot)$	co-variance operator
$\mathrm{E}(\cdot)$	expectancy operator
F	the failure domain
$\overline{F}$	the safe domain
$F_{\mathbf{X}}(\mathbf{x})$	the cumulative distribution function of $\mathbf{X}$
$F_{X_2\|X_1}(x_2, x_1)$	conditional CDF of X_2, given X_1
$L(x)$	minus log-exceedance function of X
$L'(x)$	slope of the minus log-exceedance function of X
$\widehat{\mathrm{P}}$	statistical estimator for $\Pr(F)$
P_Θ	failure probability considering model uncertainty Θ
$P_{\overline{\theta}}$	failure probability for the case $\mathbf{\Theta} = \overline{\boldsymbol{\theta}}$
$\Pr(\cdot)$	probability operator
R	(random) resistance variable
S	(random) load effect variable
X	random variable X (original space)
$\mathbf{X}$	random vector X (original space)
U	random variable U (standard normal space)
$\mathbf{U}$	random vector U (standard normal space)
$\mathrm{Var}(\cdot)$	variance operator

Lowercase Greek letters

α	reliability index sensitivity factor
β	reliability index
β^*	inflated U-contour radius
γ	omission sensitivity factor
θ	particular value of the model uncertainty Θ
θ^*	ignorance level of Θ
$\overline{\theta}$	mean value of Θ
ν_ψ	COV of multiplicative model uncertainty Ψ
σ_X	standard deviation of X
ϕ	standard normal CDF
ψ^*	ignorance level of Ψ

Uppercase Greek letters

Θ	model uncertainty
Φ	standard normal CDF
Φ^{-1}	inverse standard normal CDF
Ψ	multiplicative model uncertainty

Other Symbols

∇f	the gradient of f
$\|\mathbf{x}\|$	the norm of vector $\mathbf{x} = \sqrt{\mathbf{x}^T\mathbf{x}}$
$\lvert x \rvert$	the absolute value of x

Moving Load Problem

ei	bending stiffness
f_u	force required for a unit displacement
k	COV-ratio of the two loads
l	beam length and load spacing
m_u	bending moment required for a unit rotation
m_B	bending moment over the support B
p_i	point load on the beam
r_B	reaction force at the support B
x	position of the point load ($0 \leq x \leq l$)
$\mathrm{Covar}(P_1, P_2)$	covariance of P_1 and P_2
δ_u	displacement at D due to a unit redundant $r_B = 1$
δ_D	mid-span deflection at D
η_i	influence coefficient of load P_i
κ	load ratio $\left(\kappa = \frac{p_2}{p_1}\right)$
ξ	dimensionless load position $\left(\xi = \frac{x}{l}\right)$
$\xi_{\max}$	load position of maximum effect
ρ	correlation coefficient between P_1 and P_2

Ocean Wave Modeling

h_S	significant wave height
n	return period in years
t_P	spectral peak period
t_Z	zero-crossing period
y	crest height
$y_{0.5,q}$	median extreme crest height with exceedance probability q
J	Jacobian of the tranformation $\mathbf{X} \xrightarrow{t} \mathbf{U}$
$R(\tau)$	autocorrelation function of time-difference τ
$S_{yy}(\omega)$	spectral density function of frequency ω
$\widetilde{\beta}^*$	inflated contour level, when the sensitivity factor α is not exact
γ	peak factor of the JONSWAP-spectrum

Marine Drilling Riser

$\mathbf{c}$, c_i	residual reduced current (vector and component i)
c_d	drag coefficient
d	riser diameter
h_S	significant wave height
n	return period in years
os	offset at the top of the riser
q_c	distributed load per unit length exerted by the currents
t_{eff}	effective tension in the riser
$\mathbf{v}$, v_i	current velocity (vector and component i)
$\overline{\mathbf{v}}$	mean current velocity
$\mathbf{A}$	matrix of orthnormal eigenvectors
$\kappa_{1,i}$	skewness of c_i
$\kappa_{2,i}$	kurtosis of c_i
λ_i	eigenvalue i, variance of Y_i
ν	occurrence rate of a storm
ρ_{riser}	specific riser weight per unit length
$\rho_{\text{sea water}}$	density of the sea water [kg/m^3]
σ_i	standard deviation of c_i
φ	orientation of the plane of maximum response angle
ω	bottom response angle
$\boldsymbol{\Sigma}$	variance-covariance matrix

Chapter 1

Introduction

1.1 Structural Reliability Analysis

Engineering practice, and structural engineering in particular, is characterized by decision making under incomplete or imperfect knowledge. Examples are abundant: what is the lifetime maximum load a structure will have to withstand or the lifetime minimum strength a structural component will demonstrate?

In the early history of modern structural engineering it was believed that absolute upper and lower limits to loads and resistances could be established [35]. Safety factors then related these bounds to mean or characteristic load or resistance values. The structural uncertainty was believed to result from incomplete data rather than inherent uncertainty of the loads or resistances. Subsequently, each new type of structure developed its own safety factors based on engineering judgment and accumulated experience [35].

Due to the growing acceptance of structural design as a problem of decision making under uncertainties and risk, the reliability theory is used more and more as a control tool in the design code development process. Nowadays, most design codes are reliability based. These design codes reduce the work involved in a full probabilistic analysis to a routine check for the class of structures to which the code is meant to apply, commonly referred to as the *scope* of the code.

Structural reliability theory assumes that failures occur only by means of a finite number of *failure modes*. Even though the condition of a structural component may be described by a discrete or continuous *limit state function* (LSF), it is assumed that each mode can adopt only two states: safe or unsafe. Subsequently, these limit state functions depend on the random loads and material strengths, the geometric and other deterministic design parameters, and the remaining random model uncertainties. Generally, loads and resistances vary randomly in space and time; they are described by random fields and/or stochastic processes. Often this time- and space-dependent reliability problem can be reduced to a time-invariant equivalent. In this case the uncertain quantities are described by *basic random variables.* The failure probability $\Pr(F)$, where F stands for failure domain, is then given as the probability that one or more limit states is violated. In that case, a failure has occurred in the associated failure modes.

In this thesis, some important limitations apply to the methods presented. The limit state functions are assumed to be time- and space-independent. Consequently, the structural reliability problems are described in terms of basic random variables and not random processes in time or space. As explained in the next sections, this does not imply that time-variant reliability cannot be studied. Those problems first have to be reduced to an equivalent problem in terms of basic random variables only. In addition, failure is assumed to occur mainly due to violation of only one LSF.

1.2 The Need For Response-Based Design Criteria

Consider the time-invariant formulation of the following load-resistance problem. There is only one load effect S and one material resistance R in this problem. If the load effect variable S exceeds the resistance R, the system fails; otherwise it is safe. The LSF for this failure mode is simply given by:

$$g(R, S) = R - S \tag{1.1}$$

where uppercase notation denotes random variables and lowercase is used for a particular occurrence of this random variable. Bold typeface refers to vectors and matrices.

The LSF divides the original (r, s)-domain in a safe and failure domain:

$$\begin{aligned} \overline{F} &= \{(r,s) \mid g(r,s) > 0\} \longrightarrow \text{safe domain} \\ F &= \{(r,s) \mid g(r,s) \leq 0\} \longrightarrow \text{failure domain} \end{aligned} \tag{1.2}$$

where (r, s) stands for a particular occurrence of R and S. The structural failure probability $\Pr(F)$ is then easily obtained as the probability content of the failure domain F:

$$\Pr(F) = \Pr\left(g(R,S) \leq 0\right) = \Pr(R \leq S) \tag{1.3}$$

The simple R-S formulation reflects the two key aspects in structural engineering: loads and resistances. Traditionally, a fair share of the structural engineering research focuses on the resistance side. On the load side, however, arise similar, if not greater, challenges: different loads act simultaneously upon a typical structure. Some of the resulting load effects are correlated with each other, others may be independent. Some loads may be sustained, others are transient in nature. Load duration effects may be important when the material experiences time-dependent behavior: e.g. creep, relaxation or fatigue.

In classical civil engineering application fields, such as office buildings, the design codes have evolved from engineering practice. In recent years, however, there has been an increased need for a more quantitative assurance of the structural reliability. Additionally, new types of structures are being designed in increasingly hostile environments. The uncertainty in the loads then becomes an important issue. Since not all loads act at their maximum level at the same time, the identification of the appropriate load combinations is of primary interest for the designing engineer.

The Response-Based Design Criteria (RBDC) development process identifies those critical combinations. Risk levels are specified directly in terms of critical responses rather than input variables such as environmental loading or material strength. For each of those critical responses, corresponding to one or more limit states, the most important load combinations can then be identified.

1.3 Reliability-Based Design And Load Combination

In reliability-based design two philosophies are currently adopted: an extreme event formulation and a response based approach. According to the former philosophy, loads and resistances associated with an extreme event are used in the design. These loads and resistances are typically specified at a high return period level. In the latter case, the safety level is formulated directly for the response variables rather than for the input parameters. The design loads and resistances are then given as the input values associated with this critical response.

This difference is best illustrated by means of an example. For the design of Tension-Leg platforms (TLP), both philosophies are presently in use. The environmental load effects are caused by wind, waves and currents. The UK Department of Energy [12] adopts the design event approach and specifies a return period for these environmental parameters of 50 or 100 years. This is different from the API (American Petroleum Institute) recommended practice for TLP design [1] which stipulates the responses be calculated to have a return period of 100 years. The environmental input parameters associated with this response are used as the design loads.

For simplicity the formulation in this section will be restricted to loads only. When different loads act simultaneously, their design values have to be determined to assure that the probability of exceedance of a sum of load effects is approximately equal to the probability of exceedance of any load acting separately [53]. Usually these design combination rules depend on the required risk/reliability level. In general, the more unlikely the exceedance of the design values of the individual loads, the less important the combination problem.

For variable loads it proves to be convenient to describe the fluctuation of the loading according to a time scale corresponding to the structural natural vibration period [55]. The structural response under loads with a macro-scale fluctuation is primarily static. For loads with fluctuation periods in the vicinity of the structural period the dynamic response is important. The former can be reduced to an equivalent static loading formulated in terms of basic random variables. Stochastic process theory gives approximate expressions for the maximum of such a process. Turkstra [52] formulated a rule of thumb for design purposes resulting from an approximate combination analysis: the maximum of each individual load effect is identified and combined with the point-in-time values of the other load effects. This is repeated for all load effects and the maximum effect of all these is used for the actual design. This idea is known as Turkstra's rule.

The maximum combined load is not always given by this rule: studies of live loads in office buildings, for instance, indicate that a simultaneous occurrence of the maxima of at least some of the load processes, which is not accounted for in Turkstra's rule, may become important [8]. Nevertheless, Turkstra's rule generally gives satisfactory results when the duration of load pulses is very short. In other cases a more refined load combination model is required. Two approximate solution methods in terms of up-crossing rates are the Point Crossing Method [31], [32] and the Load Coincidence Method [46].

1.4 RBDC And Inverse Reliability

Unlike the normal, "forward" reliability problem which tries to find the failure probability $\Pr(F)$, given the distributions of the load and resistance variables and a limit state function, the development of RBDC starts from a specified failure probability

$\Pr(F)$ and identifies critical load and resistance combinations. As such, RBDC can be considered an "inverse" reliability problem.

For simplicity consider the simply supported reinforced concrete beam, subject to two random loads as given in Figure 1.1. Assume that the response quantity of interest is the mid-span deflection. The limit state model describes under which load and resistance combinations the structure has failed, which in this case is formulated as "the deflection exceeds a given, critical value δ". The loads and resistances, i.e. material strengths and geometry, are the basic variables of the problem and denoted as $\mathbf{X}$. The failure probability of this structure is calculated using forward reliability techniques. This is, therefore, a "forward" reliability problem:

$$\begin{cases} \text{find } \Pr(F) = \Pr\left(g(\mathbf{X}, \delta) \leq 0\right) \\ \text{given the parameter } \delta \end{cases} \tag{1.4}$$

In a design context, however, an "inverse" formulation is needed. Given a specified failure probability $\Pr(F) = q$, the value of a design parameter λ is to be determined. In the example this parameter could be the effective depth of the beam or the mean concrete strength, for instance. In a more general formulation, the inverse reliability problem determines the value of one scalar parameter λ, which appears in the LSF $g(\mathbf{x}, \lambda)$ or in the joint probability density function $f_{\mathbf{X}}(\mathbf{x}|\lambda)$ such that a

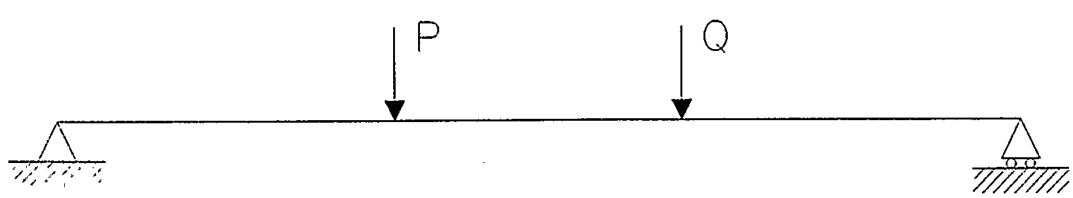

Figure 1.1: Simply supported beam

required reliability level is achieved [14]:

$$\begin{cases} \text{find the value for } \lambda \\ \text{such that } \Pr(F) = \Pr\left(g(\mathbf{X}) \leq 0 \mid \lambda\right) = q \end{cases} \tag{1.5}$$

RBDC takes us one step further. Given the failure probability q, the deflection δ_q with exceedance probability will now be determined together with the load combinations which cause this deflection. It is clear that if the unknown parameter λ in the LSF $g(\mathbf{x}, \lambda)$ is replaced by δ_q (or, in general, the critical response level y_q) in (1.5), the inverse reliability problem gives the desired extreme response level. The corresponding load values, given as the components of the vector $\mathbf{x}$, are the RBDC. As explained in the next section this solution is no longer unique, several combinations $\mathbf{x}_1, \mathbf{x}_2, \ldots$ may possibly result in the critical response. This problem arises, for instance, in code formulation and the development of design criteria for a large or new structure. The goal is to come up with input parameters (loads and/or resistances) such that the overall failure probability $\Pr(F)$ matches the target exceedance probability q.

$$\begin{cases} \text{find the value for } y_q \text{ and the corresponding } \mathbf{x} \\ \text{such that } \Pr(F) = \Pr\left(g(\mathbf{X}, y_q) \leq 0\right) = q \end{cases} \tag{1.6}$$

In the RBDC formulation this exceedance probability q is specified directly for the response variables, rather than for the input parameters.

A "forward" approach to this problem implies an iterative solution: a level for the critical response y_q is assumed and the resulting failure probability $\Pr(F)$ is compared with the target reliability q. Iteration will then yield the final design values of y_q for the applicable range of input parameters $\mathbf{X}$. The alternative, "inverse" problem, starts from $\Pr(F) = q$ and then identifies the required values for y_q from the probabilistic response model without iteration.

1.5 RBDC Problem Formulation

The most common case in which RBDC are presently used is that of a structural system which is subjected to a variety of environmental variables such as wind, waves, currents, earthquakes, heating or cooling, or live load, and denoted by $\mathbf{X} = (X_1, X_2, \ldots, X_n)$. Based on a structural analysis, certain critical responses $\mathbf{Y} = (Y_1, Y_2, \ldots, Y_n)$ can be identified in this system, e.g.: axial and shear forces, bending and twisting moments, deflections and rotations, stresses and strains. These response variables directly affect the reliability of the system, i.e. each of them appears in one or more limit states. Deflections and rotations for instance appear in the serviceability limit state equations; plastic rotations may appear in the ultimate limit state function.

In this work, the response model is assumed to be time-independent $\mathbf{Y} = h(\mathbf{X})$, where h is a static structural response model. It is therefore assumed that the response at time t is a function of the input variables $\mathbf{X}$ at time t only. In a more general approach, the time-dependent behavior can be taken into account.

In general, several combinations of the input variables result in a response with exceedance probability less than or equal to q. The determination of "the" load combination as such therefore does not exist and in their most general formulation, RBDC consist of all combinations of input variables $\mathbf{x}_{q,1}, \mathbf{x}_{q,2}, \ldots$ which produce an extreme response $\mathbf{y}_q$ with exceedance probability q. In a more restricted definition, only the most likely joint occurrence $\mathbf{x}_q^*$ is understood by the term RBDC. In the following the term RBDC is restricted to this most likely combination, other combinations are referred to as "other" or "alternative" RBDC.

Depending on which method is used, this extreme response $\mathbf{y}_q$ may have to be determined beforehand, usually from an extreme value analysis, or results from the RBDC identification procedure itself.

1.6 Examples Of RBDC Development

The following examples illustrate the concept of RBDC:

1. Consider the simply supported reinforced concrete beam in Figure 1.1 subject to two random point loads, which have a lifetime maximum magnitude described by some joint probability distribution. An upper bound for the lifetime maximum deflection δ_q with exceedance probability q can be given by the deflection of the beam when both loads are equal to their lifetime maximum level with exceedance probability q. This upper bound is exact if these maximum loads occur simultaneously. However, when a joint occurrence of these maxima is highly unlikely this upper bound is over-conservative. This may be the case if both loads are negatively correlated for instance; when one load is higher than average, the other one will then tend to be smaller than average. In general a lot of load combinations will result in the critical deflection δ_q. It then makes sense to design for the most likely, or at least a highly likely, load combination which results in this deflection δ_q.

2. Examples are common in offshore engineering. The environmental loading is described by wind and speeds, and wave heights and periods. Usually, not all of these input parameters need to be extreme to cause an extreme response. Which loads are critical also depends to some extent on the type of structure considered. For a gravity-based structure (GBS), for instance, the wave periods are not very important; for a more compliant structure they may become the main variable. In a lot of sites the extreme values of wave height and

current speed are stochastically independent [25], [47], with low probability of simultaneous occurrence of high wave heights and current speeds. This indicates that an extreme event approach, i.e. combination of extreme waves and extreme currents, will result in an over-conservative loading. RBDC may then substantially improve the efficiency of the design.

3. RBDC are not restricted to structural engineering applications only. Consider for example the following transportation engineering problem. The traffic flow, i.e. traffic volume passing a particular road section during a specified time, is function of the travel speed and car density (or its inverse, the car distance). It is clear that for low car densities the speed is independent of the density, while for high densities the speed is limited by the density. Consider now the traffic flow as a design response. RBDC will then identify critical combination(s) of speed and density resulting in the specified critical traffic flow.

1.7 Overview

Chapter 2 briefly reviews different methods used in structural reliability computation and presents different methods for time-invariant RBDC. The first one was introduced by Winterstein *et al.* [56] and is based on the First-Order Reliability Method (FORM) [35], [41], [50], [51], [54]. This method requires a transformation (or reparametrization) of the problem in the standard normal space. The second method is developed in this thesis and it is based on the maximum likelihood principle. Consequently, approximate methods which account for model uncertainty are explained as well.

Chapters 3, 4 and 5 deal with structural engineering examples: a moving load problem, ocean wave modeling and drilling riser operability are studied.

The moving load problem in Chapter 3 applies the different techniques, presented in Chapter 2, in the simplest possible way. Both RBDC methods are compared, and the effect of model uncertainty is analyzed using both an "exact" approach and approximate second moment methods. The power and limitations of the RBDC technique are demonstrated.

In Chapter 4 the maximum crest height of ocean waves is determined as a function of the significant wave height and the wave peak spectral period and is solved using exact probabilistic methods. This solution is then compared with a simplified problem formulation; relative likelihoods are estimated and a model expansion approach is presented.

In the drilling riser example (Chapter 5) considerable attention is paid to the formulation of a simple, but accurate, structural model reducing a three dimensional drilling riser model into a planar one. This is required since design criteria have to be formulated "in plane" for practical reasons. The design criteria are set in terms of operability limits. Different load combinations and their relative likelihood are analyzed using both methods and the results are compared.

Finally, a comparison of both RBDC methods and the treatment of the effects of model uncertainty, based on a discussion of the inherent strengths and drawbacks of the different techniques is made in Chapter 6. Some directions for further improvement of the RBDC methods are given and the need for an even more general reliability-based design technique is discussed.

Chapter 2

Response-Based Design Criteria

2.1 Introduction

Before the actual development of RBDC is discussed, two different methods to calculate failure probabilities are briefly presented. They form the basis for the various state-of-the-art computational techniques used in structural reliability. The first approach is based on first-order approximation methods involving the use of reliability indices. The second one evaluates failure probabilities using simulation techniques.

Then, it is explained how RBDC can be obtained as the solution of either an iterative forward or an inverse reliability problem formulation. Two inverse techniques are discussed and compared. The first one is the inverse FORM method introduced by Winterstein *et al.* [56]. Transformation of the basic random variables **X** into the standard normal **U**-space is required. The second one is based on (log-)likelihood maximization in the original variable domain.

Subsequently, RBDC development for uncertain models is discussed. Two different approaches are given: inflated contours [56], based on omission [33] or expansion [36] factors, and ignorance factors [36].

Finally, the algorithms for the determination of practical design combinations are given for the different RBDC development methods. A comparison of their overall performance is made.

2.2 Structural Reliability Integrals

The reliability of a structural element or system is described by a limit state function (LSF) $g(\mathbf{x})$ which depends on an n-dimensional random vector $\mathbf{X} = (X_1, X_2, ..., X_n)$. The components X_i of $\mathbf{X}$ describe the basic variables of the problem such as: geometry, loads and material properties. When $g(\mathbf{x}) \leq 0$ the structural element has failed, otherwise, it is safe. The domain where $g(\mathbf{x}) \leq 0$ is known as the failure domain F. In order to calculate the failure probability of this structural element both the probability density function (PDF) $f_{\mathbf{X}}(\mathbf{x})$ of the random vector $\mathbf{X}$ and the limit state function (LSF) $g(\mathbf{x})$ must be known:

$$\Pr(F) = \int_{g(\mathbf{x})\leq 0} f_{\mathbf{X}}(\mathbf{x})d\mathbf{x} \tag{2.1}$$

Usually the integral (2.1) can not be evaluated in closed form. Numerical integration is difficult as well since in many cases:

1. the failure probability $\Pr(F)$ is very small for structural applications
2. the dimension n of the problem is typically large
3. the integration domain $g(\mathbf{x}) \leq 0$ may have an irregular shape
4. the PDF $f_{\mathbf{X}}(\mathbf{x})$ may behave irregularly over the domain $g(\mathbf{x}) \leq 0$

Because of the first reason the approximation error for common numerical integration rules may be of the same order as $\Pr(F)$. The last three reasons make it difficult to implement common integration rules efficiently.

Since a straightforward solution of the basic problem (2.1) is usually impossible, various approximations and alternative methods have been introduced. Two groups can be distinguished: first, approximation methods which calculate the reliability index of the failure probability. Second, simulation methods which compute the failure probability $\Pr(F)$ in a statistical way, namely by Monte Carlo Simulation (MCS). A more extensive review of these methods can be found in various papers and textbooks [34], [35], [41].

2.3 First-Order Reliability Method (FORM)

2.3.1 The Reliability Index β

Since the actual failure probability is usually hard to obtain, the LSF $g(\mathbf{x})$ is replaced by an approximation and the reliability index β of this (simplified) problem is calculated. It will be shown that under some rather strict conditions an exact relationship exists between β and $\Pr(F)$. In these cases, finding the reliability index is equivalent to finding the actual failure probability $\Pr(F)$.

Since the normal distribution has interesting characteristics, it is not surprising that much work in structural reliability heavily relies on this distribution. In FORM, the basic random variables are always transformed to the normal space.

2.3.2 FORM-Procedure

In the First-Order Reliability Method the reliability index β associated with the failure probability $\Pr(F)$ is determined. The method consists of the following three steps:

1. The transformation t maps all basic variables and the limit state function into the standard normal space. In this **U**-space all random variables U_i are uncorrelated and have a standard normal distribution:

$$\begin{cases} \mathbf{X} \overset{t}{\mapsto} \mathbf{U} \\ g(\mathbf{x}) \overset{t}{\mapsto} g_u(\mathbf{u}) \end{cases} \tag{2.2}$$

2. Determine the point $\mathbf{u}^*$ on the LSF $g_u(\mathbf{u}) = 0$ for which the distance to the origin is minimized. This minimal distance point is often called the design point.

3. The First-Order reliability index β is now defined as this shortest distance $\|\mathbf{u}^*\|$.

Since the standard normal distribution is rotationally symmetric, it is clear that for a linear LSF:

$$\Pr(F) = \Phi(-\beta) \tag{2.3}$$

where Φ stands for the standard normal cumulative distribution function (CDF). Consequently, the FORM method actually replaces the evaluation of the failure probability integral (2.1) by the constrained optimization problem:

$$\begin{aligned} &\text{Find } \beta = \min \|\mathbf{u}\| = \|\mathbf{u}^*\| \\ &\text{subject to } g_u(\mathbf{u}) = 0 \end{aligned} \tag{2.4}$$

2.3.3 Discussion

Transformation Into The Standard Normal u-Space

For independent basic variables a transformation which maps non-normal vectors $\mathbf{x}$ into the standard normal space $\mathbf{u}$ is:

$$u_i = \Phi^{-1}(F_{X_i}(x_i)) \tag{2.5}$$

where F_{X_i} is the CDF of X_i and Φ^{-1} the inverse standard normal CDF.

A further extension of the method to dependent variables was made by Hohenbichler and Rackwitz [24]. They suggested to use the Rosenblatt-transformation to map the correlated variables x_i onto mutually independent standard normal variables u_i:

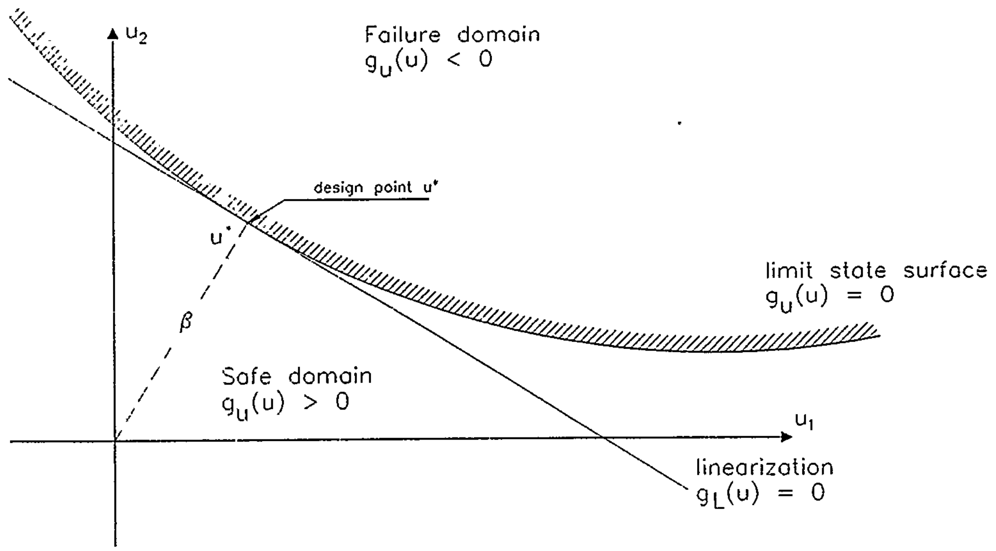

Figure 2.1: Definition of the first-order reliability index β

$$\begin{cases} u_1 = \Phi^{-1}(F_{X_1}(x_1)) \\ u_2 = \Phi^{-1}(F_{X_2 \,|\, X_1}(x_2 \,|\, x_1)) \\ \vdots \\ u_n = \Phi^{-1}(F_{X_n \,|\, X_{n-1},\ldots,X_1}(x_n \,|\, x_{n-1}, \ldots, x_1)) \end{cases} \tag{2.6}$$

with $F_{X_i \,|\, X_{i-1},\ldots,X_1}(x_i \,|\, x_{i-1}, \ldots, x_1)$ the CDF of X_i conditional upon $X_{i-1}, \ldots, X_1$.

It is to be noted that the transformation (2.6) is usually difficult to implement since, in many cases, the conditional CDF is not available in an analytical form. Moreover, the transformed vector $\mathbf{u}$ can be obtained in numerical form only, since the inverse standard normal CDF Φ^{-1} can not be expressed in closed form. Accurate approximations for the standard normal CDF can be found in the literature [28]. When the problem dimension is high, the numerical stability of this transformation must be considered carefully.

Linearization Of The Limit State Function

In the FORM method, a non-linear transformed LSF $g_u(\mathbf{u})$ is approximated by its tangent hyperplane $g_L(\mathbf{u})$ at the design point $\mathbf{u}^*$

$$g_L(\mathbf{u}) \simeq g_u(\mathbf{u}^*) + \sum_{i=1}^{n} \left.\frac{\partial g_u}{\partial u_i}\right|_{\mathbf{u}^*} (u_i - u_i^*) \tag{2.7}$$

The relationship between β and $\Pr(F)$ is only valid as a first-order approximation (see Figure 2.1):

$$\Pr(F) \simeq \Phi(-\beta) \tag{2.8}$$

because of the linearization (2.7), whence the name First-Order Reliability Method (FORM). For a non-linear transformed LSF $g_u(\mathbf{u})$, the first order approximation at the design point $\mathbf{u}^*$ may be rather poor. In the situation on the left of Figure 2.2 the failure probability is overestimated, while the situation on the right side leads to an underestimation. The so-called Second Order Reliability Method (SORM) remedies this imperfection by accounting for curvature information of the limit state function at the design point. This method and the use of asymptotic techniques form today's state-of-the-art in reliability analysis.

2.3.4 First-Order Approximations In The Original Domain

The classical state-of-the-art structural reliability computational methods rely on the transformation (2.5) or (2.6) of the original variables $\mathbf{X}$ to the standard normal space $\mathbf{U}$. It is already mentioned that this numerical transformation may be hard when the original basic variables are not independent.

In addition, modern structural reliability analysis does not only require an accurate evaluation of the probability integral (2.1) but the sensitivity of this result with respect to some design parameters as well. It is not immediately clear how sensitivity factors resulting from a FORM analysis in the standard normal space $\mathbf{U}$,

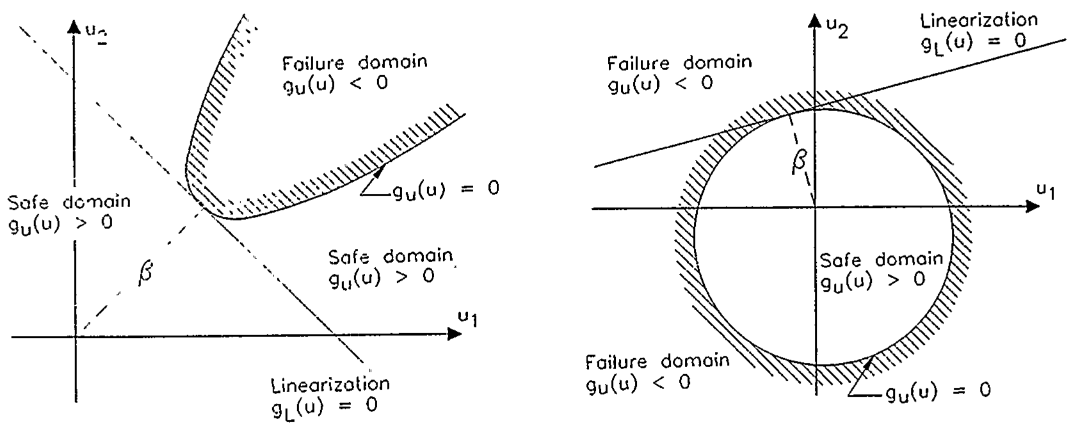

Figure 2.2: Linearization of the limit state surface in FORM

can be expressed in terms of those design parameters. This explains the need for complementary methods in the original variable domain $\mathbf{X}$.

In 1991, Breitung [5] shows that the transformation to the standard normal space can be avoided: the minimization of the distance to the origin in the standard normal U-space is asymptotically equivalent to the maximization of the log-likelihood function $\ell_{\mathbf{X}}(\mathbf{x}) = \ln(f_{\mathbf{X}}(\mathbf{x}))$.

For a standard normal vector $\mathbf{U}$, the density and log-likelihood functions are:

$$\begin{aligned} &f_{\mathbf{U}}(\mathbf{u}) = \frac{1}{\sqrt{(2\pi)^n}} \exp\left(-\tfrac{1}{2}\,\mathbf{u}^T\,\mathbf{u}\right) \\ &\Rightarrow \ell_{\mathbf{U}}(\mathbf{u}) = -\tfrac{1}{2}\left(n\,\ln(2\pi) + \|\mathbf{u}\|^2\right) \end{aligned} \tag{2.9}$$

The point $\mathbf{x}^*$ where this log-likelihood function is maximal, is known as the point of maximum likelihood (PML) and assumes the role of the minimal distance point $\mathbf{u}^*$ in the original domain.

$$\begin{array}{lcl} \min\ \|\mathbf{u}\| = \|\mathbf{u}^*\| & \Longleftrightarrow & \max\ \ell(\mathbf{u}) = \ell(\mathbf{u}^*) \\ \text{subject to } g_u(\mathbf{u}) = 0 & & \text{subject to } g_u(\mathbf{u}) = 0 \end{array} \tag{2.10}$$

From the latter equation in (2.9), it is clear that iso-log-likelihood lines are given by a circle in the U-space. Maximization of the log-likelihood $\ell(\mathbf{u})$ is then equivalent to minimization of $||\mathbf{u}||$, the distance to the origin (2.10).

For all other distributions, proof of (2.10) is based on asymptotic approximations of the reliability integral using the Laplace-integration method for small failure probabilities [4], [5]. This implies that all methods developed for the standard normal U-space can equally well be applied in the original X-domain. The role of the design point $\mathbf{u}^*$ is then assumed by the PML $\mathbf{x}^*$ which allows a direct probabilistic interpretation of the results rather than a geometrical one [6, pp.107-108]. This opens a whole new perspective for structural reliability computation since sensitivity factors for the results are now directly formulated in terms of the original design parameters. Especially asymptotic approximations of the reliability integral will prove useful.

2.4 Simulation Methods

2.4.1 Crude Monte Carlo

Crude Monte Carlo simulation is used primarily to approximate high dimensional integrals for which common numerical integration methods such as Simpson's rule or Newton-Côtes formulas are not effective [43]. The failure probability is now estimated as a frequency statistic. A sample point $\mathbf{x}$ in the n-dimensional original basic variable domain is drawn from the joint distribution $f_{\mathbf{X}}(\mathbf{x})$. The limit state function $g(\mathbf{x})$ is evaluated and the failure frequency $\hat{\mathrm{P}}$ is an estimate for the failure probability $\Pr(F)$.

This hit-and-miss algorithm overcomes the first 3 difficulties mentioned in Section 2.2. Moreover, $\hat{\mathrm{P}}$ is unbiased and asymptotically exact, which means that the estimate $\hat{\mathrm{P}}$ converges to the true failure probability $\Pr(F)$ as the number of samples m increases. Unfortunately, this convergence rate is very low, the coefficient of variation of $\hat{\mathrm{P}}$ is given by:

$$\mathrm{COV}(\hat{\mathrm{P}}) \simeq \frac{1}{\sqrt{m\,\hat{\mathrm{P}}}} \tag{2.11}$$

which indicates very slow decay ($\sim m^{-1/2}$) of the approximation error compared to the widely used Simpson integration rule ($\sim m^{-4}$) for instance. This makes the method computationally expensive for structural reliability problems since $\Pr(F)$ is typically very small in these cases (see point 4 of the list in Section 2.2). E.g.: to obtain an estimate for $\Pr(F) = 10^{-5}$ with COV less than 10%, at least 10^7 simulations are required!

2.4.2 Importance Sampling

To circumvent the excessive computational cost of crude Monte Carlo simulations, different variance reduction techniques are available.

The most important technique is importance sampling [3], [30], [48], [57]. A new sampling density is selected such that the variance of the probability failure estimator $\hat{\mathrm{P}}$ is reduced. The failure probability estimate remains unbiased as long as the new sampling density covers the entire failure domain. It can be shown that the variance of the estimator is minimal if the new sampling density is proportional to the original one in the failure domain. In the safe domain, however, the PDF of the new sampling density should be as close to zero as possible in order to save computer time.

It is clear that all these objectives are somehow conflicting. In addition, importance sampling results strongly depend on the appropriate selection of the new sampling density. Failure to do so may bias the outcome of the estimation process. Since failure probability estimation is a key-point in reliability analysis, it is not surprising that a wide variety of alternative sampling algorithms has been developed. A concise overview with further references can be found in [18]. Many of these commonly used simulation methods rely on a transformation of the random variables to the standard normal space. An alternative is the Asymptotic Importance Sampling (AIS) method [37]. It is based on identification of the PML and asymptotic approximations of the failure probability integral in the original basic variable domain.

2.5 RBDC Development Methods

Different RBDC methods will be presented here. First, the algorithms for each of the methods will be given. At the end of this section the intrinsic strengths and shortcomings of the methods will be compared briefly.

We recall from Chapter 1 that RBDC consist of the most likely combinations of input variables $\mathbf{x}^*$, which produce an extreme response $\mathbf{y}_q$, or y_q for a scalar response, with specified exceedance probability q. To simplify the notations, only scalar responses Y are considered.

2.5.1 RBDC Using Iterative Forward FORM

The FORM Method does not only result in an estimate for the failure probability but in the minimal distance point $\mathbf{u}^*$ as well. This point represents the most likely combination of input parameters in the $\mathbf{U}$-space which yields a response $Y = y_q$.

Consequently, straightforward application of the FORM method yields the RBDC if the critical response y_q is known. Based on an iterative step-by-step method, this critical response level y_q and the RBDC can be obtained from forward reliability techniques:

1. Assume a value for the critical response y_{trial} for which the RBDC are to be developed

2. Find the reliability index β from the optimization problem (2.4) and the corresponding first-order estimate for the failure probability $\Pr(F)$ from (2.8)

3. Compare $\Pr(F)$ with q and adjust y_{trial} accordingly.

4. Repeat steps 1-3 until $\Pr(F) = q$

5. The resulting value for Y from this iteration process is a first-order estimate for y_q.

6. After back-transformation of $\mathbf{u}^*$, $\mathbf{x}^* = t^{-1}(\mathbf{u}^*)$ gives the RBDC

For completeness, it should be mentioned that RBDC development using forward reliability techniques is not restricted to FORM only. Every method which identifies the PML, such as SORM or AIS, can be used in the iterative scheme to find the RBDC.

2.5.2 RBDC Using Inverse FORM

The RBDC development can be formulated as an "inverse" reliability problem [14]. Even though it is strictly speaking not necessary for the method to be applicable, the problem solution is simplified considerably if the LSF is of the form:

$$g_u(\mathbf{U}, Y) = Y - h_u(\mathbf{U}) \tag{2.12}$$

where h_u is the response model in the U-space and Y represents the scalar response of interest.

In contrast to forward FORM, the exceedance probability q is now given. This defines an n-dimensional hypersphere surface with radius $\|\mathbf{u}\| = \beta$ in the standard normal space, where $\beta = -\Phi^{-1}(q)$ (2.8). All combinations $\mathbf{u}$ of the input variables $\mathbf{U}$ on this surface have a FORM probability of joint occurrence equal to q. Consequently, the maximum response y_q produced by one of these combinations $\mathbf{u}$ has an exceedance probability q.

As a matter of fact, this is strictly speaking correct only if the maximum response $y_{\max}(\beta)$ on a surface $\|\mathbf{u}\| = \beta$ is a monotonically increasing function of β. But this is generally true since, due to the nature of the problem, extreme responses are caused by unlikely joint occurrences of the input variables. The more extreme a joint occurrence is, the higher the response level will be. If this condition is not satisfied, the critical response is given as the maximum response in the sphere $\|\mathbf{u}\| \leq \beta$, which indicates that even though the critical response has an exceedance probability larger than q, it is caused by input variable combinations with probability of joint occurrence greater than q. This could be the case for discontinuous or step-wise continuous responses, for instance.

The method can therefore be summarized as follows [56]:

1. Given q, determine the reliability index β from (2.8)

2. Solve the constrained optimization problem

$$\begin{cases} \text{Find } y_q = \max\left[h_u(\mathbf{u})\right] \\ \text{subject to } \|\mathbf{u}\| = \beta \end{cases} \tag{2.13}$$

3. After back-transformation of $\mathbf{u}^*$, $\mathbf{x}^* = t^{-1}(\mathbf{u}^*)$ gives the RBDC

2.5.3 RBDC Using Maximum Likelihood Method

Consider the joint PDF of the input variables in the original domain. Unlike in the U-space, the distance from the PML to the mean is no longer a simple measure for the failure probability. It is generally not straightforward to determine contours of constant exceedance probability. Actually, this would almost always require a transformation similar to (2.5) or (2.6). Instead we now consider contours of constant response y. Generally, different combinations of input variables $\mathbf{x}_1$ and $\mathbf{x}_2$ yielding the same response y will have different likelihoods $f_{\mathbf{X}}(\mathbf{x}_1)$ and $f_{\mathbf{X}}(\mathbf{x}_2)$ where $f_{\mathbf{X}}$ stands for the joint PDF of $\mathbf{X}$. This likelihood can be used to assess how likely, or unlikely, the occurrence of $\mathbf{x}_1$ is compared with $\mathbf{x}_2$. The most likely combination on the limit state surface $y = y_q$ is the solution to the RBDC problem. This point is known as the PML $\mathbf{x}^*$.

For computational reasons, it is much easier to maximize the log-likelihood function instead of the joint PDF. The different steps involved in the computation are:

1. Determine the extreme response y_q corresponding to the chosen exceedance probability q

2. Set up the joint log-likelihood model and solve:

$$\begin{cases} \max \ell_{\mathbf{X}}(\mathbf{x}) = \ln\left(f_{\mathbf{X}}(\mathbf{x})\right) \\ \text{subject to } g(\mathbf{x}, y_q) = 0 \end{cases} \tag{2.14}$$

3. The solution $\mathbf{x}^*$ of this non-linear optimization problem gives the RBDC

2.5.4 Discussion

An inverse reliability formulation holds clear computational advantages over a forward approach: iteration is no longer required. In addition, inverse FORM allows, at least theoretically, an uncoupling of the environmental input variables $\mathbf{X}$ and the response Y as well. In principle, the contours of $\mathbf{X}$ can be determined from an inverse Rosenblatt transformation first, see (2.6). Then, the maximum response is sought along these contours in a second step.

So far it is assumed that the critical response y_q corresponding to the exceedance probability q is known when the Maximum (Log-)Likelihood (MLL) method is used.

This is totally different from the inverse FORM approach where the value for y_q results from the analysis itself. One, but definitely not the best, way to find this critical response y_q could be using iterative, forward FORM. Of course this is not very efficient, since an inverse FORM approach would give this very same result at once!

The advantage of the proposed MLL method is precisely located in its very flexible format. Due to the uncoupling of the determination of the extreme response y_q and the actual RBDC, a wide range of methods is at hand, such as: extreme value analysis, Second-Order Reliability Methods (SORM), asymptotic approximations, and simulation methods. Generally these methods are superior (faster and/or more accurate) to forward FORM. Unfortunately, their formulation is not suited for an inverse reliability approach. Consequently, the proposed MLL method is application dependent and can be customized to the specific needs of the problem.

In short, inverse FORM seems to be computationally the most efficient solution; while the MLL method is the most versatile one. Additionally, the validity of the MLL results is not jeopardized by the linearization of the LSF, which may adversely affect the quality of the inverse FORM solution.

2.6 Model Uncertainty

2.6.1 Introduction

Der Kiureghian [13] distinguishes three basic sources of uncertainties, other than *human and organizational errors*,

1. *Inherent randomness* is described by the probability density functions $f_{\mathbf{X}}(\mathbf{x})$.

2. *Statistical uncertainty* is reflected in uncertainty associated with the parameters $\boldsymbol{\theta}$ in the PDF and denoted as $f_{\mathbf{X},\Theta}(\mathbf{x},\boldsymbol{\theta})$.

3. *Model uncertainty* is due to model inexactness and is reflected by uncertainties in the LSF $g(\mathbf{x}, \boldsymbol{\theta})$.

The vector $\mathbf{X}$ describes the basic random variables (point 1) and $\boldsymbol{\Theta}$ describes the model uncertainties (point 2 and 3). When the state of knowledge is perfect (no model uncertainty) $\boldsymbol{\Theta}$ is deterministically known: $\boldsymbol{\Theta} = \boldsymbol{\theta}$ and is a deterministic parameter in the distribution and LSF. To explicitly delineate the dependence of the model on $\boldsymbol{\Theta}$, the probabilistic model and LSF can be formulated as conditional upon $\boldsymbol{\Theta}$: $f_{\mathbf{X}|\boldsymbol{\Theta}}(\mathbf{x}|\boldsymbol{\theta})$ and $g(\mathbf{x}|\boldsymbol{\theta})$. Otherwise, the degree of model imperfection is reflected in the distribution of $\boldsymbol{\Theta}$, the parameter $\boldsymbol{\Theta}$ then may then be considered an additional random variable in the models $f_{\mathbf{X},\boldsymbol{\Theta}}(\mathbf{x}, \boldsymbol{\theta})$ and $g(\mathbf{x}, \boldsymbol{\theta})$ [15].

Unlike inherent variability, statistical and model uncertainties can be reduced, e.g. by collecting additional data or using more refined models. Model imperfection arises from two sources: one is lack of understanding of the physical phenomenon itself and the other is the use of simplified models. Quite often a model has to be simplified to keep the formulation mathematically tractable. So many variables may be involved in the analysis, such as in stochastic finite elements, that there is a need for simplification. Variables that do not greatly affect the response or that do not demonstrate much variation are then considered to be deterministic and are fixed at some value, typically the median or the mean. Since design codes have to be kept simple, these issues are closely related to the RBDC development as well.

This important problem of simplifying a probabilistic analysis has attracted considerable attention in recent years. Two, approximate methods are discussed here: they are based on "omission" of variables and "expansion" of a simplified analysis to a full one. Afterwards, it will be shown how they can be used in RBDC development, based on a second moment approximation of the model uncertainty.

2.6.2 Omission Factors In U-Space

Omission sensitivity factors give the relative error in the reliability index β when a basic variable is replaced by a deterministic number [33]. They are primarily used in the iterative determination of the design point $\mathbf{u}^*$ in forward FORM (2.4). The idea is that variables u_i with small omission factors do not greatly affect the reliability index, and can therefore be replaced by a fixed value for all subsequent iterations at a minimal penalty. This reduces the dimension of the optimization problem and hence substantially decreases the computer time. Once the reduced optimization problem has converged, one or two more iterations can be performed on the full problem. The omission sensitivity factor $\gamma_i\left(u_i^f\right)$ of the i-th variable, fixed at the value u_i^f, is defined as the ratio between the β-index, resulting from a simplified analysis with U_i fixed at the value u_i^f, and the β-index resulting from a full analysis, where U_i is a random variable.

In the following, the case where a model uncertainty Θ is fixed at its median value, i.e. $u_\theta = 0$, will be of practical interest. Madsen [33] proves that, when Θ is an independent basic variable, the omission sensitivity factor γ_i is:

$$\gamma_i\left(u_\theta = 0\right) \simeq \frac{1}{\sqrt{1-\alpha_\theta^2}} \tag{2.15}$$

where the approximation (2.15) is exact to first order and asymptotically true as $\alpha_\theta \rightarrow 0$. This is illustrated in Figure 2.3 for a non-linear LSF; the first order approximation will coincide with the exact value as $\alpha_\theta \rightarrow 0$. The factor α_i is a measure for both the sensitivity of the reliability index to inaccuracy in u_i at the design point $\mathbf{u}^*$:

$$\alpha_i = \left.\frac{\partial\beta}{\partial u_i}\right|_{\mathbf{u}^*} \tag{2.16}$$

and for the fraction of total uncertainty due to the uncertainty on u_i:

$$\mathbf{u}^* = \beta\,\boldsymbol{\alpha} \tag{2.17}$$

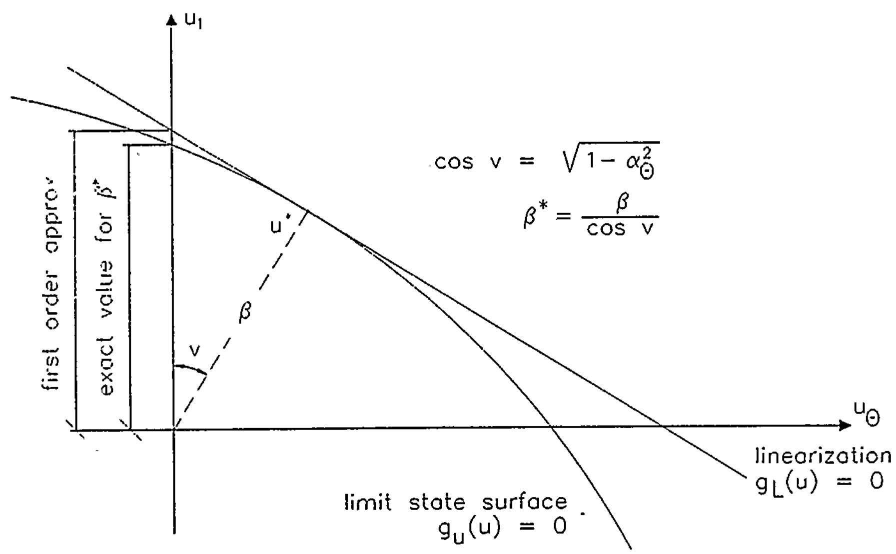

Figure 2.3: Illustration of the omission sensitivity factor $\gamma = \beta^*/\beta$ for the case of only one model uncertainty Θ

2.6.3 Model Expansion Factors In X-Space

Maes [36] estimates the failure probability of the full analysis P_Θ based on information resulting from the reduced analysis only. In this context the term "reduced" or "simplified" analysis refers to an analysis without consideration of model uncertainty, while the "full" analysis takes this model uncertainty into account as an additional random variable Θ. The failure probability $\Pr(F)$ of the full and reduced analysis are denoted as P_Θ and $P_{\overline{\theta}}$ respectively.

In this formulation the parameters Θ are fixed at their mean value $\overline{\boldsymbol{\theta}}$ in the reduced analysis. Based on the total probability theorem, the exact failure probability P_Θ can be found as:

$$P_\Theta(\mathbf{X},\Theta) = \int_\theta \Pr\left(g(\mathbf{X},\boldsymbol{\theta}) \le 0 \,|\, \boldsymbol{\theta}\right)\; f_\theta(\boldsymbol{\theta})\, d\boldsymbol{\theta} \tag{2.18}$$

Based on a Taylor-expansion of the integrand in (2.18) about the mean $\overline{\boldsymbol{\theta}}$ and asymptotic expressions for the second order sensitivities of the failure probabilities, a first-order second moment (FOSM) approximation for P_Θ can be obtained, based on $P_{\overline{\theta}}$, the failure probability in the reduced analysis where $\Theta = \overline{\boldsymbol{\theta}}$. For the practical case where only a single model uncertainty Θ is considered, the following result is obtained [36]:

$$P_\Theta \simeq P_{\overline{\theta}} \left\{ 1 + \tfrac{1}{2}\sigma_\theta^2 \left(\left[\frac{\partial g}{\partial \theta} \frac{|\nabla \ell|}{|\nabla g|} \right]_{\Theta=\overline{\theta},\mathbf{X}=\mathbf{x}^*} \right)^2 \right\} \tag{2.19}$$

where the gradient ∇ is taken with respect to $\mathbf{x}$, and $\mathbf{x}^*$ represents the PML in the original variable space.

2.6.4 Application To RBDC Development

Model uncertainty may result from two different sources:

1. Simplification when an exact or less inaccurate model is known

2. Inexactness due to lack of understanding of the physical phenomena

In any event, a central modeling of this uncertainty, i.e. second moment information, is readily available. For instance, this can be obtained from a comparison of model predictions with experimental evidence. The approximate methods, presented in the previous sections, can now be applied to develop RBDC when model uncertainty is present.

It is clear from the discussion in Section 2.5 that the iterative forward FORM method is computationally not efficient. It merely serves as a theoretical justification for the compact inverse FORM algorithm. Hence, model uncertainty discussion will be restricted to the inverse FORM and MLL methods only.

Inverse FORM

Winterstein *et al.* [56] assume the model uncertainty in the response model is represented by an additive, independent, zero mean, normally distributed random error term Θ. The "exact" response model is then:

$$Y_u(\mathbf{U}, \Theta) = h_u(\mathbf{U}) + \Theta \tag{2.20}$$

An exact RBDC formulation using inverse FORM for (2.20) considers Θ as an additional random variable. Without loss of generality, it can be assumed that Θ is a standard normal variable. This can always be achieved by multiplying Θ in (2.20) with the standard deviation σ_θ of the model uncertainty. The resulting inverse FORM problem (2.13) is:

$$\begin{cases} \text{Find } y_q = \max\,[Y_u(\mathbf{u}, \theta)] = \max\,[h_u(\mathbf{u}) + \sigma_\theta\,\theta] \\ \text{subject to } \sqrt{\|\mathbf{u}\| + \theta^2} = \beta \simeq -\Phi^{-1}(q) \end{cases} \tag{2.21}$$

To avoid explicit inclusion of this additional uncertainty Θ, Winterstein *et al.* [56] suggest to seek a new, inflated contour $\beta^* \geq \beta$, along which the simplified response model yields the correct capacity:

$$\begin{cases} \text{Find } y_q = \max\,[Y_u(\mathbf{u} \mid \theta = 0)] = \max\,[h_u(\mathbf{u})] \\ \text{subject to } \|\mathbf{u}\| = \beta^* \end{cases} \tag{2.22}$$

This argument is somehow circular, since the new value of β^* is unknown and dependent on the model uncertainty Θ. However, Winterstein *et al.* suggest that growing experience with this format for different structures will identify a reasonable range for the required correction β^*/β. The inflated contour level β^* reflects the additional safety required to compensate for the model uncertainty Θ. The exact value for β^* can only be obtained from a full analysis:

1. determine the maximum response y_q from (2.21)

2. find β^* from a forward FORM (2.4) with the simplified model $h_u(\mathbf{U})$ and the exact response y_q, obtained is step 1.

Theoretically, for each assumption about Θ and every response Y this ratio can be determined exactly. The forward FORM in this two step determination of β^*/β can actually be avoided.

An asymptotically exact value for β^* can be obtained from Madsen's omission sensitivity factors [33]:

$$\gamma_\theta(u_\theta = 0) = \frac{\beta(\Theta = \overline{\theta})}{\beta} = \frac{\beta^*}{\beta} \tag{2.23}$$

Substitution of (2.15) in (2.23) yields the inflated contour level:

$$\beta^* = \gamma_\theta \, \beta = \frac{\beta}{\sqrt{1-\alpha_\theta^2}} \tag{2.24}$$

This result is correct only for a linear LSF, otherwise it is an asymptotic approximation as $\alpha_\theta \to 0$. For relatively small α_θ, (2.24) may remain accurate.

In short, an asymptotic estimate for β^* can be obtained as:

1. determine the maximum response y_q from (2.21)

2. find β^* from (2.24)

The inconvenience of the use of omission sensitivity factors is that still one full analysis is required to identify α_θ and the inflated contour level β^* (2.24). The expansion factor derived by Maes [36] avoids this problem since only information available from the reduced analysis is used. An asymptotic result for the inflated contour level β^* can then be determined from (2.19):

$$\begin{aligned} \beta^* &\simeq -\Phi^{-1}(P_{\overline{\theta}}) \\ \Rightarrow \beta^* &\simeq -\Phi^{-1}\left(\Phi\left(-\beta\right)\frac{P_{\overline{\theta}}}{P_{\Theta}}\right) \end{aligned} \tag{2.25}$$

When (2.25) is used the two-step determination of β^* actually reduces to a single step, where only information from the reduced analysis is used.

Maximum Likelihood Method

When RBDC are developed using the MLL method, the critical response y_q is assumed to be known. The exceedance probability q_Θ for a given response y when model uncertainty is accounted for, will be different from the exceedance probability $q_{\overline{\theta}}$, when this uncertainty is fixed at its mean level. When model uncertainty is present, the MLL method is only useful if the "exact" response level $y_{q,\Theta}$ can be estimated directly from $y_{q,\overline{\theta}}$, i.e. the critical response when model uncertainty is not considered. In other words, there is a need for techniques which allow to obtain the required change of the limit state function Δg compensating for the model uncertainty and keeping the "exact" failure probability equal to the target exceedance probability q.

Maes suggests to achieve this by means of so-called ignorance factors θ^* [36]. The required change Δg is then obtained by replacing the model uncertainty parameter Θ by θ^* instead of $\overline{\theta}$, while the other input variables $\mathbf{x}$ remain unaffected. This approach allows to keep the same design parameters $\mathbf{x}^*$, which resulted from the simplified analysis, while still achieving the required "exact" exceedance probability q. An additional advantage of this format is that it provides a clear incentive to reduce the model uncertainty.

These ignorance factors result from the model expansion technique. They can be used directly in the simplified LSF model by replacing $\overline{\theta}$ by θ^*. For an additive and multiplicative model uncertainty Θ and Ψ, asymptotic approximations are respectively [36]:

$$\theta^* \sim \overline{\theta} - \tfrac{1}{2}\sigma_\theta^2 \left[\frac{\partial g}{\partial \theta} \frac{|\nabla \ell|}{|\nabla g|}\right]_{\overline{\theta},\mathbf{x}^*} \tag{2.26}$$

$$\psi^* \sim 1 - \tfrac{1}{2}\nu_\psi^2 \left[1 + \frac{\partial g}{\partial \psi} \frac{|\nabla \ell|}{|\nabla g|}\right]_{\overline{\psi}=1,\mathbf{x}^*} \tag{2.27}$$

where σ_θ is the standard deviation of Θ, ν_ψ is the COV of Ψ, and $\mathbf{x}^*$ is the PML for the simplified model analysis ($\Theta = \overline{\theta}, \Psi = \overline{\psi} = 1$).

2.7 Alternative RBDC

2.7.1 General

In the preceding sections, only the most likely combination of input variables giving a extreme response y_q was identified. Various other combinations will cause the same extreme response.

For practical design purposes one may wish to fix some input variables at a convenient value: the median, a suitably high or low percentile or a selected return period level. This is best illustrated by means of an example.

Assume now that RBDC have to be developed for different response variables $\mathbf{Y} = (Y_1, \ldots, Y_m)$ in a particular structure subject to various loads $\mathbf{X}$. The most likely combinations of input variables $\mathbf{x}^*$, which result from the RBDC development process, will consist of different load levels $\mathbf{x}_i$ for each response $\mathbf{y}_{q_i}$, where the subscript i indicates which one of the m responses is considered. Typically, the resulting load levels for the load variables governing the response will be extreme (high or low) while the RBDC levels for the remaining load variables will be located in the central part of their marginal distributions. In this case, it makes sense from a design point of view to bundle the various load combinations. One may wish to fix the non-governing variables at their mean level and adjust the other ones accordingly such that the exact response is obtained. Or, just the other way around, when one variable seems to govern the response, it makes sense to relate this load directly to the response in terms of return periods. Again, all remaining variables of the particular problem will have to be adjusted accordingly. E.g. the 100-year bending moment is caused by the 100-year wind load, combined with other loads which are specified at a different level.

They may also be used to compare two different design philosophies. The RBDC in strict sense determines the environmental parameters associated with the recurrence interval of the responses. The other RBDC can reflect an extreme event philosophy in which return period levels for at least some of the input variables are used. The RBDC development will then give the most likely values for the non specified variables, conditional upon those fixed return period levels.

That the exact response y_q and corresponding input variables $\mathbf{x}^*$ are known already from the first step, the actual RBDC development. The n basic variables are now partitioned in two groups: j variables are somehow fixed, the remaining n-j variables are still random. In this context, fixed means a deterministic relation to find them is available, rather than fixed at one particular deterministic value; they are no longer stochastic variables:

$$\begin{aligned} &\text{original variable domain:} \quad \mathbf{X} = [\mathbf{x}_j,\, \mathbf{X}_{n-j}] \\ &\text{standard normal space:} \quad \mathbf{U} = [\mathbf{u}_j,\, \mathbf{U}_{n-j}] \end{aligned} \tag{2.28}$$

The objective is now to determine the most likely combination of the remaining input variables $\mathbf{X}_{n-j}$ when y_q and $\mathbf{x}_j$ are given. This is discussed for all three RBDC development methods, independent from which method is used to determine the critical response y_q, the PML $\mathbf{x}^*$ and the fixed input parameters $\mathbf{x}_j$.

2.7.2 Forward FORM

A forward FORM analysis with the problem dimension reduced to n-j will give the practical design combination $\mathbf{x}^*_{n-j}$. The reliability index resulting from this analysis can be interpreted as an inflated contour level β^*. This increased reliability level indicates how much further the new minimal distance point is away from the origin compared with the actual design point $\mathbf{u}^*$.

In the case of independent variables the transformation (2.5) is straightforward. It is to be noted, however, that for correlated basic variables the implementation of the Rosenblatt transformation (2.6) has to be considered on a case by case basis. When the dependent original variable x_i is specified at some fixed level this does no longer imply a fixed value for the corresponding standard normal u_i-variable. It rather defines a deterministic equation for u_i. Generally, the inverse tranformation $t^{-1} : \mathbf{u} \mapsto \mathbf{x}$ has to be re-arranged. This is illustrated in the drilling riser application in Chapter 5.

2.7.3 Inverse FORM

Since the design point of the full analysis is known, the omission factors and the increased contour level can be determined from (2.24). A new inverse FORM in the n-j−dimensional U-space will then give the practical design combination. However, this solution is only asymptotically correct for $\alpha_j \to 0$ if the LSF is non-linear [33]. Given this β^*, an inverse FORM will then yield the RBDC. The full analysis result provides a good starting value for $\mathbf{u}^*_{n-j}$. Even though the method is not exact in most cases, it provides an internal quality check. If the resulting y_q from the reduced analysis is much different from the full analysis result, this is a clear indicator that the LSF is too non-linear for the given α_j-values.

2.7.4 Maximum Likelihood Method

In this method the dimension of the optimization problem (2.14) is directly reduced to n-j. The method is applicable without modification. The likelihood of the most likely combination (the "PML" $\mathbf{x}^*_{n-j}$) in the n-j-dimensional problem will be less than for the true PML $\mathbf{x}^*_n$, resulting from the n-dimensional full analysis. The ratio of both likelihoods indicates how less likely this "constrained PML" $\mathbf{x}^*_{n-j}$, yielding the same response y_q as the actual PML $\mathbf{x}^*_n$, is to occur compared with the combination given by the actual PML $\mathbf{x}^*_n$.

2.7.5 Comparison Of Results

When these other RBDC are determined using the FORM method the new minimal distance $\|\mathbf{u}^*\|$ can be interpreted as a measure of the relative likelihood of occurrence of the design combination with some fixed parameters, compared to the most likely design combination. Both design combinations, however, result in the same response level y_q, with exceedance probability q.

When the MLL method is used for this purpose, a relative likelihood is obtained at once. This is a relative probability density, rather than a relative probability.

2.8 Comparison

2.8.1 General

All RBDC development methods discussed in this chapter are now compared with each other on the basis of 6 criteria: *required input*, *produced output* and *computa-*

tional effort are self explanatory terms. The *applicability* of the method combines both the versatility and accuracy of the technique and explains for what type of PDF and LSF the method can be applied successfully. The item *model uncertainty* describes how second moment information about model uncertainty can be used to determine the RBDC. Eventually, the term *alternative design combinations* stands for the computational effort involved and accuracy obtained when the method is used to determine other than "most likely" design combinations, given the solution to the actual RBDC problem.

2.8.2 Forward FORM

1. *required input:* required reliability level q
2. *produced output:* RBDC $\mathbf{x}^*$ and critical response y_q
3. *computational effort:* requires iterative solution, each iteration is of a similar computational complexity as the inverse FORM calculation itself.
4. *applicability:* only exact for LSF which is linear in the standard normal **U**-space. A non-linear LSF $g_u(\mathbf{u})$ may influence the quality of the results.
5. *model uncertainty:* inflated contours are most convenient, but only asymptotically correct. If $\frac{|\nabla \ell|}{|\nabla g|}$ is easily determined, ignorance factors can be used straightaway.
6. *alternative design combinations:* new n-j−dimensional forward FORM

2.8.3 Inverse FORM

1. *required input:* required reliability level q
2. *produced output:* RBDC $\mathbf{x}^*$ and critical response y_q

3. *computational effort:* concise and straightforward

4. *applicability:* only exact for LSF which is linear in the standard normal **U**-space. A non-linear LSF $g_u(\mathbf{u})$ may influence the quality of the results.

5. *model uncertainty:* inflated contours based on omission or expansion factors

6. *alternative design combinations:* approximate solution from inverse FORM using inflated contour level; exact solution from n-j−dimensional forward FORM

2.8.4 Maximum Likelihood

1. *required input:* the critical response level y_q

2. *produced output:* RBDC $\mathbf{x}^*$

3. *computational effort:* actual RBDC development is of same computational complexity as inverse FORM. Determination of y_q increases computing cost.

4. *applicability:* is applicable to all problems. Output quality depends only on the accuracy of y_q, which may be determined using any structural reliability computational method.

5. *model uncertainty:* ignorance factors

6. *alternative design combinations:* new n-j−dimensional log-likelihood maximization

2.9 Summary

In this chapter, the structural reliability integral is defined and some structural reliability computation methods are reviewed briefly.

Then, three methods for RBDC development are presented. Iterative forward FORM and inverse FORM rely on the transformation of the basic variables to the normal space and the First-Order reliability index β. Aside from the RBDC they also give a first-order estimate of the extreme response y_q. In the maximum likelihood method this extreme response has to be determined beforehand. This opens the option to use a more refined method to find the critical response y_q.

It is shown how model uncertainty can be handled if only second moment information is available and the practical development of design combinations is discussed as well. Finally, the methods are compared with each other for different criteria.

Chapter 3

Application To A Moving Load Problem

3.1 Overview

In this chapter a first application is given which demonstrates the different methods presented in the previous chapter. It concerns a two-span continuous beam subjected to two moving point loads. The example is intended to illustrate, in the simplest possible way, the various methodologies for RBDC. To limit the computational work, a bivariate normal distribution is chosen for the two loads.

First, the influence of the correlation coefficient between the loads is studied with respect to three response variables specified at the 10^{-4} level: the middle support reaction, the bending moment over the support, and the mid-span deflection. The load combinations yielding these critical responses are determined using both the inverse FORM and Maximum Likelihood methods.

Subsequently, model uncertainty is introduced by assuming an uncertain settlement of the middle support. The performance of the omission factor and ignorance factor approaches is measured against "exact" results for the bending moment and support reaction.

3.2 Problem Description

3.2.1 General

Consider the two-span statically indeterminate beam shown in Figure 3.1. Both spans have equal length l and constant bending stiffness ei. Two moving point loads, P_1 and P_2, act on the beam; their spacing is l and it is assumed that there is

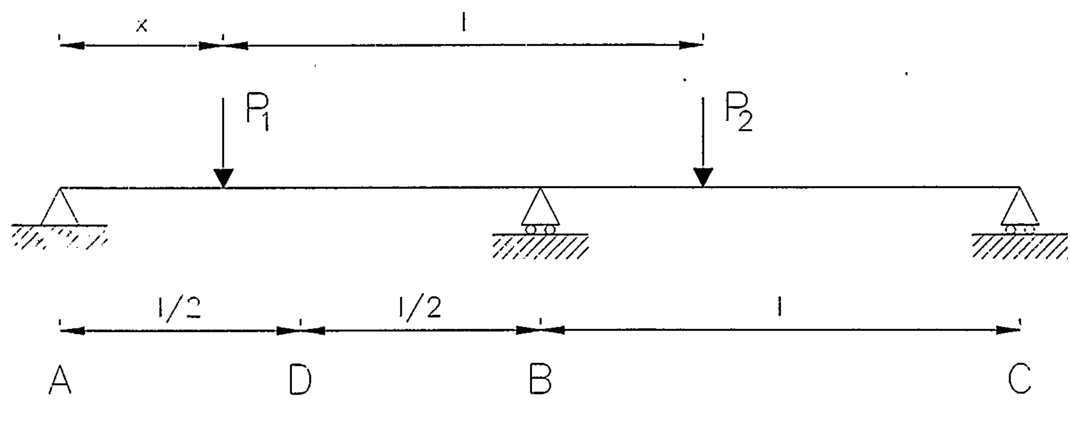

Figure 3.1: Moving load problem on a two-span continuous beam

always one load acting on each span (i.e. $0 \leq x \leq l$). It is worthwhile re-stating that the notation followed here is consistent with common practice in reliability analysis: uppercase letters are used for random variables, while lowercase notation is used for deterministic values of these random variables. Consequently, P_1 stands for a random load variable, whereas p_1 is used for a particular occurrence of this random load P_1. This is in contrast with the notation usually adopted in structural analysis where lowercase denotes distributed loads.

In this example three structural responses are studied: the reaction force R_B and bending moment M_B at the middle support and the deflection Δ_D at mid-span. The following sign convention is adopted: an upward support reaction R_B is considered positive, the bending moment M_B is positive if it produces tension in the top fibre of the beam and the deflection Δ_D is measured positively in downward direction.

3.2.2 Load Modeling

The loads P_1 and P_2 are assumed to be jointly normal: their mean value p is the same, but their standard deviation and correlation are different. The coefficient of variation (COV) of the load in the second span is selected at 10%. The parameter k

expresses the ratio of the two standard deviations and ρ is the correlation coefficient ($-1 \le \rho \le 1$). Only $k > 1$ is analyzed since the largest critical load level will always occur in the first span in that case. This simplifies the formulas a lot and it can be done without actual loss of generality since the problem geometry is symmetric. The mean vector $\boldsymbol{\mu}_{\mathbf{P}}$ and covariance matrix $\Sigma_{\mathbf{P}}$ are:

$$\boldsymbol{\mu}_{\mathbf{P}} = \mathrm{E}(\mathbf{P}) = \begin{Bmatrix} \mathrm{E}(P_1) \\ \mathrm{E}(P_2) \end{Bmatrix} = \begin{Bmatrix} p \\ p \end{Bmatrix} \tag{3.1}$$

$$\Sigma_{\mathbf{P}} = \begin{bmatrix} \mathrm{Var}(P_1) & \mathrm{Covar}(P_1, P_2) \\ \mathrm{Covar}(P_1, P_2) & \mathrm{Var}(P_2) \end{bmatrix} = \begin{bmatrix} (0.1k\,p)^2 & \rho\,k\,(0.1p)^2 \\ \rho\,k\,(0.1p)^2 & (0.1p)^2 \end{bmatrix} \tag{3.2}$$

In the original basic variable space, this joint probability density function is consequently given as:

$$f_{\mathbf{P}}(p_1, p_2) = \frac{1}{2\pi\sigma_{P_1}\sigma_{P_2}\sqrt{1-\rho^2}} \exp\left\{ \frac{-\left[\left(\frac{p_1-p}{\sigma_{P_1}}\right)^2 - 2\rho\left(\frac{p_1-p}{\sigma_{P_1}}\right)\left(\frac{p_2-p}{\sigma_{P_2}}\right) + \left(\frac{p_2-p}{\sigma_{P_2}}\right)^2\right]}{2(1-\rho^2)} \right\} \tag{3.3}$$

and the log-likelihood function is then:

$$\ell_{\mathbf{P}}(p_1, p_2) = -a\left[\left(\frac{p_1-p}{\sigma_{P_1}}\right)^2 - 2\rho\left(\frac{p_1-p}{\sigma_{P_1}}\right)\left(\frac{p_2-p}{\sigma_{P_2}}\right) + \left(\frac{p_2-p}{\sigma_{P_2}}\right)^2\right] + b \tag{3.4}$$

where a, b are constants and $a > 0$.

The Rosenblatt-transformation (2.6) which is generally required to map the original variables into the standard normal space is greatly simplified here since the original variables are already normally distributed:

$$\begin{Bmatrix} u_1 \\ u_2 \end{Bmatrix} = \frac{1}{\cos(2\varphi)} \begin{bmatrix} \cos\varphi & \sin\varphi \\ \sin\varphi & \cos\varphi \end{bmatrix} \begin{Bmatrix} \frac{p_1-p}{\sigma_{P_1}} \\ \frac{p_2-p}{\sigma_{P_2}} \end{Bmatrix} \tag{3.5}$$

where $\varphi = \frac{1}{2}\arcsin(-\rho)$. In the standard normal space the joint PDF (3.3) is given as:

$$f_{\mathbf{U}}(u_1, u_2) = \tfrac{1}{2\pi}\exp\left\{-\tfrac{1}{2}\left(u_1^2 + u_2^2\right)\right\} = \tfrac{1}{2\pi}\exp\left\{-\tfrac{1}{2}\|\mathbf{u}\|^2\right\} \tag{3.6}$$

3.3 Derivation Of Influence Lines

3.3.1 General

In this section the structural models $h(P_1, P_2)$ for the three responses of interest are developed. The actual RBDC formulation afterwards is then as follows: find the most likely combination of P_1 and P_2 yielding the response $y_q = h(P_1, P_2)$ where y_q has an exceedance probability q. Here, $h(P_1, P_2)$ is formulated in terms of influence ordinates:

$$h(P_1, P_2) = \eta_1(x)P_1 + \eta_2(x)P_2 \tag{3.7}$$

where x denotes the position of the loads P_1 and P_2 on the span.

The derivation of the influence lines is based on the Müller-Breslau technique [19]. Since the loads in this problem are moving, the position of the moving loads which results in the maximum effect of the action considered has to be determined from:

$$\max_{0<x<l} h(P_1, P_2) \Rightarrow \frac{d}{dx}\left[\eta_1(x)P_1 + \eta_2(x)P_2\right] = 0 \tag{3.8}$$

3.3.2 Support Reaction R_B

To determine the influence line for the reaction force at B, the support B is removed and a unit displacement in downward direction introduced at B. The corresponding force f_u required is:

$$f_u = \frac{6ei}{l^3} \tag{3.9}$$

The deflected shape of the beam subjected to this load f_u at point B represents the influence line for r_B. The influence ordinates for the first and second span (load P_1 and P_2 respectively) are:

$$\begin{aligned} \eta_1 &= \tfrac{3}{2}\xi - \tfrac{1}{2}\xi^3 \\ \eta_2 &= 1 - \tfrac{3}{2}\xi^2 + \tfrac{1}{2}\xi^3 \end{aligned} \tag{3.10}$$

where $\xi = \frac{x}{l}$ is the so-called natural coordinate for the position of the point load P_i on span i.

The structural response r_B (3.7) is:

$$r_B(p_1, p_2) = p_1\left(\tfrac{3}{2}\xi - \tfrac{1}{2}\xi^3\right) + p_2\left(1 - \tfrac{3}{2}\xi^2 + \tfrac{1}{2}\xi^3\right) \tag{3.11}$$

and has to be maximized with respect to ξ according to (3.8). It can be shown that (3.11) is maximal when:

$$\xi_{\max} = \frac{\kappa - \sqrt{\kappa^2 - \kappa + 1}}{\kappa - 1} \tag{3.12}$$

with $\kappa = \frac{p_2}{p_1}$. If $\kappa = 1$, (3.11) is maximal for $\xi = 0.5$.

It is interesting to see how much $\xi_{\max}$ varies in function of κ:

- $\kappa = 0 \Rightarrow \xi_{\max} = 1$: load p_1 acts at point B, and p_2 $(= 0)$ at the right end C.
- $\kappa = 1 \Rightarrow \xi_{\max} = 0.5$: both load p_1 and p_2 act at mid-span (at D and E).
- $\kappa = \infty \Rightarrow \xi_{\max} = 0$: load p_1 $(= 0)$ acts at the left end A, and p_2 at point B.

The maximum load effect for every occurrence (p_1, p_2) can be determined from (3.11). Since p_1 and p_2 are random, the load ratio κ and position for maximum effect ξ (3.12) will be random as well.

3.3.3 Bending Moment M_B

To determine the influence line for the bending moment at B, a hinge and a unit rotation are introduced at the support B. The moment m_u required to do so is [19, App. B]:

$$m_u = \frac{3ei}{2l} \tag{3.13}$$

The deflected shape of the beam subjected to this bending moment m_u at point B represents the influence line for m_B. The influence ordinates for the first and second span (load P_1 and P_2 respectively) are:

$$\begin{aligned} \eta_1 &= \tfrac{l}{4}\left(\xi - \xi^3\right) \\ \eta_2 &= \tfrac{l}{4}\left(\xi^3 - 3\xi^2 + 2\xi\right) \end{aligned} \tag{3.14}$$

where $\xi = \frac{x}{l}$ is the so-called natural coordinate for the position of the point load P_i.

The structural response m_B (3.7) is:

$$m_B(p_1, p_2) = p_1 l \left[\frac{(\xi - \xi^3) + \kappa\,(\xi^3 - 3\xi^2 + 2\xi)}{4}\right] \tag{3.15}$$

with $\kappa = \frac{p_2}{p_1}$ and (3.15) has to be maximized with respect to ξ according to (3.8). It can be shown that (3.15) is maximal when:

$$\xi_{\max} = \frac{3\kappa - \sqrt{3\left(\kappa^2 + \kappa + 1\right)}}{3\left(\kappa - 1\right)} \tag{3.16}$$

It is observed that the variation of (3.16) as function of κ is a lot less for the bending moment m_B compared with the support reaction m_B. For $\kappa = 0$, (3.15) is maximal at $\xi_{\max} = \frac{1}{\sqrt{3}} \simeq 0.577$ and for $\kappa = 1$, (3.16) yields $\xi_{\max} = 0.5$.

As before, p_1 and p_2 are random. Consequently, the load ratio κ and position for maximum effect ξ (3.16) will be random as well.

3.3.4 Mid-span Deflection Δ_D

From Betti's theorem, it follows that the influence line for the deflection at D is given as the deflected shape of the beam when a unit load is applied at this point D. Since the two-span continuous beam is statically indeterminate to the first degree, the influence line will be obtained through the following procedure [19, pp. 381-382]:

1. determine the influence coefficient of the deflection $\eta_{\delta_{rel}}$ in the released structure
2. determine the influence coefficient η_{r_B} for the redundant force r_B
3. determine the value of the deflection due to unit redundants δ_u
4. the influence coefficient for the deflection at D η_{δ_D} in the statically indeterminate beam is then $\eta_{\delta_D} = \eta_{\delta_{rel}} + \eta_{r_B}\,\delta_u$

The support reaction force r_B is chosen as the redundant in the structure. According to step 1, a unit load is now introduced at $x = l/2$ in the released structure and the deflected shape is determined:

$$\begin{array}{ll} x \le l/2 & \eta_{\delta_{rel}} = \frac{3x}{96ei}\left(7l^2 - 4x^2\right) \\ x \ge l/2 & \eta_{\delta_{rel}} = \frac{1}{96ei}\left(4x^3 - 24x^2 l + 33xl^2 - 2l^3\right) \end{array} \tag{3.17}$$

It is clear from Figure 3.1 that the load p_2 will always be located to the right of D. Consequently, the influence coefficient of the deflection δ_D for the load in the second span in the released structure $\eta_{\delta_{rel,2}}$ is given as:

$$\begin{array}{l} \eta_{\delta_{rel,2}} = \frac{1}{96ei}\left(4(x+l)^3 - 24(x+l)^2 l + 33(x+l)l^2 - 2l^3\right) \\ \Rightarrow \eta_{\delta_{rel,2}} = \frac{1}{96ei}\left(4x^3 - 12x^2 l - 3xl^2 + 11l^3\right) \end{array} \tag{3.18}$$

The influence line for the redundant force r_B was already obtained before, see (3.11). Now, the value of δ_D due to a unit redundant $r_B = 1$ is calculated:

$$\delta_u = -\frac{11l^3}{96ei} \tag{3.19}$$

Eventually, the influence coefficients η_1 and η_2 in (3.7) are obtained as $\eta_{\delta_{rel}} + \eta_{r_B}\,\delta_u$:

$$\begin{aligned} x \leq l/2\text{:} \quad & \eta_1 = \tfrac{1}{192ei}\left(-13x^3 + 9xl^2\right) \\ x \geq l/2\text{:} \quad & \eta_1 = \tfrac{1}{192ei}\left(19x^3 + 33xl^2 - 48x^2l - 4l^3\right) \\ \text{for all } x\text{:} \quad & \eta_2 = \tfrac{-1}{64ei}\left(x^3 - 3x^2l + 2xl^2\right) \end{aligned} \tag{3.20}$$

After substitution for (3.20), The maximum of (3.7) is given by the formula for $x \leq l/2$ if $\kappa \leq 1$ and obtained at:

$$\xi_{\max} = \frac{3\kappa + \sqrt{3\kappa^2 - 17\kappa + 39}}{3\kappa + 13} \tag{3.21}$$

and is given by:

$$\delta_D(p_1, p_2) = \frac{p_1 l^3}{192ei}\left[\left(9\xi - 13\xi^3\right) - 3\kappa\left(\xi^3 - 3\xi^2 + 2\xi\right)\right] \tag{3.22}$$

The position $\xi_{\max}$ where the maximum is obtained is now almost invariant with respect to κ. For $\kappa = 0$, $\xi_{\max} = \sqrt{\frac{3}{13}} \simeq 0.480$ and for $\kappa = 1$, $\xi_{\max} = 0.5$. Since, as before, p_1 and p_2 are random, the load ratio κ and position for maximum effect $\xi_{\max}$ (3.21) will be random as well.

3.4 RBDC By Inverse FORM And Maximum Likelihood

3.4.1 Inverse FORM

According to the methodology outlined in the previous chapter, we first have to determine the reliability index corresponding to the desired risk level. Here, an arbitrary level of $q = 10^{-4}$ is chosen which yields $\beta = -\Phi^{-1}(q) = 3.72$. Then, the inverse reliability problem is formulated as an inverse FORM problem (2.13). In order to solve (3.24) the structural response function h_u has to be known in terms of the standard normal vector $\mathbf{u}$ whose components u_i are mutually independent. Therefore, the transformation (3.5) is inverted:

$$\left\{ \begin{array}{c} p_1 \\ p_2 \end{array} \right\} = \left\{ \begin{array}{c} p \\ p \end{array} \right\} + \left[\begin{array}{cc} \sigma_{p_1} \cos\varphi & -\sigma_{p_1} \sin\varphi \\ -\sigma_{p_2} \sin\varphi & \sigma_{p_2} \cos\varphi \end{array} \right] \left\{ \begin{array}{c} u_1 \\ u_2 \end{array} \right\} \tag{3.23}$$

and the inverse FORM problem can be formulated as:

$$\left\{ \begin{array}{l} \text{Find } r_{B,q} = \max \left[h_u \left(p_1(\mathbf{u}), p_2(\mathbf{u}) \right) \right] \\ \text{subject to } \|\mathbf{u}\| = \beta = 3.72 \end{array} \right. \tag{3.24}$$

3.4.2 Maximum Likelihood

When the maximum likelihood (MLL) method is used, the RBDC are obtained through:

$$\left\{ \begin{array}{l} \max \ell(p_1, p_2) = -a \left[\left(\frac{p_1 - p}{\sigma_{P_1}} \right)^2 - 2\rho \left(\frac{p_1 - p}{\sigma_{P_1}} \right) \left(\frac{p_2 - p}{\sigma_{P_2}} \right) + \left(\frac{p_2 - p}{\sigma_{P_2}} \right)^2 \right] + b \\ \text{subject to } h(p_1, p_2) = p_1\, \eta_1(\xi) + p_2\, \eta_2(\xi) = y_q \end{array} \right. \tag{3.25}$$

where a, b are constants and $a > 0$.

In this method the critical response y_q, corresponding to the risk level q, must be known beforehand. In this example, y_q is determined directly from the distribution for the response variable of interest, which is obtained by Monte Carlo Simulation (MCS).

Applying a basic variance reduction technique [3], the required number of simulations can be substantially reduced. Since the correlation coefficient ρ is considered as a parameter in this problem, the relative performance of the inverse FORM and MLL methods, is of interest as well. This relative performance indicates whether both methods reflect the sensitivity of the result to ρ correctly or not. Symbolically, the differences

$$d_{y_q} = y_q(\rho = -1) - y_q(\rho) \tag{3.26}$$

are of interest. The objective of the variance reduction technique is now to reduce the uncertainty, typically measured as the sample variance, on the estimate of $d_{r_{B,q}}$. From

$$\begin{aligned} \operatorname{Var}\left[d_{y_q}\right] &= \operatorname{Var}\left[y_q(\rho = -1) - y_q(\rho)\right] \\ &= \operatorname{Var}\left[y_q(-1)\right] + \operatorname{Var}\left[y_q(\rho)\right] - 2\operatorname{Cov}\left[y_q(-1), y_q(\rho)\right] \end{aligned} \tag{3.27}$$

it follows that making the Cov-term positive reduces the variance of y_q. The Cov-term in (3.27) is maximal if the random numbers used to calculate $y_q(-1)$ and $y_q(\rho)$ are the same. This is easily achieved in simulation: using the same initial seed for the random number generator (RNG) reproduces the stream of pseudo-random numbers.

Even when the absolute performance $y_q(\rho)$ is of primary interest, the former method can be used to reduce the computer time. Once a specific value $y_q(\rho_0)$ is obtained sufficiently accurate (e.g. from a long simulation) each additional point $y_q(\rho)$ can be obtained at a marginal cost by in fact estimating the difference $y_q(\rho) - y_q(\rho_0)$ rather than $y_q(\rho)$.

It is obvious that this simple variance reduction technique is helpful only if a parameter sensitivity analysis (ρ in this example) is to be performed. If only one value y_q is of interest, more refined variance reduction techniques, such as described in [3], [30], [48], and [57], must be used to cut the excessive computational costs of crude MCS.

3.4.3 Middle Support Reaction R_B

Figure 3.2 compares the results for $r_{B,q}$, p_1^*, and p_2^*, obtained from inverse FORM and Maximum Likelihood for the case $k = 1.01$ as a function of the correlation coefficient ρ $(-1 \leq \rho \leq 1)$. The main conclusion from the graph is that both methods yield almost identical results for the critical response $r_{B,q}$. This will be discussed in more detail in Section 3.4.6.

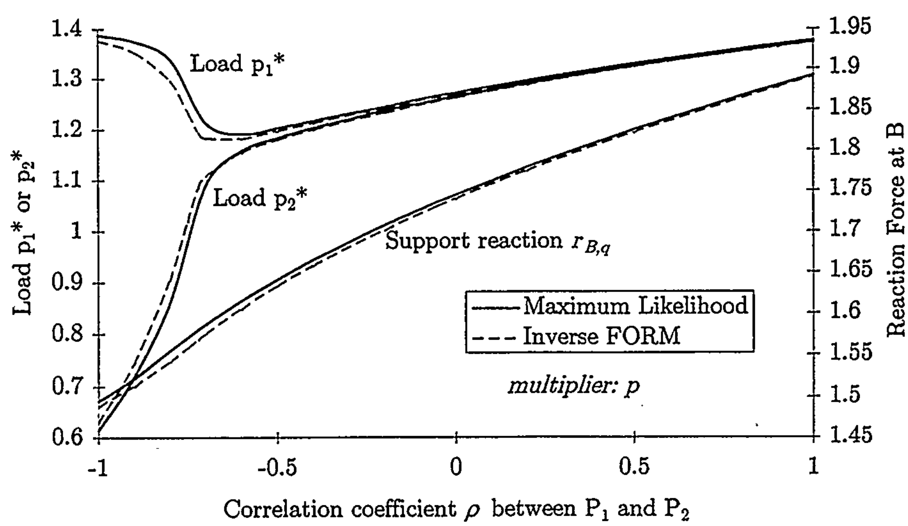

Figure 3.2: Comparison between inverse FORM and MLL for $k = 1.01$

In a second step, the influence of the parameter k is studied. Figure 3.3 shows the RBDC for k-values of 1.01, 1.1, 1.25, 1.5 and 2. The arrows on the graph point in the direction of increasing k. Since the results for the inverse FORM and MLL methods are almost identical, only one set of solutions (inverse FORM) is presented. The following conclusions can be drawn:

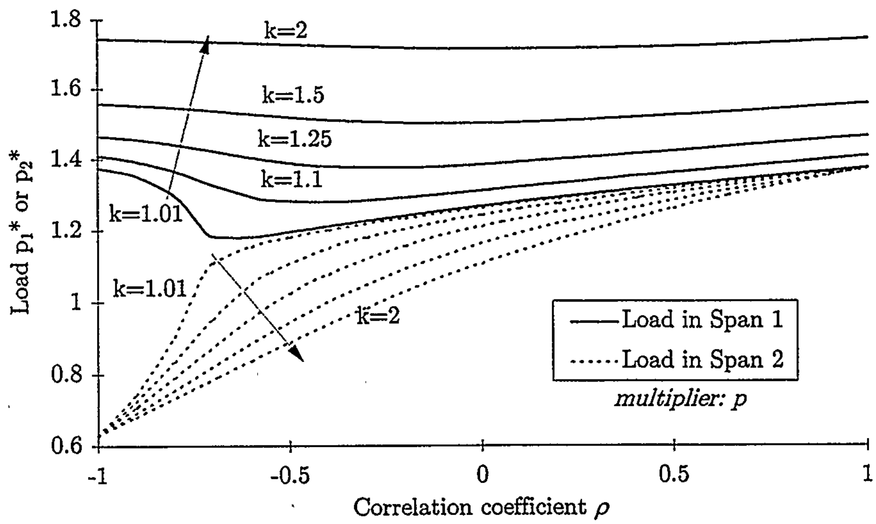

Figure 3.3: RBDC for p_1^* and p_2^*, plotted as a function of the correlation coefficient ρ and the COV-ratio k, for the reaction force at support B, obtained using Inverse FORM.

- The critical response $r_{B,q}$ increases as k, and thus the variance of the load in the first span, increases. To avoid overloading of the graph, the values for $r_{B,q}$ are not plotted. Their values are listed in Table 3.1 for $\rho = -1$, 0, and +1. As $k \rightarrow \infty$, the level for $r_{B,q}$ becomes independent of ρ. Since the load p_1^* is then much higher than p_2^*, P_1 governs the response whence $u_1^* \simeq \beta$ while $u_2^* \simeq 0$.

- The load levels (after division by the standard deviation σ_{P_i}) corresponding to $\rho = \pm 1$ are invariant of k: $\frac{p_1^* - p}{\sigma_{P_1}} = \beta$, $\frac{p_2^* - p}{\sigma_{P_2}} = -\beta$ for $\rho = -1$ and β for $\rho = 1$. $\frac{p_1^* - p}{\sigma_{P_1}}$ is always positive since the variance of P_1 is greater than for P_2. The actual load levels p_2^* are invariant of k for $\rho = \pm 1$ in the original domain as well because the variance of load P_2 does not depend on k.

COV-ratio	Correlation between P_1 and P_2		
k	$\rho = -1$	$\rho = 0$	$\rho = +1$
1.01	1.488	1.739	1.889
1.10	1.519	1.756	1.912
1.25	1.571	1.788	1.952
1.50	1.657	1.850	2.019
2.00	1.882	1.992	2.161
4.00	2.549	2.651	2.785

Table 3.1: Critical response $r_{B,q}$ for different values of ρ and k (multiplier: p)

COV-ratio	Correlation between P_1 and P_2		
k	$\rho = -1$	$\rho = 0$	$\rho = +1$
1.01	0.1886	0.2226	0.2576
1.10	0.1918	0.2393	0.2607
1.25	0.1971	0.2433	0.2660
1.50	0.2060	0.2504	0.2747
2.00	0.2237	0.2657	0.2922

Table 3.2: Critical response $m_{B,q}$ for different values of ρ and k (multiplier: pl)

- For low values of k, p_1^* and p_2^* (or better, $\frac{p_1^*-p}{\sigma_{P_1}}$ and $\frac{p_1^*-p}{\sigma_{P_1}}$) are almost identical, even for rather strong negative correlation ($\rho = -0.6$). This trend decreases with increasing k. In the limit for $k \to \infty$, p_2^* is a linear function of ρ which implies $p_2^* = p$ ($u_2^* = 0$) when the loads are mutually independent ($\rho = 0$). This corresponds to what one intuitively expects: the response level is actually governed by the variability of the more important load.

3.4.4 Support Moment M_B

As before, the inverse FORM and MLL solutions are compared for a particular value of k (Figure 3.4). Figure 3.5 shows the influence of the parameter k on the RBDC; these results are obtained using inverse FORM. To avoid overloading the graph, only the loads p_1^* and p_2^* yielding the critical response $m_{B,q}$ are drawn. The actual support bending moment $m_{B,q}$ is not shown on the graph, the trend as function of ρ can be seen from Figure 3.4. The critical bending moment level $m_{B,q}$ varies with k in a way similar to the support reaction $r_{B,q}$ (see Table 3.2). Comparing these figures with the ones for the support reaction response $r_{B,q}$ from the previous section, we may conclude:

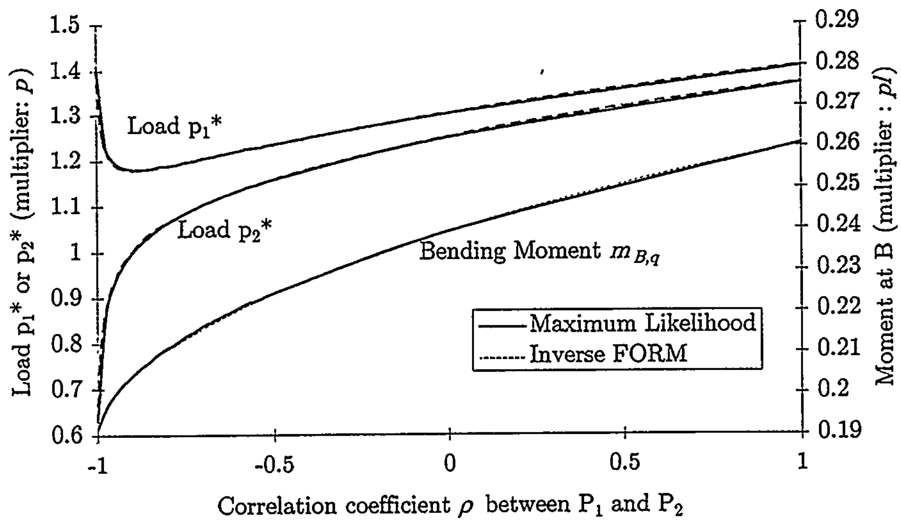

Figure 3.4: Comparison between inverse FORM and MLL for $k = 1.1$

- The discrepancy between inverse FORM and MLL is even smaller here. A more detailed discussion is presented in Section 3.4.6.

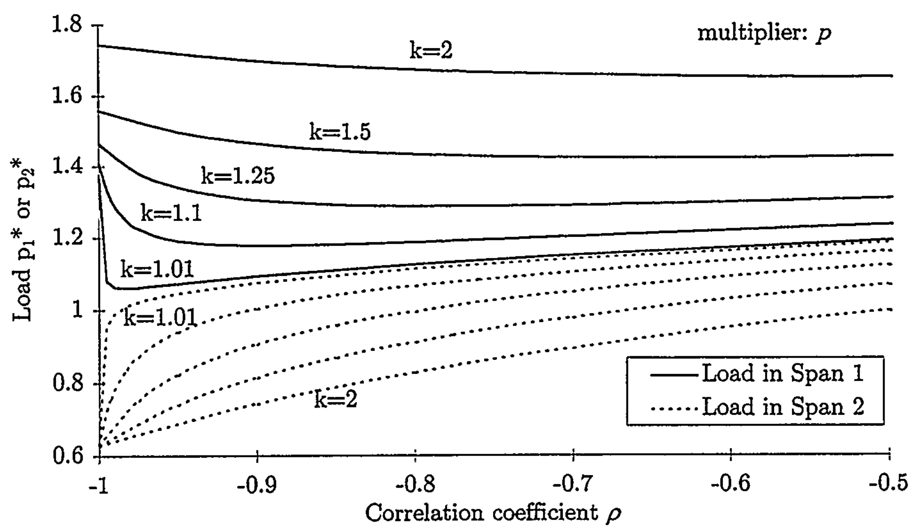

Figure 3.5: RBDC for p_1^* and p_2^*, plotted as a function of the correlation coefficient ρ and the COV-ratio k, for the bending moment at support B, obtained using Inverse FORM.

- As before, the load levels (after division by the standard deviation σ_{P_i}) corresponding to $\rho = \pm 1$ are invariant of k: $\frac{p_1^* - p}{\sigma_{P_1}} = \beta$, $\frac{p_2^* - p}{\sigma_{P_2}} = -\beta$ for $\rho = -1$ and equal to β for $\rho = 1$.

- The same trend to have u_1^* and u_2^* almost identical is observed as for the support reaction response $r_{B,q}$. The trend is much stronger though than for $r_{B,q}$. For $k = 1.01$, an almost pathological case is obtained, p_1^* and p_2^* differ only significantly when $-1 \leq \rho < -0.97$. For this reason the curves in Figure 3.5 were cut off at $\rho = -0.5$. Figure 3.6 shows this effect in a different way: the total load $p_1^* + p_2^*$ increases a lot faster for the bending moment $m_{B,q}$ than for the support reaction $r_{B,q}$. This difference between the two RBDCs is even more pronounced for $k = 1.01$ but vanishes as $k \to \infty$.

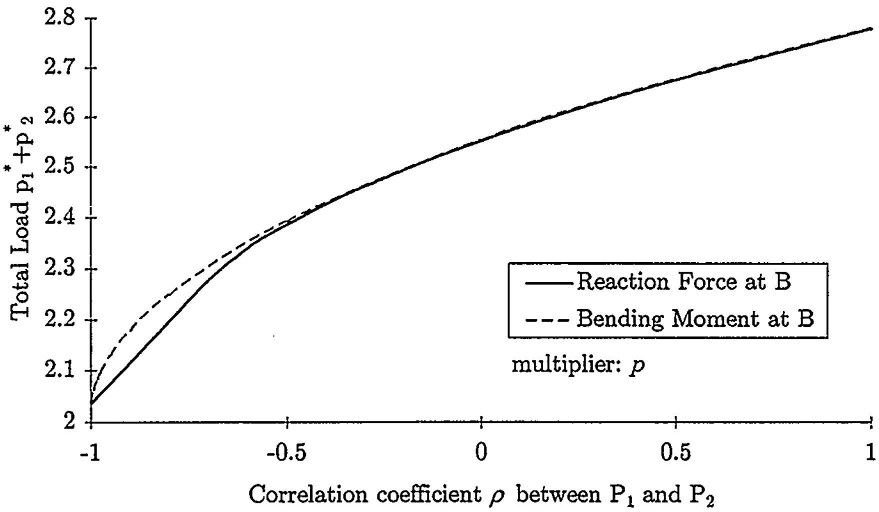

Figure 3.6: Total load $p_1^* + p_2^*$ resulting from the RBDC for R_B and M_B ($k = 1.1$)

- As before, the trend to have u_1^* and u_2^* almost identical decreases with increasing k and in the limit for $k \rightarrow \infty$, p_2^* is a linear function of ρ, similar to the previous case.

3.4.5 Midspan Deflection Δ_D

First, the inverse FORM and MLL methods are compared for $k = 1.01$ (Figure 3.7). Figure 3.8 shows the influence of the parameter k on the RBDC; these results are again obtained using inverse FORM. To avoid overloading of the graph, only the loads p_1^* and p_2^* yielding the critical response $\delta_{D,q}$ are drawn. The values for the critical deflection $\delta_{D,q}$ are listed in Table 3.3.

- The actual mid-span deflection $\delta_{D,q}$ is not shown on the graph. The trend as function of ρ can be seen from Figure 3.7: $\delta_{D,q}$ now decreases with ρ. Since the influence coefficient η_2 is negative (3.20), the mid-span deflection will decrease as P_2 becomes more and more important, i.e. as ρ increases.

COV-ratio k	Correlation between P_1 and P_2 $\rho = -1$	$\rho = 0$	$\rho = +1$
1.01	3.2520	2.9099	2.4117
1.10	3.3485	3.0003	2.5080
1.25	3.5092	3.1526	2.6684
1.50	3.7772	3.4101	2.9360
2.00	4.3132	3.9326	3.4712

Table 3.3: Critical response $\delta_{D,q}$ for different values of ρ and k (multiplier: $\frac{pl^3}{192ei}$)

- The RBDC resulting from inverse FORM and MLL actually coincide now. This is not surprising when we consider that the influence coefficients η_i are now almost constant because the position for maximal effect is practically invariant of the relative magnitude of P_1 and P_2 ($0.480 < \xi \leq 0.5$). Consequently, the LSF in the **u**-space is almost perfectly linear resulting in an exact result using First-Order reliability techniques.

- Once more, the load values (after division by their standard deviation σ_{P_i}) corresponding to $\rho = \pm 1$ are invariant of k: $\frac{p_1^* - p}{\sigma_{P_1}} = \beta$, $\frac{p_2^* - p}{\sigma_{P_2}} = -\beta$ for $\rho = -1$ and equal to β for $\rho = 1$.

- Because the influence coefficients η_1 and η_2 have different sign, the loads p_2^* tends to be as small as possible. However, in the limit for $k \to \infty$, p_2^* is a linear function of ρ, similar to the previous cases. This limit is now approached from the lower side.

- The actual loads p_1^* are now almost independent of ρ while p_2^* hardly depends on k: there is only 15% variation on p_2^* in the range $k \in (1, \infty)$. For the more practical range $k \in (1, 2)$, this variation is even less than 8%.

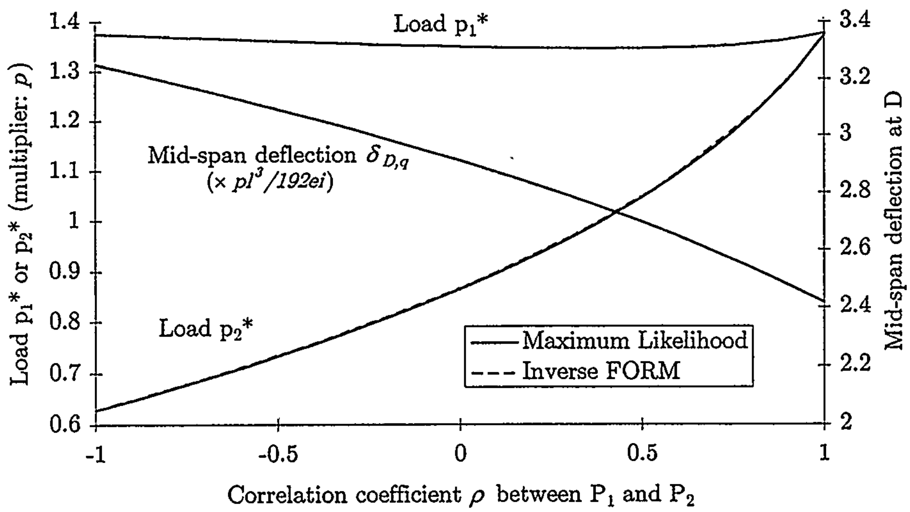

Figure 3.7: Comparison between inverse FORM and MLL for $k = 1.01$

3.4.6 Discussion Of FORM Performance

Comparison Inverse FORM and Maximum Likelihood Method

As discussed in Chapter 2, both RBDC development methods are conceptually different. Inverse FORM first determines load combinations with a given exceedance probability q, referred to as U- or β-contours, and then finds the maximum response due to these loads. It is conceptually appealing that these circles are response independent. For a given exceedance probability q, the contour surface is always the same. This is shown for the support reaction at B in Figure 3.9. The iso-response curves vary with ρ, but the β-contour remains invariant. Maximization of the response along this circle gives the critical support reaction $r_{B,q}$. The critical iso-response lines for the bending moment $m_{B,q}$ and mid-span deflection $\delta_{D,q}$ are also tangent to this circle, but they are omitted from Figure 3.9 for clarity.

The MLL method on the other hand first searches all combinations yielding the critical response y_q, and then looks for the most likely load combination among

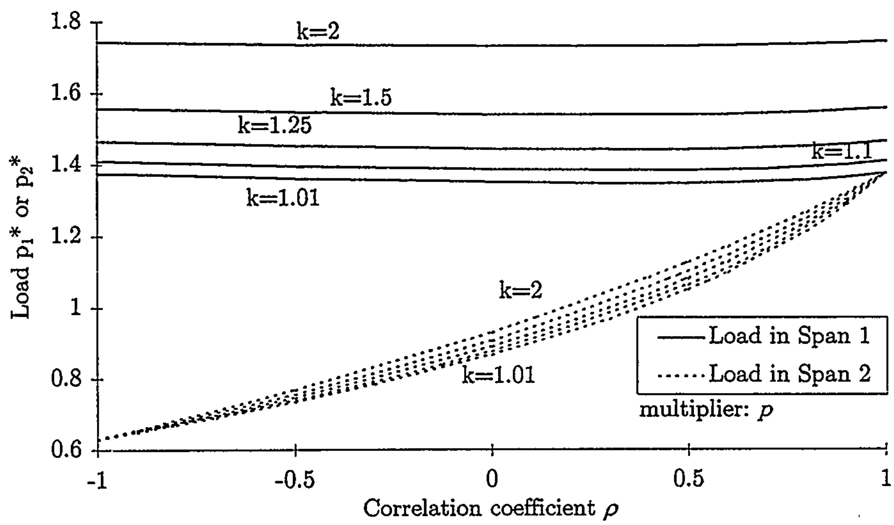

Figure 3.8: RBDC for p_1^* and p_2^*, plotted as a function of the correlation coefficient ρ and the COV-ratio k, for the mid-span deflection of the first span, obtained using Inverse FORM.

these. For a joint normal distribution the contour lines of the log-likelihood function $\ell_{\mathbf{P}}(p_1, p_2)$ and the **U**-contours actually coincide.

After back-transformation to the original variable domain, these contours are presented in Figure 3.10 for $k = 1.01$ and in Figure 3.11 for $k = 2$. In this case the back-transformed **U**-contours are ellipses:

$$\mathbf{U}\text{-contour} = \{\mathbf{p} \mid \|\mathbf{u}\| = \|t(\mathbf{p})\| = \beta\} \tag{3.28}$$

and coincide with the log-likelihood contours:

$$\ell\text{-contour} = \{\mathbf{p} \mid \ell_{\mathbf{P}}(\mathbf{p}) = \ell(p_1, p_2) = \text{ constant}\} \tag{3.29}$$

The parameter k determines the ratio of the lengths of the axes of the ellipses while

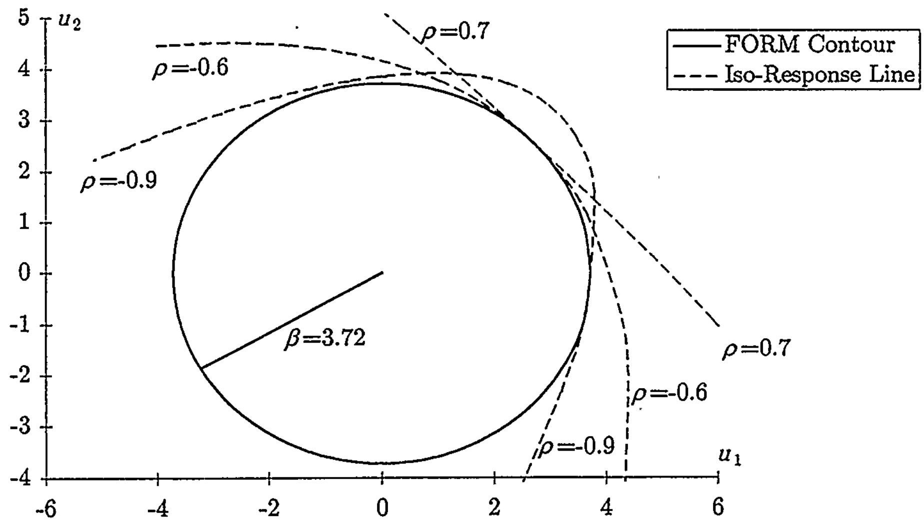

Figure 3.9: β-circle and iso-response lines for $r_{B,q}$ in the standard normal space for $k = 1.01$ and different values of ρ

the correlation coefficient ρ indicates the orientation of those axes [29]. The center of the ellipses is located at the mean $(1, 1)$.

Since the loads are jointly normal, the PML $\mathbf{p}^*$ and minimal distance point $\mathbf{u}^*$ are perfectly interchangeable through the transformation t. For $k = 1.01$ two local PMLs can be identified for negative ρ, they correspond to two points in the standard normal space whose distance to the origin is almost minimal (see Figure 3.9). As ρ increases, the two local PML points merge into one global PML. For $k = 2$ only one PML is found for the full range $-1 \leq \rho \leq 1$.

The First-Order approximation formula

$$q \simeq \Phi(-\beta) \tag{3.30}$$

is based on the assumption that there is only 1 unique minimal distance point $\mathbf{u}^*$ and is consequently no longer correct for the case $k = 1.01$. If the design points are

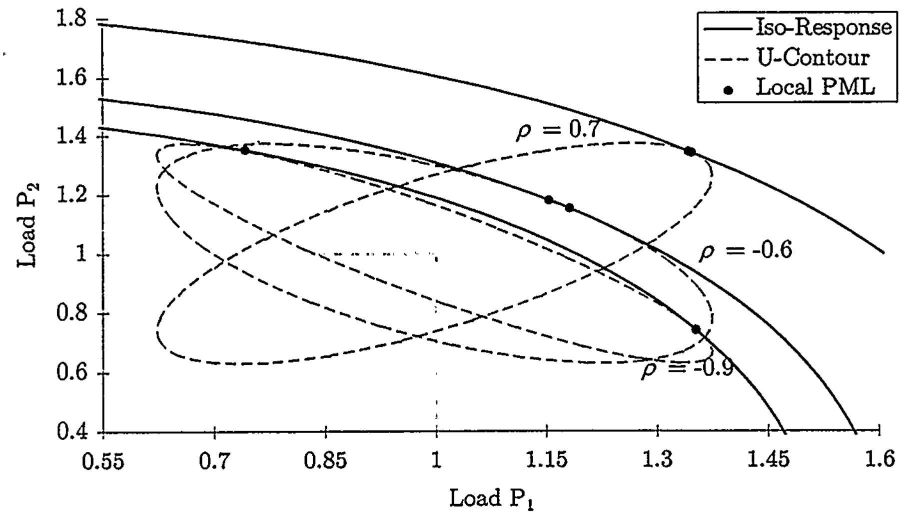

Figure 3.10: Contour lines of log-likelihood and response $r_{B,q}$ for $k = 1.01$

sufficiently far away from each other, a pragmatic adjustment for (3.30) consists of adding the contribution of all design points $\mathbf{u}_i^*$ towards the failure probability:

$$q \simeq \sum_i \Phi(-\beta_i) \tag{3.31}$$

where β_i represents the distance from design point $\mathbf{u}_i^*$ to the origin.

Consequently, we may conclude that in this particular application an underestimation of the failure probability by 50% still results in an accurate estimate for $r_{B,q}$ (see Figure 3.2).

Linearization of $g_u(\mathbf{u}) = 0$ In Inverse FORM

From a comparison of the Figures 3.2, 3.4, and 3.7, it can be concluded that the difference between the inverse FORM and MLL solution vanishes more and more. At least for the positive range of ρ-values this is to be contributed to the nearly linear shape of the limit state surface $g_u(\mathbf{u}) = 0$.

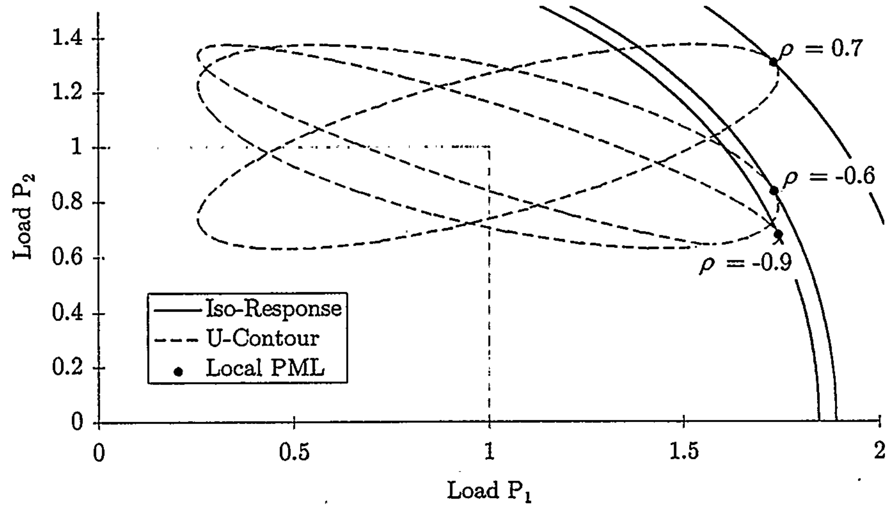

Figure 3.11: Contour lines of log-likelihood and response $r_{B,q}$ for $k = 2$

When the influence line for M_B was developed (see Section 3.3.3), it was pointed out that the support bending moment was maximal when the loads P_1 and P_2 are positioned between $0.5\,l$ and $0.557\,l$. The same rationale can be made for the deflection Δ_D where $0.480 < \xi_{\max} \leq 0.5$. This implies that the influence coefficients η_1 and η_2 are not very variable and that, as a result, the structural response function h (3.7) is almost linear in P_1 and P_2. This quasi-linearity is not affected by the transformation to the $\mathbf{u}$-space because (3.5) represents a shift, a scaling and a rotation, operations which do not affect the linearity. In short, the LSF in the $\mathbf{u}$-space is quasi-linear whence the very good performance of First-Order reliability techniques.

Quality Of Inverse FORM

It is observed that in this application the inverse FORM method always gives very good results even though the First-Order failure probability estimate is not necessarily accurate. As a matter of fact, the error on the response y_q is more of interest than the error on the exceedance probability q. In structural reliability applications, q is usually very small. Consequently the tail behavior of the distribution then becomes important. The minus log-exceedance function:

$$L(y) = -\ln(q) \tag{3.32}$$

is widely used for the estimation of large quantiles y_q of a random variable Y [2]. This function is plotted in Figure 3.12 for the response $r_{B,q}$ and will be referred to as the (L, y)-plot. For a wide class of distributions, this function becomes more and more linear as $q \to 0$ [7]. A linearization is then justified, whence the following error-estimate for the critical response y_q:

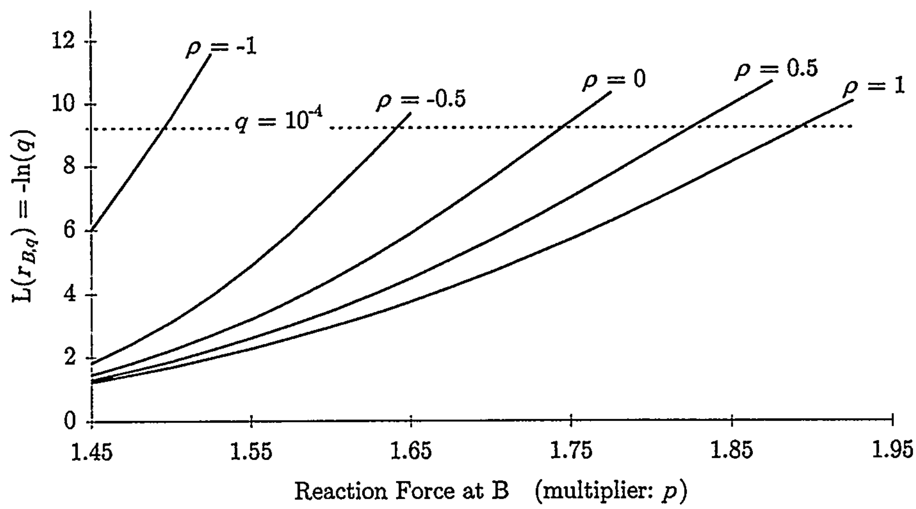

Figure 3.12: Minus log-exceedance function for R_B, $k = 1.01$, and different ρ-values

$$|\Delta y_q| = \left|\frac{\Delta \ln q}{L'(y_q)}\right| \tag{3.33}$$

where $L'(y_q)$ is the slope of the (L, y)-plot at the estimate for y_q. From (3.33) it follows that a crude estimate for q may be satisfactory as long as the slope $L'(y_q)$ is not too small.

For $\rho = -1$ and $k = 1.01$, the error $\Delta \ln q \simeq \ln 2 = 0.69$, the slope $L'(r_{B,q}) = 74.5$, whence $\Delta r_{B,q} = \frac{0.69}{74.5} = 0.0093$. As a result, an error of 50% on q is reduced to an error of only 0.6% on $r_{B,q}$. This corresponds to the difference between the inverse FORM and MCS result for $r_{B,q}$. For $\rho = 1$, this slope $L'(r_{B,q})$ is smaller, which requires a more accurate estimate of the exceedance probability q to maintain the same accuracy on $r_{B,q}$.

It is important to stress that this tail behavior accounts for all sources of error: both non-linearity of the LSF and multiple PML problems. In this particular application the tail behavior of r_B compensates for the error on q.

3.4.7 Comparison Of Design Criteria

It may be concluded from the Figures 3.2, 3.4, and 3.7 that the load levels p_1^* and p_2^* are very different for the three responses. Since the influence coefficient η_2 in (3.20) is negative, this is to be expected for the deflection response. This is also reflected in the marginal exceedance probabilities for p_2^*. Figure 3.13 clearly indicates that the load P_2 tends to be as low as possible. It also shows, however, that the RBDC for R_B and M_B are quite different as well. This seems in contradiction with what one expects since both responses are clearly strongly correlated. Figure 3.14 explains this difference.

The arrows in Figure 3.14 point at the position of maximum effect for p_1^* and p_2^*. The load values for $k = 1.01$ are printed above the beam, and for $k = 2$ under the beam. The values s_i between brackets indicate the number of standard deviations this load value p_i^* is away from the mean and is related to the marginal exceedance

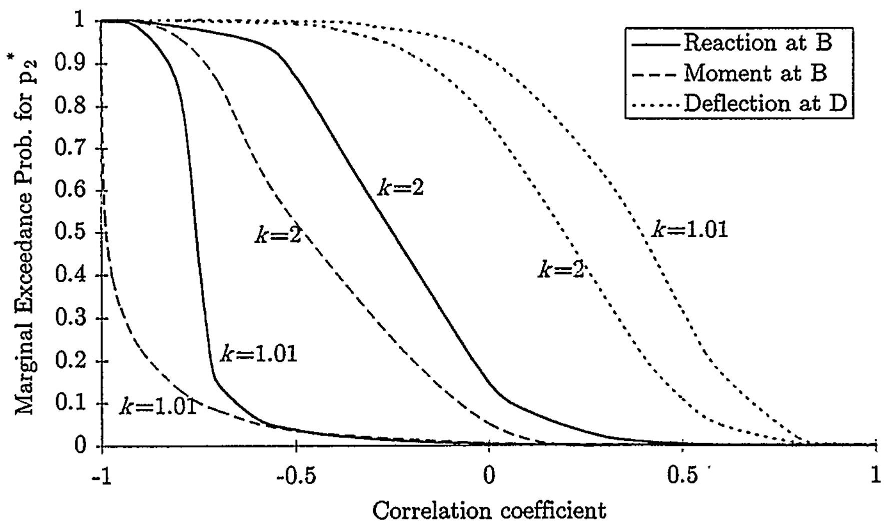

Figure 3.13: Marginal exceedance probability for load p_2^* as a function of ρ and k for the three responses

probability plotted in Figure 3.13:

$$\Pr(P_i > p_i^*) = 1 - \Phi(s_i) \tag{3.34}$$

Figure 3.14 shows that the difference between the two RBDC is caused by a different position of maximum effect $x_{\max}$. Even though R_B and M_B are correlated for most values of P_1 and P_2, their extremes are different. Assume for instance $P_1 \gg P_2$, the maximum reaction force R_B is then obtained when P_1 is located near the support B. This causes only a very small bending moment though. Recall that the position $x_{\max}$ for maximum bending moment is always located between $0.5\,l$ and $0.577\,l$, while this range is much wider for the reaction force: $0.5\,l \le x_{\max} \le l$.

It is most pronounced for strong negative correlation between P_1 and P_2 and is stronger for increasing values of k as well. This can also be seen from Figure 3.13: for $k = 1.01$ the marginal distributions of p_2^* almost coincide for $\rho > -0.6$, while for

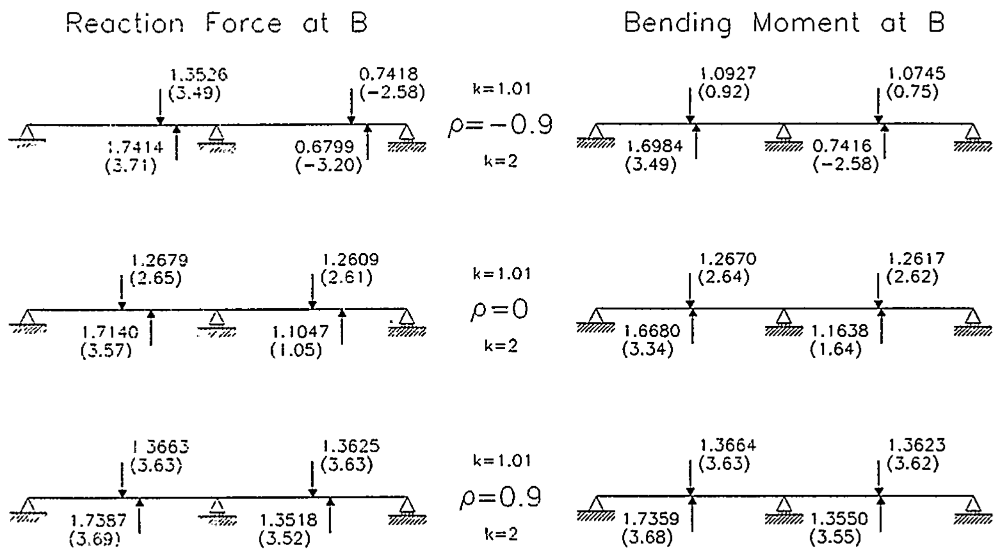

Figure 3.14: Comparison of p_1^* and p_2^* (multiplier: p) for the critical support reaction and bending moment at B as a function of k and ρ.

$k = 2$ they are clearly different until $\rho > 0.5$.

The RBDC development clearly indicates these different extremes and consequently provides a better understanding of the underlying (extreme) behavior.

3.5 Model Uncertainty

3.5.1 Problem Description

The performance of the approximate methods accounting for model uncertainty, presented in the previous chapter, is now examined. In this example, model uncertainty is introduced through an uncertain settlement of the middle support at B, which is treated as a model error here.

It was already pointed out in the previous chapter that the approximate methods dealing with model uncertainty (e.g. ignorance factors) are accurate only as long as the model uncertainty does not govern the response. Since it is clear that the mid-span deflection δ_D is highly affected by a support settlement δ_B, this response variable will be excluded from this model uncertainty analysis.

Because the mean value of this support settlement is not equal to zero, the response levels obtained before can not directly be compared to the new ones, a shift is required.

The exact, modified, structural response model h, resulting from a structural analysis is [19]:

$$r_B(p_1, p_2, \delta_B) = p_1\left(\tfrac{3}{2}\xi - \tfrac{1}{2}\xi^3\right) + p_2\left(1 - \tfrac{3}{2}\xi^2 - \tfrac{1}{2}\xi^3\right) - \frac{6ei}{l^3}\delta_B \tag{3.35}$$

$$m_B(p_1, p_2, \delta_B) = p_1 l\left[\frac{(\xi - \xi^3) + \kappa\,(\xi^3 - 3\xi^2 + 2\xi)}{4}\right] - \frac{3ei}{l^2}\delta_B \tag{3.36}$$

For the subsequent analysis, it is convenient to express this support settlement as:

$$\delta_B = \theta\,\frac{pl^3}{ei} \tag{3.37}$$

where θ is a parameter, indicating the magnitude of the support settlement. This selection for δ_B expresses the model uncertainty in (3.35) and (3.36) with the same multipliers p and pl as the actual responses R_B and M_B and allows a more elegant formulation of the results. Substituting (3.37) in (3.35) and (3.36), we obtain:

$$r_B(p_1, p_2, \theta) = p_1\left(\tfrac{3}{2}\xi - \tfrac{1}{2}\xi^3\right) + p_2\left(1 - \tfrac{3}{2}\xi^2 - \tfrac{1}{2}\xi^3\right) - 6\,\theta\,p \tag{3.38}$$

$$m_B(p_1, p_2, \theta) = p_1 l\left[\frac{(\xi - \xi^3) + \kappa\,(\xi^3 - 3\xi^2 + 2\xi)}{4}\right] - 3\,\theta\,pl \tag{3.39}$$

Now consider θ to be uncertain with a lognormal distribution for Θ. Note that this distribution becomes more and more skew with increasing COV. The mean $\overline{\theta}$ of Θ then describes the magnitude of the mean support settlement, while the variation of Θ represents the actual uncertainty around this mean value.

3.5.2 "Exact" Results

General

When Θ is considered an additional random variable in the problems (3.38) and (3.39), "exact" results for the RBDC can be obtained. In this section we compare the solution obtained using inverse FORM with the MLL method and an omission factor approach using the exact lognormal distribution for Θ. In the following the COV of Θ is studied as a parameter of the problem.

Since $\overline{\theta} \neq 0$ in general, the response levels obtained before can not be directly compared to the new ones. A shift over $\delta_{R_B} = \mathrm{E}(\Delta_{R_B}) = -6\overline{\theta}p$ or $\delta_{M_B} = \mathrm{E}(\Delta_{M_B}) = -3\overline{\theta}pl$ is required.

Middle Support Reaction R_B

First, the "exact" solution is obtained directly from the distribution for R_B, which is obtained by Monte Carlo Simulation (MCS). Then this is compared with an inverse FORM solution, including a third standard normal variable U_3, representing the model uncertainty parameter Θ after transformation into the **u**-space:

$$\begin{aligned} u_3 &= \frac{\ln(\theta) - \mathrm{E}(\ln(\Theta))}{\sigma_{\ln(\Theta)}} \\ \text{with } &\mathrm{E}(\ln(\Theta)) = \ln(\mathrm{E}(\Theta)) - \tfrac{1}{2}\sigma^2_{\ln(\Theta)} \\ \text{and } &\sigma_{\ln(\Theta)} = \sqrt{\ln(1+\sigma^2_{\Theta})} \end{aligned} \tag{3.40}$$

Figure 3.15 compares the RBDC using inverse FORM with the results using MCS for $k = 1.01$, $\rho = 0$ and $\overline{\theta} = 0.1$. The third line shown on the figure represents the RBDC when an "exact" omission factor is used. This result is listed in Table 3.4 obtained as follows:

1. determine the sensitivity factor: $\alpha_3 = u_3/\beta$

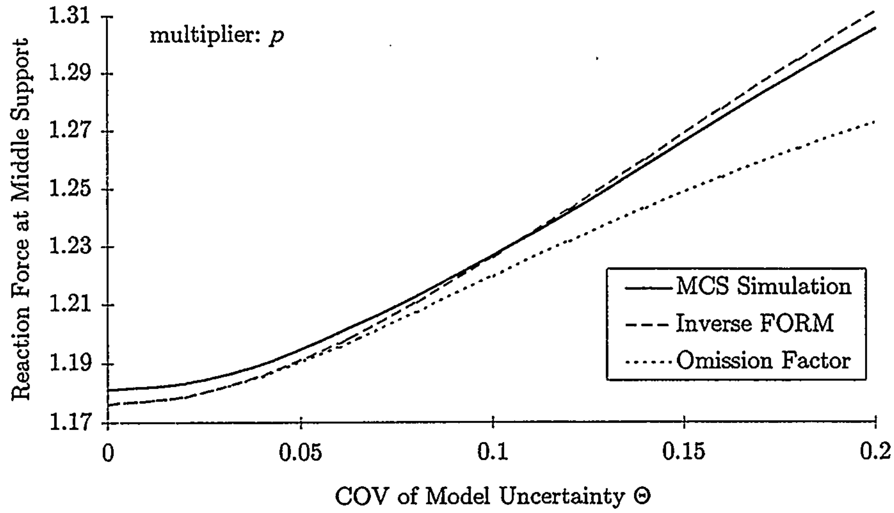

Figure 3.15: Comparison of "exact" $r_{B,q}$ for $k = 1.01$, $\rho = 0$ and $\overline{\theta} = 0.1$

2. calculate the inflated contour level β^* from the omission sensitivity factor:

$$\beta^* = \frac{\beta}{\sqrt{1 - \alpha_3^2}}$$

3. find the approximate response level using inverse FORM, with $u_3 = 0$ as the omitted variable.

A few remarks may to be added here: step 2 is correct only if the LSF is linear, for non-linear limit states this valid in an asymptotic sense as $\alpha \longrightarrow 0$. The approximation gradually worsens as α increases. This is also clear from the Table 3.4 which shows the monotonic relationship between model uncertainty COV and α as well.

It may be worth noting that $u_3 = 0$ fixes Θ at its median level and not the mean. This median value depends on the COV and can be calculated from (3.40).

COV (%)	α_3	Relative Error (%)
0	0	-0.5
5	-0.26	-0.4
10	-0.44	-0.6
15	-0.53	-1.4
20	-0.59	-2.5

Table 3.4: Error on $r_{B,q}$ using an "exact" omission factor

COV (%)	α_3	Relative Error (%)
0	0	-0.08
20	-0.31	-0.07
40	-0.39	-0.54
60	-0.40	-1.00
80	-0.39	-1.17
100	-0.38	-1.08

Table 3.5: Error on $m_{B,q}$ using an "exact" omission factor

Support Bending Moment M_B

Similar to the support reaction, Figure 3.16 compares the RBDC for the bending moment M_B using inverse FORM with the results using MCS for $k = 1.01$, $\rho = 0$ and $\overline{\theta} = 0.01$. The third line shown on the figure shows $m_{B,q}$ when an "exact" omission factor, outlined in the previous section, is used. This approximation gradually worsens as α_3 increases (see Figure 3.16 and Table 3.5). Since the model uncertainty is a lot less ($\overline{\theta} = 0.01$), the induced error is now much smaller than for the support reaction and stabilizes around 1% ($\alpha_3 \simeq 0.4$).

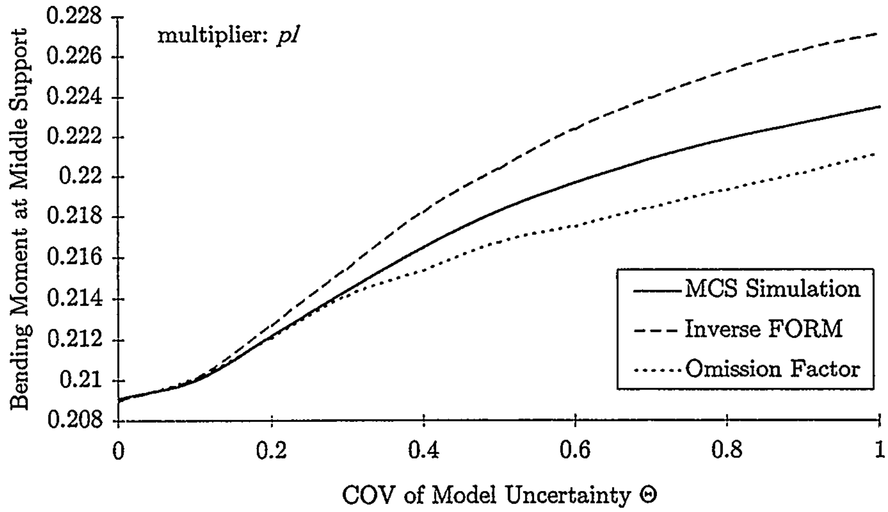

Figure 3.16: Comparison of "exact" $m_{B,q}$ for $k = 1.01$, $\rho = 0$ and $\overline{\theta} = 0.01$

3.5.3 Approximate Second Moment Solutions

General

These methods use only first and second moment information of the model error Θ. Basically, this comes down to assuming a normal distribution for the model uncertainty. For both responses an omission and ignorance factor approach are compared with the "exact' value obtained using MCS. For the omission factor approach the sensitivity of the RBDC to the α-value is studied as well. The standard normal variable U_3, representing the model uncertainty parameter Θ after transformation into the **u**-space, is now obtained as:

$$u_3 = \frac{\theta - \mathrm{E}(\Theta)}{\sigma_\Theta} \tag{3.41}$$

In this case an inverse FORM and omission factor approach are almost identical since the model uncertainty is represented by an independent, normally distributed random variable and both approaches use the same linearization of the LSF at the design point $\mathbf{u}^*$ (see Chapter 2 and [33]) Since the LSF is almost linear, there is hardly a difference between the linearization of the LSF at the slightly different design points $\mathbf{u}^*$. Because α_3 can only be obtained from a full analysis (including U_3), the omission factor approach will usually be based on an estimate of α_3 [56]. Therefore, the effect of a 10% error on α_3 is analyzed as well. The method works as follows:

1. perform an inverse FORM analysis based on (3.41)
2. determine the sensitivity factor: $\alpha_3 = u_3/\beta$
3. modify α_3 by 10% $\rightarrow \tilde{\alpha}_3$
4. calculate the approximate inflated contour level $\tilde{\beta}^*$ from the omission sensitivity factor:
$$\tilde{\beta}^* = \frac{\beta}{\sqrt{1-\tilde{\alpha}_3^2}}$$
5. find the approximate RBDC using inverse FORM, with $u_3 = 0$, i.e. $\Theta = \overline{\theta}$, as the omitted variable.

Support Reaction R_B

Figure 3.17 shows $r_{B,q}$ using inverse FORM for the inflated contour level β^* with the results obtained from MCS for $k = 1.01$, $\rho = 0$ and $\overline{\theta} = 0.1$. The inflated contour level becomes quite sensitive to a correct estimate of α_3 when α_3 becomes rather large, say for COV > 0.1 (see Table 3.6). It may be interesting to point out that $\beta = 3.72$ corresponds to an exceedance probability $q = 10^{-4}$, $\beta^* = 5.67$ to $q = 7.2 \times 10^{-9}$, $\tilde{\beta}^*_{-10\%} = 5.07$ to $q = 2.0 \times 10^{-7}$, and $\tilde{\beta}^*_{+10\%} = 6.68$ to $q = 1.2 \times 10^{-11}$.

The ignorance factor for the additive model uncertainty in (3.38) is calculated as well and the result is compared with the inflated contour results. Based on (3.35)

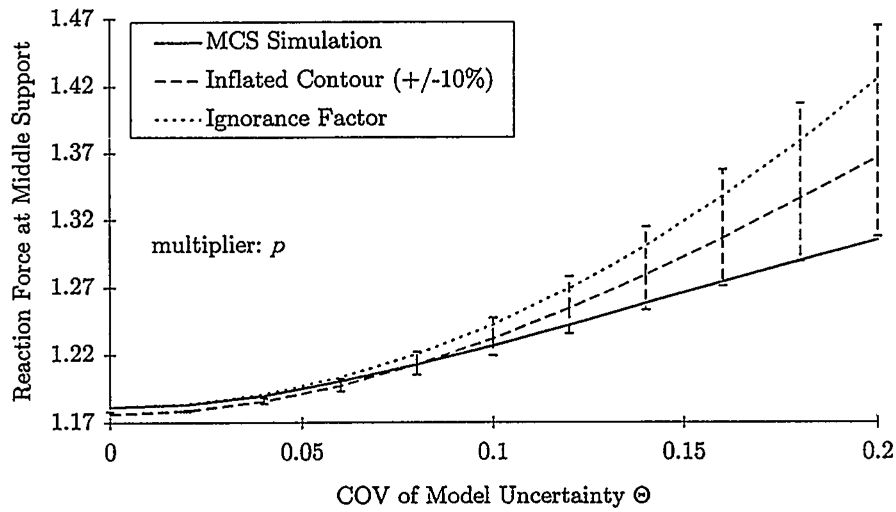

Figure 3.17: Comparison of second moment approximations for $r_{B,q}$ for $k = 1.01$, $\rho = 0$ and $\overline{\theta} = 0.1$

and (3.38), the LSF can be written as:

$$g(\mathbf{P}, \Theta) = r_{B,q} - [h(P_1, P_2) - 6\,p\,\Theta] \tag{3.42}$$

We can now calculate the asymptotic ignorance factor for additive model uncertainty for this LSF [36]:

$$\theta^* \sim \overline{\theta} - \tfrac{1}{2}\sigma_\theta^2 \left[\frac{|\nabla \ell|}{|\nabla g|}\frac{\partial g}{\partial \theta}\right]_{\mathbf{p}^*,\overline{\theta}} \tag{3.43}$$

$$\begin{aligned}
|\nabla \ell| &= \sqrt{\left(\frac{p_1^* - p}{\sigma_{p_1}^2}\right)^2 + \left(\frac{p_2^* - p}{\sigma_{p_2}^2}\right)^2} = \frac{37.5422}{p} && (3.44)\\
|\nabla g| &= \tfrac{1}{2}\sqrt{\left(3\xi_{\max}^* - \xi_{\max}^{*^3}\right)^2 + \left(2 - 3\xi_{\max}^{*^2} + \xi_{\max}^{*^3}\right)^2} = 0.9723 && (3.45)\\
\frac{\partial g}{\partial \theta} &= -6\,p && (3.46)
\end{aligned}$$

COV (%)	α_3	$\tilde{\beta}^*_{-10\%}$	β^*	$\tilde{\beta}^*_{+10\%}$
0	0	3.72	3.72	3.72
5	-0.28	3.84	3.88	3.82
10	-0.50	4.16	4.29	4.45
15	-0.65	4.60	4.92	5.37
20	-0.76	5.07	5.67	6.68

Table 3.6: Inflated contour level β^* for $r_{B,q}$ using approximate second moment methods

$$\sigma_\theta = \overline{\theta}\,\mathrm{COV}(\Theta) = 0.1\,\mathrm{COV}(\Theta) \tag{3.47}$$

Substituting (3.44) to (3.47) in (3.43), the following asymptotic result is obtained:

$$\theta^* - \overline{\theta} \sim 1.158\,[\mathrm{COV}(\Theta)]^2 \tag{3.48}$$

The model uncertainty in (3.38) or (3.42) is now fixed at the ignorance factor level θ^* instead of the mean $\overline{\theta}$ and the RBDC are determined in the two-dimensional $\mathbf{u}(u_1, u_2)$-space. Maes [36] proves that the value for $r_{B,q}$, resulting from this analysis, is a second order approximation for the true value of $r_{B,q}$ around $\Theta = \overline{\theta}$. The graph supports this finding.

It can be concluded that both approaches are equally valuable. Even though inverse FORM using the "exact" second moment inflated contour seems more accurate, it has to be considered that this "exact" second moment sensitivity factor α is generally not available. The α-value must then be estimated [56]. The ignorance factors, however, can be obtained exactly from the reduced analysis results (where $\Theta = \overline{\theta}$).

Support Moment M_B

Figure 3.18 shows the RBDC for the bending moment at the support M_B using inverse FORM for the inflated contour level β^* with the results obtained from MCS for $k = 1.01$, $\rho = 0$ and $\overline{\theta} = 0.01$. Even though the average magnitude of the model error is now a lot smaller, it is observed that this model error Θ gradually dominates the problem as its COV increases ($|\alpha_3|$ approaches 1). Since the lognormal distribution for the model error becomes skewer and skewer with increasing COV, the second moment approximation for the model error (which has zero skewness) deteriorates. As a result, the inverse FORM method using inflated contour levels can not accurately account for the model uncertainty.

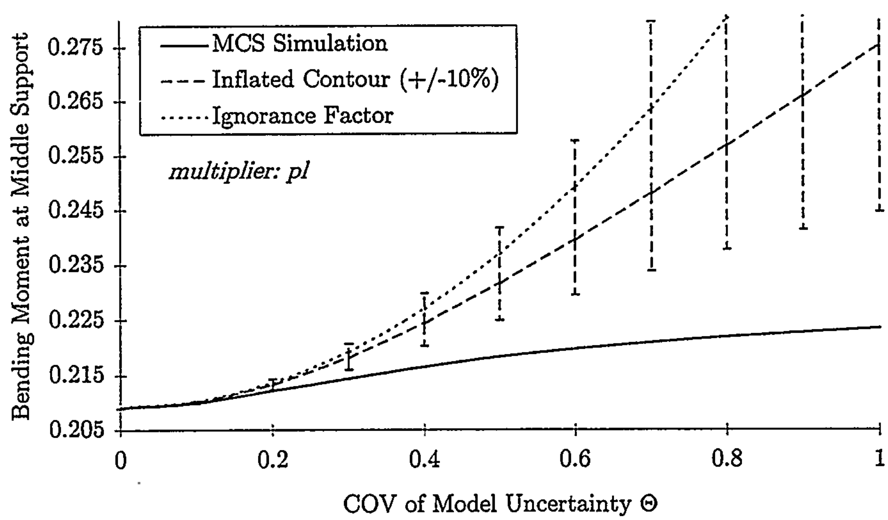

Figure 3.18: Comparison of second moment approximations for $m_{B,q}$ for $k = 1.01$, $\rho = 0$ and $\overline{\theta} = 0.01$

It is again observed that the ignorance factor approach yields a second-order approximation for the true response level $m_{B,q}$ around $\Theta = \overline{\theta}$.

As long as the model error COV is not excessively large (say less than 0.5), both

COV (%)	α_3	$\tilde{\beta}^*_{-10\%}$	β^*	$\tilde{\beta}^*_{+10\%}$
0	0	3.72	3.72	3.72
20	-0.39	3.97	4.04	4.12
40	-0.65	4.57	4.87	5.28
60	-0.78	5.26	6.00	7.37
80	-0.86	5.88	7.30	11.53
100	-0.90	6.39	8.69	34.23

Table 3.7: Inflated contour level β^* for $m_{B,q}$ using approximate second moment methods

approaches yield equally accurate results. For larger values of the COV, the α_3-values clearly indicate that these approximate solution methods can not work any longer since the model error which is excluded from the analysis obviously governs the problem. Consequently, a 10% variation of α_3 yields useless estimates for β^* (see Table 3.7) and the response level $m_{B,q}$ (error bars on Figure 3.18).

3.6 Summary

In this chapter the performance of the various methods and techniques described in Chapter 2 are compared and evaluated by means of an application, taken from structural analysis. RBDC for the design of a two-span continuous beam, subject to two moving loads, are developed for three responses: middle support reaction force, support bending moment and mid-span deflection.

In this problem the inverse FORM and MLL methods yield almost identical results since the limit state function (in the standard normal **u**-space) is almost linear. The inverse FORM method is computationally more efficient since it automatically yields the critical response y_q as well. When MLL is used, the response is obtained through simulation.

It is demonstrated that an omission sensitivity factor and an ignorance factor approach yield equally valuable results when model uncertainty is present. These shortcut, approximate, procedures are compared with "exact" results for a lognormal model error Θ.

It is shown that an ignorance factor approach yields a second-order approximation for the critical response around $\Theta = \overline{\theta}$. In this example, their performance is found to be satisfactory as long as the COV of the model uncertainty does not exceed 0.2.

In this example, it is observed that an inflated contour approach based on the model uncertainty sensitivity factor α, yields good results too as long as $|\alpha_\Theta| < 0.4$, i.e. when the model uncertainty does not govern the problem. This is in agreement with results reported by Winterstein [56]. An estimate for α, within 10% of the exact sensitivity factor α, is sufficiently accurate in this particular example.

Chapter 4

Application To Ocean Wave Modeling

4.1 Introduction

In this example, RBDC for an extreme wave crest height Y are determined. The input environmental parameters are the significant wave height H_s and the peak spectral period T_P. This example is of practical interest since Y determines the deck level of a fixed offshore structure which is required to avoid wave impact loading. The data for this problem are taken from Winterstein *et al.* [56].

First, the extreme wave crest height Y is replaced by its median value $y_{0.5}$ and the critical response is determined for return periods of 10, 100 and 1000 years. Then, an "exact" solution, assuming Poisson upcrossings for Y, is computed. Finally, the approximate methods accounting for model uncertainty (inflated contours and ignorance factor) are compared with this exact result.

4.2 Problem Formulation

4.2.1 Definitions

In ocean wave modeling the term "wave height" is used for the vertical distance between a crest and the preceding trough (Figure 4.1). The "crest height" is defined as the vertical distance between a crest , i.e. wave maximum, and the mean water level. In the zero-crossing method, the time T_Z between two consecutive zero up-crossings of the wave is defined as the zero (up-)crossing wave period [42].

From these definitions, it is clear that the crest height is a more meaningful design parameter than the wave height for fixed, bottom-founded offshore structures [27].

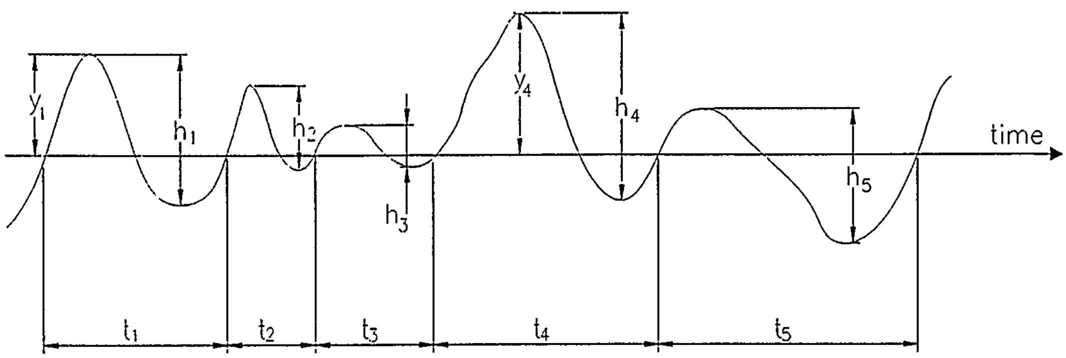

Figure 4.1: Definition of wave height h, crest height y, and zero-crossing period t

The platform deck elevation must be selected on the basis of a "maximum" crest elevation.

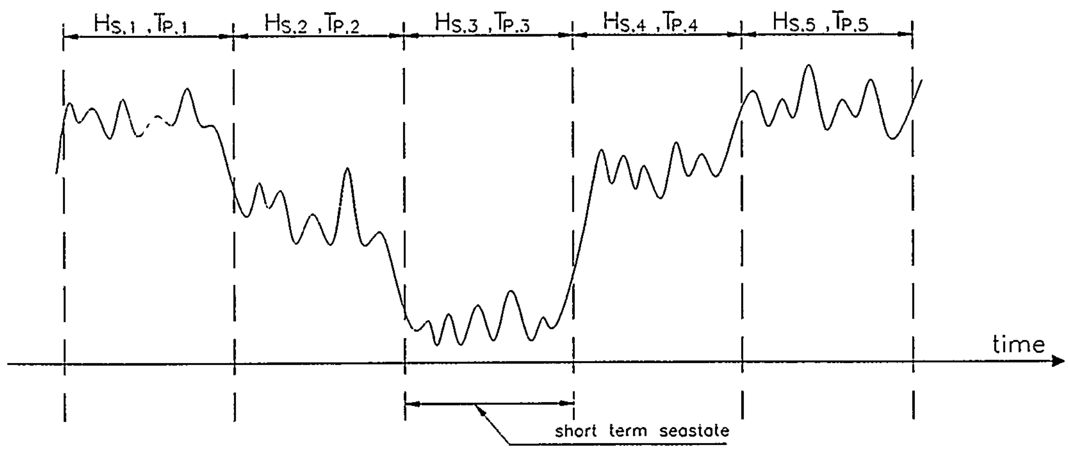

Figure 4.2: Long term modeling as a series of stationary, short term seastates

Long term predictions are modeled as a series of stationary seastates in which the seastate parameters are constant (see Figure 4.2). The stochastic process theory gives the distribution of the crest height of a wave conditional upon the seastate under the following assumptions [45]:

1. Ocean waves are taken to be a wide sense stationary, zero mean, ergodic,

Gaussian process

2. Wave spectral density functions are narrow banded
3. Wave crest maxima are statistically independent
4. The statistical properties of ocean waves are homogeneous, i.e. independent of the local position

4.2.2 Wave Climate Description

For short term periods, the wave elevation $y(t)$ can be described as a realization of a zero mean stationary Gaussian process. Consequently, this process is completely described by the spectral density function $S_{yy}(\omega)$ which is the Fourier transform of the autocorrelation function $R(\tau)$ [44]:

$$S_{yy}(\omega) = \int_{-\infty}^{+\infty} R(\tau) e^{-j\omega\tau} d\tau \tag{4.1}$$

where $j = \sqrt{-1}$, ω denotes the frequency and τ the time difference. The autocorrelation function of the $y(t)$ is defined as:

$$R(\tau) = \mathrm{E}\left[y(t+\tau)\, y(t)\right] \tag{4.2}$$

For long term predictions, this model is extended over a series of stationary seastates which are parameterized by the significant wave height H_S (in meter) and the peak spectral period T_P (in seconds). The significant wave height is defined as the average of the highest one-third of the waves. The spectral peak period is the period T_P corresponding to the frequency ω where $S_{yy}(\omega)$ is maximal.

The wave climate model considered is this application was developed by Haver and Nyhus for the North Sea [21], [22]. For the northern part of the North Sea they suggest the following Weibull distribution for H_S:

$$\Pr(H_S < h_S) = F_{H_S}(h_S) = 1 - \exp\left\{-\left(\frac{h_S}{2.822}\right)^{1.547}\right\} \tag{4.3}$$

A lognormal distribution is used for T_P, conditional upon the value for H_S. Its parameters are:

$$\begin{aligned} \mathrm{E}\left(\ln\left(T_P\right)|h_S\right) &= 1.59 + 0.42\ln\left(h_S + 2\right) && (4.4) \\ \mathrm{Var}\left(\ln\left(T_P\right)|h_S\right) &= 0.005 + 0.085\exp\left(-0.13\, h_S^{1.34}\right) && (4.5) \end{aligned}$$

For the JONSWAP wave spectrum, which is most commonly used for the North Sea, the average zero up-crossing period is approximately given as:

$$T_Z \simeq T_P\left(1 - 0.29\,\gamma^{-0.22}\right) \tag{4.6}$$

where γ is the peak factor of the JONSWAP spectrum [9].

4.2.3 Maximum Crest Height Prediction

For a short term seastate, the relative frequency of large crest heights Y is modeled by the Rayleigh distribution when a narrow band spectrum is assumed. The CDF is:

$$F_{Y|h_S}(y) = 1 - \exp\left\{-8\left(\frac{y}{h_S}\right)^2\right\} \tag{4.7}$$

Y-upcrossings of a high level y can be accurately described by a Poisson process since they are rare events. The expected number of waves in one seastate with duration T_{SS} is Tss/Tz. Consequently, the CDF of Y over the full seastate is then

$$\Pr(Y \;>\; y) = \exp\left\{-\left(\frac{T_{SS}}{T_Z}\right)\left[1 - F_{Y|h_S}(y)\right]\right\}$$

$$= \exp\left\{-\left(\tfrac{T_{SS}}{T_Z}\right)\exp\left[-8\left(\tfrac{y}{h_S}\right)^2\right]\right\} \tag{4.8}$$

Using 3 hour seastates and a peak factor $\gamma = 3.3$ in the JONSWAP wave spectrum, the following result is obtained for the up-crossing problem:

$$\Pr(Y > y|t_P, h_S) = \exp\left\{-\left(\tfrac{13899.8}{t_P}\right)\exp\left[-8\left(\tfrac{y}{h_S}\right)^2\right]\right\} \tag{4.9}$$

4.2.4 Solution Approach

Winterstein *et al.* [56] break the extreme crest height determination up in 2 steps:

1. ignore the uncertainty on Y, given the seastate parameters H_S and T_P. This is achieved by using the median response level $y_{0.5}$ from (4.9) for H_S and T_P corresponding to the required reliability level, i.e. return period.

2. compensate for the uncertainty in Y, by selecting H_S and T_P, corresponding to a higher reliability than required such that the median response $y_{0.5}$ for these new H_S and T_P values equals the correct value y_q.

4.3 Median Extreme Crest Height

4.3.1 RBDC Using Inverse FORM

The median extreme crest height $Y_{0.5}$ is found by setting (4.9) equal to 0.5:

$$Y_{0.5}\left(H_S, T_P\right) = H_S\sqrt{\frac{\ln\left(\frac{20053.2}{T_P}\right)}{8}} \tag{4.10}$$

The different steps of the inverse FORM method are:

1. Determine the reliability index β for the different risk levels. For this purpose the return period n must be formulated in terms of the exceedance probability

q for a 3-hour seastate. Since there is 2920 3-hour seastates in a year

$$q = 1 - \sqrt[2920]{1 - \tfrac{1}{n}} \tag{4.11}$$

where $1/n$ is the annual exceedance probability corresponding to a return period n. Finally, we obtain the following expression for β:

$$\beta = -\Phi^{-1}\left(1 - \sqrt[2920]{1 - \tfrac{1}{n}}\right) \tag{4.12}$$

2. Transform the standard normal vector $\mathbf{U}$ to the original basic variable space, e.g. using an inverse Rosenblatt-transformation:

$$\begin{cases} H_S = F_{H_S}^{-1}\left(\Phi\left(U_1\right)\right) \\ T_P = F_{T_P|h_S}^{-1}\left(\Phi\left(U_2\right)|h_S\right) \end{cases} \tag{4.13}$$

whence

$$\begin{cases} H_S = 2.822\ \sqrt[1.547]{-\ln(1-\Phi(U_1))} \\ T_P = \exp\left\{\mathrm{E}(\ln(T_P)|h_S) + U_2\sqrt{\mathrm{Var}(\ln(T_P)|h_S)}\right\} \end{cases} \tag{4.14}$$

3. Solve the inverse FORM problem:

$$\begin{aligned} &\text{Find } y_{0.5} = \max\left[h_S(\mathbf{u})\sqrt{\frac{\ln\left(\frac{20053.2}{t_P(\mathbf{u})}\right)}{8}}\right] \\ &\text{subject to } |\mathbf{u}| = \beta = -\Phi^{-1}(q) \end{aligned} \tag{4.15}$$

The results obtained by Winterstein *et al.* [56] for (4.15) for return periods of 10, 100 and 1000 years are given in Table 4.1.

Return Period n [yr]	$y_{0.5,q}$ [m]	h_S^* [m]	t_P^* [s]
10	12.1	12.69	15.05
100	13.7	14.51	15.80
1000	15.2	16.18	16.46

Table 4.1: Inverse FORM results for the median extreme crest height $y_{0.5}$

4.3.2 RBDC Using Maximum Likelihood

Determination Of The Critical Response Level

When using the MLL method for RBDC development the critical response level $y_{0.5,q}$, corresponding to the median extreme crest height for a return period n, must be known beforehand. This level can be determined exactly from the distribution for $Y_{0.5}$. Consider the PDF for H_S and $T_P|h_S$; from (4.3), (4.4) and (4.5) follows:

$$\begin{aligned} f_{H_S}(h_S) &= \tfrac{1.547}{2.822}\left(\tfrac{h_S}{2.822}\right)^{0.547}\exp\left\{-\left(\tfrac{h_S}{2.822}\right)^{1.547}\right\} && (4.16)\\ f_{T_P|H_S}(t_P|h_S) &= \tfrac{1}{\sqrt{2\pi}\,\sigma_{\ln(T_P)|h_S}\,t_P}\exp\left\{-\tfrac{1}{2}\left(\tfrac{\ln(t_P)-\mathrm{E}(\ln(T_P)|h_S)}{\sigma_{\ln(T_P)|h_S}}\right)^2\right\} && (4.17)\end{aligned}$$

Now, the distribution for $Y_{0.5}$ is determined from the joint density for H_S and T_P:

$$f_{H_S,T_P}(h_S,t_P) = f_{H_S}(h_S)\, f_{T_P|H_S}(t_P|h_S) \tag{4.18}$$

Consider the transformation:

$$\begin{cases} x_1 = y_{0.5} = h_S\sqrt{\dfrac{\ln\left(\frac{20053.2}{t_P}\right)}{8}} \\ x_2 = h_S \end{cases} \tag{4.19}$$

The joint density f_{X_1,X_2} is then given by (see [23]):

$$f_{X_1,X_2}(x_1, x_2) = f_{X_2}(x_2)\, f_{X_1|X_2}(x_1|x_2)\; |J| \tag{4.20}$$

where $|J|$ is the Jacobian of the transformation (4.19):

$$J = \begin{vmatrix} \frac{\partial h_S}{\partial x_1} & \frac{\partial h_S}{\partial x_2} \\ \frac{\partial t_P}{\partial x_1} & \frac{\partial t_P}{\partial x_2} \end{vmatrix} = 320850.72 \left(\tfrac{x_1}{x_2^2}\right) \exp\left\{-2\left(\tfrac{2x_1}{x_2}\right)^2\right\} \tag{4.21}$$

This exceedance probability q is:

$$q = \int_0^{\infty} dx_2 \int_{y_{0.5,q}}^{\infty} f_{X_2}(x_2)\, f_{X_1|X_2}(x_1|x_2)\; |J|\, dx_1 \tag{4.22}$$

This density function is plotted in Figure 4.3 and indicates that solution of (4.22) by numerical integration is not straightforward. Since the integrand is almost a spike function, the integration domain and quadrature rule must be carefully selected on a case by case basis. Therefore, evaluation of small failure probabilities by common integration rules is to be avoided in general. The integration error easily amounts to the order of magnitude of the failure probability.

After substitution of (4.11) in (4.22), the critical response $y_{0.5,q}$ can be determined as function of the return period n. This was done using three different methods: direct numerical evaluation using Newton-Côtes integration, using Breitung's Second-Order asymptotic probability integral approximations [6] and using Asymptotic Importance Sampling [39]. The results are practically identical to the inverse FORM critical response levels and listed in Table 4.2.

RBDC Development

The RBDC development using the MLL method can now be applied:

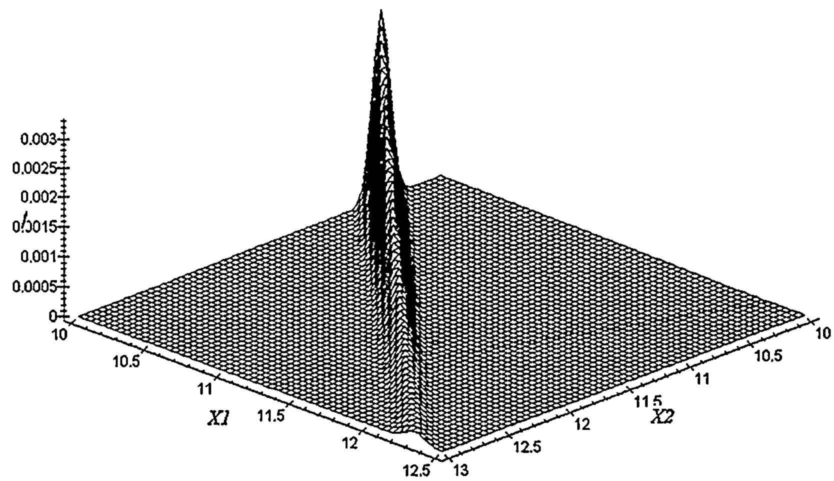

Figure 4.3: Joint density plot for $f_{X_1,X_2}(x_1,x_2) = f_{Y_{0.5},H_S}(y_{0.5},h_S)$

1. The critical response levels $y_{0.5,q}$ are known and given in Table 4.2.

2. From the joint PDF (4.18), the log-likelihood function is determined:

$$\begin{aligned}\ell\left(h_S,t_P\right) &= 0.547\ln(h_S) - \left(\tfrac{h_S}{2.822}\right)^{1.547} - \ln\left(\sigma_{\ln(T_P|h_S)}\right) - \ln(t_P) \\ &\quad -\tfrac{1}{2}\left(\tfrac{\ln(t_P)-\mathrm{E}(\ln(T_P|h_S))}{\sigma_{\ln(T_P|h_S)}}\right)^2 + \text{constants}\end{aligned} \tag{4.23}$$

Return Period n [yr]	Newton-Côtes	SO-Asymptotic	AIS
10	11.99	12.00	12.03
100	13.74	13.75	13.70
1000	15.25	15.26	15.24

Table 4.2: Estimation of median extreme crest height $y_{0.5,q}$ using different methods

Return Period n [yr]	y_q [m]	h_S^* [m]	t_P^* [s]
10	12.03	12.68	14.95
100	13.70	14.49	15.70
1000	15.24	16.16	16.34

Table 4.3: RBDC results using the MLL-method for the median extreme crest height $y_{0.5}$

3. The solution (h_S^*, t_P^*) to the problem

$$\begin{aligned} &\max \ell(h_S, t_P) = \ln\left(f_{H_S,T_P}(h_S, t_P)\right) = (4.23) \\ &\text{subject to } h_S\sqrt{\frac{\ln\left(\frac{20053.2}{t_P}\right)}{8}} = y_{0.5,q} \end{aligned} \tag{4.24}$$

represents the most likely combination of the environmental input variables, yielding the critical response.

The resulting RBDC are given for the various return periods in Table 4.3. The results are almost identical to the inverse FORM solution.

4.3.3 Comparison Of Inverse FORM And MLL

Both RBDC development methods are conceptually different. This is illustrated in Figure 4.4 Inverse FORM searches for the maximum response $y_{0.5,\max}$ along the transformed U-contour. The MLL method searches for the PML along the iso-response line $y_{0.5} = y_{0.5,q}$.

In this case, the transformed U-contour lines and the iso-loglikelihood contours are no longer identical. Recall that the U-contour connects all points with joint occurrence equal to $q = \Phi(-\beta)$, while the iso-loglikelihood line is a line of equal probability density.

At the RBDC combination the iso-response line is tangent to the transformed U-

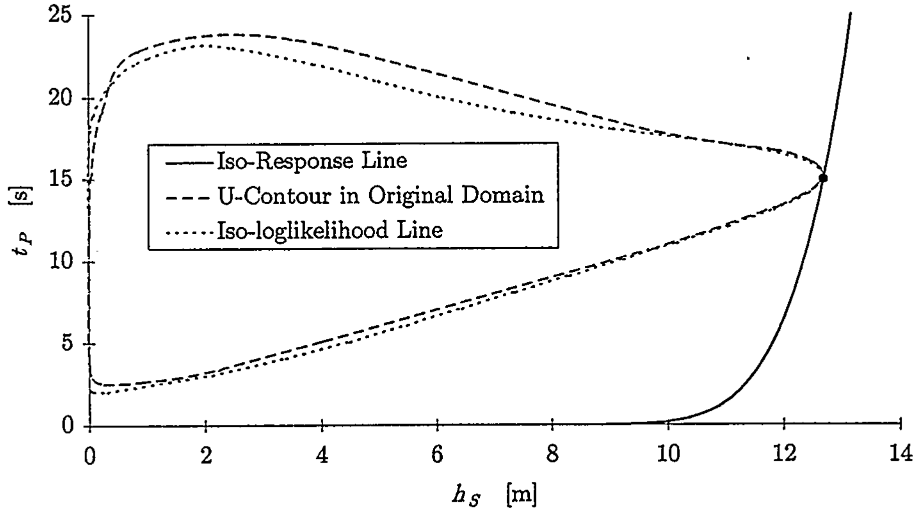

Figure 4.4: Comparison of Inverse FORM and Maximum Likelihood Method to find the RBDC

contour, since it represents the maximum response along this contour line. At this point the iso-loglikelihood contour is tangent to this response line, since it represents the maximum loglikelihood along this response line. Consequently, the gradient of the transformed U-contour and of the log-likelihood function coincide at the PML.

4.4 Maximum Extreme Wave Crest Height

4.4.1 Exact Solutions

General

So far, the uncertainty on the maximum crest height Y, given h_S and t_P, has been ignored. Using the upcrossings result (4.9), an exact solution can be obtained. Figure 4.5 shows the distribution for Y, given h_S^* and t_P^*, i.e. h_S and t_P at the PML of the simplified analysis when Y is replaced by the median $y_{0.5}$, for the three return periods of interest. The plots show increasing scatter for the response Y as the return period

n increases. Consequently, it is expected that the differences between the maximum extreme wave height y_q and the median extreme wave height $y_{0.5,q}$ will increase with the return period n.

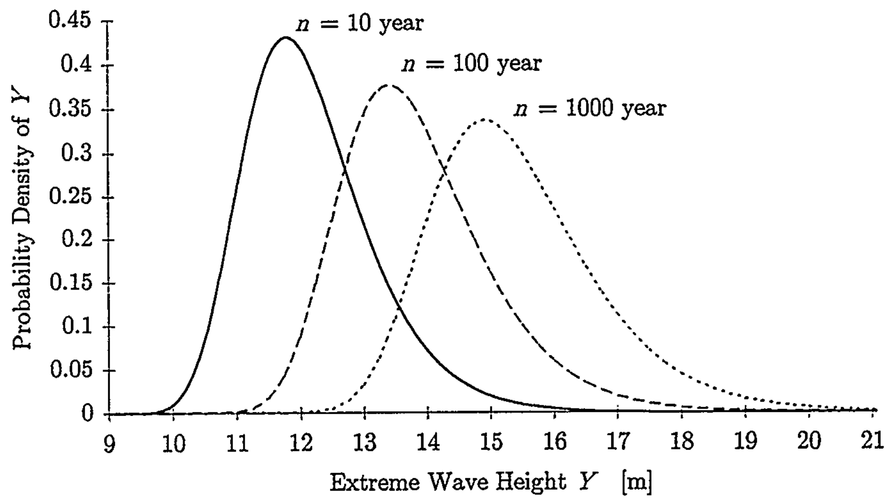

Figure 4.5: PDF of response Y, conditional upon h_S^* and t_P^*

RBDC Using Inverse FORM

When Y is considered a third random variable of the problem, an inverse FORM yields the RBDC results given in Table 4.4. The omission sensitivity factor $\alpha_Y = u_Y^*/\beta$ is listed as well. α_Y^2 indicates the fraction of the total uncertainty caused by the uncertainty on Y. Since α_Y increases with the return period n, the difference between y_q and $y_{0.5,q}$ increases (see Figure 4.6). This is expected since the scatter on Y increases for higher return periods (see Figure 4.5). It is to be noted that the values for h_S^* and t_P^* are now consistently lower than for the median extreme wave height.

Return Period n [yr]	β	y_q [m]	h_S^* [m]	t_P^* [s]	α_Y
10	3.97	12.78	11.83	14.76	0.36
100	4.50	14.86	13.21	15.36	0.40
1000	4.97	16.87	14.40	15.85	0.44

Table 4.4: Inverse FORM results for the maximum extreme crest height

Return Period n [yr]	q	y_q [m]	h_S^* [m]	t_P^* [s]
10	3.61×10^{-5}	12.82	12.06	14.68
100	3.44×10^{-6}	14.85	13.38	15.26
1000	3.43×10^{-7}	16.75	14.45	15.71

Table 4.5: RBDC results for the maximum extreme crest height using the MLL method

RBDC Using Maximum Likelihood

The exact maximum extreme wave crest height y_q for a particular return period n is now found as the solution of:

$$\Pr(Y > y_q) = \int_{y_q}^{\infty} dy \int_0^{\infty} dt_P \int_0^{\infty} f_{Y|H_S,T_P}(y)\ f_{T_P|H_S}(t_P)\ f_{H_S}(h_S)\, dh_S = q \quad (4.25)$$

where q is the exceedance probability per seastate corresponding to the return period n (4.11). The values for y_q and the input parameters h_S^* and t_P^* resulting from the RBDC development for the various return periods are estimated using MCS and listed in Table 4.5. Figure 4.6 shows that these results are practically identical to the inverse FORM solution.

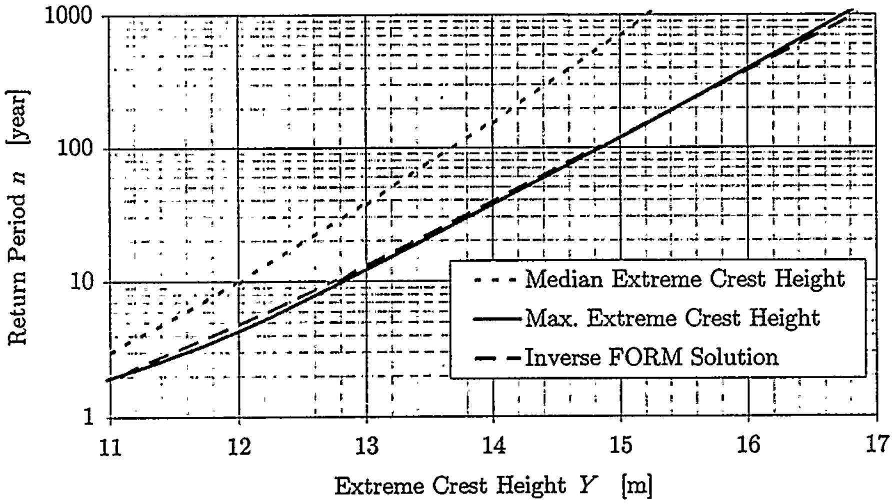

Figure 4.6: Median and Maximum Extreme Wave Crest Height

4.4.2 Second Moment Approximations

Inverse FORM Results

Winterstein *et al.* [56] approximate the real PDF $f_{Y|H_S,T_P}(y)$, shown in Figure 4.5, by

$$Y(H_S, T_P, \Theta) = y_{0.5} + \Theta \tag{4.26}$$

where Θ is a normal distribution with mean $\overline{\theta} = 0$. The standard deviation of Θ is readily obtained as the second moment of the actual PDF $f_{Y|h_S,t_P}(y)$ about $y_{0.5}$. It is important to note that this normal "model uncertainty" distribution actually depends on the PML and the PMLs are different for the various return period (see Tables 4.1, 4.3 and Figure 4.5).

For this normal approximation, the maximum extreme wave height for the three return periods is estimated using MAIS [39]. For this purpose the program MAIS was modified to allow for conditional sampling. The COV on the MAIS results is less than 0.3%. The obtained maximum extreme crest heights are shown in Figure 4.7.

Winterstein *et al.* [56] used an inverse FORM approach to determine these maximum extreme crest heights; their results are practically identical to the AIS results (see Table 4.7).

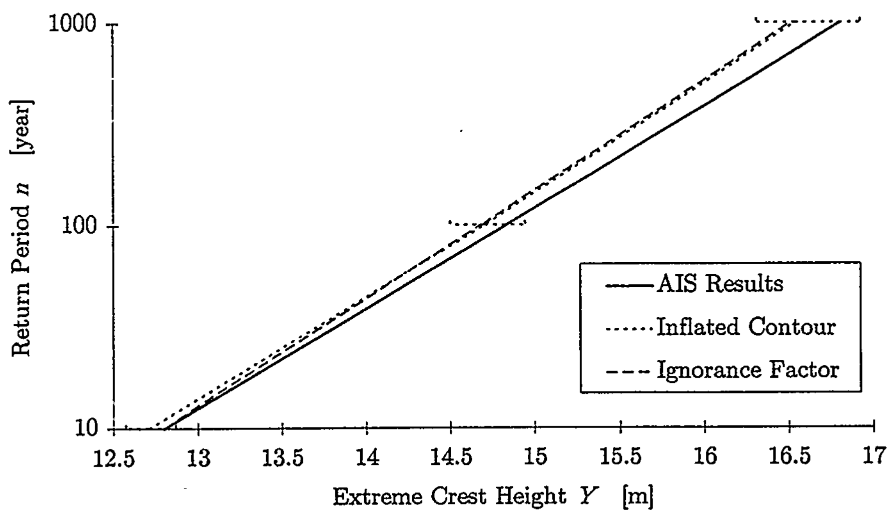

Figure 4.7: Second Moment Approximations for Θ

Table 4.6 shows the impact of replacing the exact distribution for Y, given $y_{0.5}$, by the normal approximation Θ. It may be concluded that the normal approximation is justified in this case. Because the model uncertainty is not too important (α_Y is relatively small), a central modeling is sufficiently accurate. Since the sensitivity factors α_Y are slightly higher for the actual distribution than for the normal approximation Θ, the resulting critical responses y_q are a bit higher as well.

Return Period n	Exact Distribution for Y α_Y^2	β^*	β^*/β	y_q	Normal Approx. Θ α_Y^2	β^*	β^*/β	y_q
10	0.13	4.25	1.07	12.78	0.10	4.19	1.05	12.69
100	0.16	4.91	1.09	14.86	0.12	4.81	1.07	14.67
1000	0.19	5.53	1.11	16.87	0.14	5.37	1.08	16.54

Table 4.6: Comparison of Inverse FORM solutions using the exact distribution for $Y|h_S, t_P$ and the normal approximation Θ

Inflated Contours

Unlike the previous example, the inverse FORM results for the full problem, including Y, no longer coincide with the ones obtained from an inflated contour approach using the exact omission sensitivity factor. This can be understood as follows. The "model uncertainty", i.e. the standard normal Θ, now depends on the basic variables in the simplified problem, H_S and T_P in this case. Consequently, the design point $\mathbf{u}^* = \left(u^*_{H_S}, u^*_{T_P}\right)$, or its equivalent in the original variable domain, the PML (h^*_S, t^*_P) will be different for both cases. As a result, the LSF will be linearized in a different point. Depending on how much the PMLs differ for both cases and how non-linear the LSF is near those PMLs, the inverse FORM and inflated contour results will differ more or less. Typically, the PMLs will be close to each other, at least when the model uncertainty is not too important. As a consequence, the difference between the two results will generally be small for not too non-linear LSF.

The exact sensitivity factor α is usually not available, unless a full analysis is performed. Winterstein *et al.* [56] acknowledge this problem and suggest a reasonable range for α^2 for offshore structures: $0.05 - 0.25$, and most commonly $0.1 - 0.2$. Here, the exact α-value was modified by $\pm 10\%$, similar to the procedure used in the previous example. The consequence of replacing β^* by this modified $\tilde{\beta}^*$ on the maximum extreme wave height response y_q is shown as the horizontal error bars in

Return Period n	MAIS	Inv. FORM	β^*	$\widetilde{\beta}^*_{-10\%}$	$\widetilde{\beta}^*_{+10\%}$	Ign. Fact.
10	12.80	12.69	12.71	12.57	12.87	12.80
100	14.83	14.67	14.70	14.50	14.94	14.69
1000	16.80	16.54	16.54	16.31	16.92	16.52

Table 4.7: Comparison of estimate for y_q using various approximate second moment formulations

Figure 4.7 and in Table 4.7.

Ignorance Factors

The ignorance factor approach suggested by Maes [36] avoids the estimation of omission or sensitivity factors. This (multiplicative) ignorance factor can be derived from the simplified analysis results, i.e. where the maximum extreme crest height Y is replaced by its median value $Y_{0.5}$. Multiplication of the critical response obtained from the simplified analysis by this ignorance factor compensates for the model uncertainty, i.e. yields an second moment estimate for the actual critical response. His results are presented in Figure 4.7 as well for comparison.

4.5 Summary

In this chapter a wave forecasting RBDC problem is analyzed. The practical case of the determination of the maximum extreme crest height is studied. An exact solution for the problem is obtained and compared with an approach where the uncertainty on the crest height, given the sea state parameters H_S and T_P, is approximated by a normally distributed variable Θ.

In this particular example the t_P^*-values for the RBDC are always close the conditional median value of $T_P|h_S$. As a matter of fact, the formula (4.10) suggests that the n-year extreme crest values $Y_{0.5}$ will essentially be produced by the n-year

H_S. This is typically the case for gravity dominated phenomena while for dynamic phenomena the wave period becomes more important and the values for t_P^* will be different from the conditional median of $T_P|h_S$. It is a conceptual advantage from the Inverse FORM method that the same (h_S, t_P)-contours can be used for other responses as well. This allows, at least theoretically, for an uncoupling of the environmental modeling and the structural design process.

The first-order estimate of the critical response is very accurate. It can be shown that the limit state function in the standard normal space is almost linear near the design point $\mathbf{u}^*$.

It is also shown that model uncertainty can successfully be accounted for by a second moment formulation (inflated contours or ignorance factors) as long as the sensitivity factor α for the model uncertainty is not too large. An estimate for α within 10% of the exact sensitivity factor seems to be sufficiently accurate for this purpose.

Chapter 5

Application To A Marine Drilling Riser

5.1 Introduction

In this third application, a deep-sea drilling riser, located in the Gulf of Mexico, is studied. The input variables are the significant wave height H_s and the sea current velocity $\mathbf{V}$. The critical response is the angle ω between the riser and the vertical at the bottom of the riser. This angle is of practical interest since it limits the drilling operability: as the angle increases, the friction between the drill and the pipe becomes more and more important. This critical ω_q is determined from a separate response analysis of hindcast storm data.

The goal is to identify the most likely sets as well as some other practical design combinations of the environmental variables which produce the extreme response with the specified return period. Three return period levels are studied: 10, 100 and 200 years [25], [38].

5.2 Drilling Risers

Floating structures are economically attractive for deep water drilling and production. A marine riser is essentially a conductor pipe, connecting the floating platform and the bore hole (see Figure 5.1). An excellent description of marine risers can be found in [49]. At the top, the riser pipe ends at a telescopic joint beneath the vessel. This slip joint allows change in riser length as the vessel heaves or moves laterally. The operability of drilling risers is expressed in terms of maximum angles from the vertical. To increase the riser stiffness, and thus limit these angles, tensioning de-

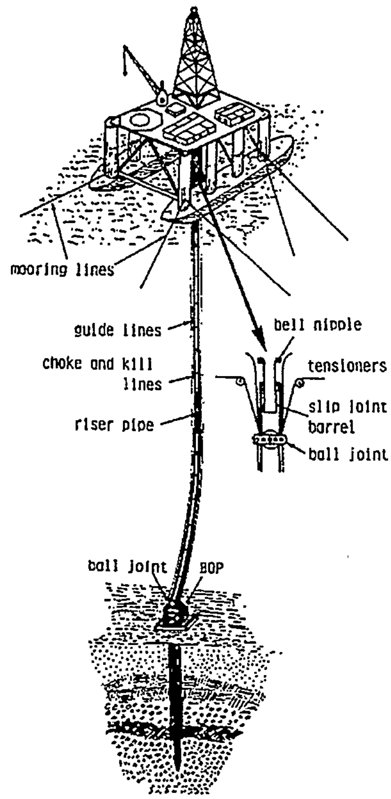

Figure 5.1: Schematic of a drilling riser [49]

vices are installed at the top joint. Buoyancy devices may be added to limit the maximum tension in the riser pipe. For deep-water conditions, dynamic positioning of the vessel considerably improves the drilling operability and reduces the required tension [10], [16].

5.3 Riser Model

5.3.1 General

This section describes the structural analysis model for the riser. The riser is modeled as a 3D tensioned string. Since, for reasons of practical design, the RBDC must be

Section	Distance above well head	c_d	d	Specific Weight (riser+mud)
1	> 0 m	0.5	1.118 m	64.3 kg/m
2	> 594.4 m	0.5	1.143 m	69.2 kg/m
3	> 914.4 m	0.5	1.086 m	73.0 kg/m
4	> 1371.6 m	0.5	1.067 m	76.8 kg/m
5	> 2286 m	0.0	0.473 m	713.2 kg/m

Table 5.1: Assumed riser characteristics

two-dimensional, this 3D model is reduced to an equivalent 2D model, which gives the same bottom angle ω as the 3D model for the equivalent 2D current pattern.

5.3.2 Riser Specification

The riser specifications in this case study are taken from [40] and are listed in Table 5.1. The drag coefficient is denoted as c_d and d stands for the riser (drag-)diameter. The operating tension t_{eff} at the bottom of the riser is fixed at 450 kN ($\simeq$ 100 kips). The buoyancy rate is assumed to vary with the water depth from 98% up to 99.5%.

5.3.3 Metocean Data

The riser is assumed to be located at the grid point: latitude 27.08, longitude 88.42 in the Gulf of Mexico. All storms in the Gulf of Mexico starting 1900 were hindcast [20]. The current data were taken from the central portion of the model for the Gulf of Mexico. Two data sets are available:

1. Hourly data for the significant wave height h_S during each storm period

2. Current velocities $\mathbf{v}$ in x- and y-direction at 9 different water depths: 5, 17.5, 37.5, 75, 137.5, 212.5, 525, 1200 and 2000 meter. In this model these velocities are assumed to be constant in each range.

5.3.4 Rig Offset

The rig offset is the horizontal distance from the well head and the rig position. Here they are taken to be identical to the "Jack Bates" rig offsets [10] with an intact mooring system and 60% thruster assist. These offsets are given as a function of the significant wave height h_S through the Response Amplitude Operators (RAO) of the rig. The total offset os, i.e. the sum of the mean offset, surge and slow drift, for these conditions is given as:

$$\begin{aligned} h_S \leq 1.5 \text{ m:} \quad & os = 0.05 \text{ m} \\ h_S > 1.5 \text{ m:} \quad & os = \max\{4.5, 7.835\, h_S - 20\} \end{aligned} \tag{5.1}$$

5.3.5 3D Riser Analysis

The riser is modeled as a tensioned string. The model used in this case study is the 3D extension of a model described by Garrett [17]. The riser bending stiffness is assumed to be negligible though. The 3D equilibrium equation of a tensioned string is (small angle assumption):

$$(t_{eff}\; u_i')' = -q_i \tag{5.2}$$

where t_{eff} is the effective tension in the riser, u the component in x- or y-direction of the lateral riser displacement, $q = \frac{1}{2}\rho_{\text{sea water}} c_d\, d\, v\; |v|$ the distributed load on the riser, c_d the drag coefficient, d the drag diameter, and v the current velocity. A prime denotes differentiation with respect to distance along the vertical z-axis.

For simplicity, consider the distance s along the riser to be measured positive from the bottom of the riser. The top is then at $s = L$.

As a result, the following integral expressions can be derived for the riser angle at the bottom [38]:

$$\begin{cases} \omega_x = u_x'(0) = \dfrac{u_x(L) + \displaystyle\int_0^L \left(\frac{\int_0^z \frac{1}{2}\rho_{\text{sea water}}\, c_d(\varsigma)\, d(\varsigma)\, v_x(\varsigma)\, |v_x(\varsigma)|\, d\varsigma}{t_{eff}(z)} \right) dz}{\displaystyle\int_0^L \frac{t_{eff}(0)}{t_{eff}(z)} dz} \\ \omega_y = u_y'(0) = \dfrac{u_y(L) + \displaystyle\int_0^L \left(\frac{\int_0^z \frac{1}{2}\rho_{\text{sea water}}\, c_d(\varsigma)\, d(\varsigma)\, v_y(\varsigma)\, |v_y(\varsigma)|\, d\varsigma}{t_{eff}(z)} \right) dz}{\displaystyle\int_0^L \frac{t_{eff}(0)}{t_{eff}(z)} dz} \end{cases} \tag{5.3}$$

For a 3D analysis (bi-planar motion), this integration has to be performed in both the x- and y-directions. This implies that the rig offset $u(L)$ must be known in these directions. Due to lack of more detailed information, it is assumed, however, that the offsets are aligned with the top (sea surface) current. This is justified for this current profile [26]. The total angular response ω and the orientation φ of the plane in which the response angle is maximal, can be determined from the projected responses (5.3).

The 3D analysis results are now reduced to one single plane. This is done by projecting currents and rig offset onto the plane of the total response angle ω in such a way that the projected offsets are always positive (the response angles, however, can be either positive or negative). The 2D reduction is considered necessary since the resulting design criteria will have to be formulated in two dimensions for practical design purposes. In general, the loads associated with the projected rig offset and current profile v_φ, will not yield exactly the same response angle in 2D as in 3D. Consequently, the projected offset has to be rescaled, while keeping the projected currents $v_{1,\varphi}, \ldots, v_{9,\varphi}$ constant, to come up with the same in-plane response as in the three dimensional analysis. After rescaling, the $h_{S,\varphi}$ value corresponding to the projected and rescaled offset is determined from the h_S-offset relation (5.1). In this particular case the required rescaling is usually negligible, say less than 0.5%. However, if the angle between the plane of the response angle and the plane containing the top current is large, the required correction may be important.

If both top and bottom angles are considered, this operation is to be performed separately for each response. Since the rescaling factor will generally be different for the top and the bottom angle, the analysis results in two data sets for $h_{S,\varphi}$ and projected currents $\mathbf{v}_\varphi$; a first one for the top angle and another one for the bottom angle response [38]. Here, only the bottom response is analyzed. Since the subsequent analysis is entirely two-dimensional, the subscript φ will be omitted. The rescaled significant wave height is denoted as h_S while $\mathbf{v}$ stands for the current velocity vector, projected on the plane of the bottom angular response.

5.4 Metocean Probabilistic Modeling

5.4.1 General

Several joint probability models for waves and currents have been proposed. Most of them are to some extent restrained by the use of the Rosenblatt transformation. In these models the joint PDF is defined as a marginal distribution and a series of conditional density functions. The advantage of this approach is that one environmental parameter, like H_S in this case, dominates the loading so that errors in the conditional models are not critical.

An alternative approach was recently used by Prince-Wright [47]. He argues there is no theoretical method for selecting the variable for the marginal distribution and suggests to transform all basic variables into a near-normal vector. Uncorrelated standard normal variates then result from a diagonalization of the variance-covariance matrix.

This avoids the computationally expensive Rosenblatt-transformation but may affect the tail behavior of the dominating variable(s).

Since the wave height clearly is the dominating variable in this application, a conditional model will be set up. H_S is selected as the marginal distribution and the currents are modeled conditional upon H_S.

5.4.2 Significant Wave Height H_S

Storm Occurrences

The approach is to analyze storm events using a generalized extreme value distribution. The storm occurrences are modeled as a Poisson process and combined with the conditional distribution of the peak significant wave height, given a storm event, to describe the annual maximum significant wave height distribution.

During the 89 year period (1900-1988) for which data are available, 38 severe storm events are observed. The expected value of the occurrence rate in the Poisson process is then $\nu = \frac{38}{89} = 0.427$ storms per year.

Due to limited availability of data, statistical uncertainty is associated with the estimate for ν. This mean value is only one possible estimator for the occurrence rate. Least squares estimation, assuming a Poisson process, yields an average of 0.451 storms per year. In a Bayesian approach to include this uncertainty, a (Gamma) distribution is assigned to the occurrence rate V (uppercase ν), which is now a considered as a random variable. Since a Gamma distribution is a conjugate prior for Poisson observations, the posterior distribution is also Gamma [11]. This posterior distribution for V can subsequently be used to assess the uncertainty associated with the design criteria. This issue is not further pursued here.

Distribution For The H_S Storm-Maxima

The distribution of the H_S storm peaks, given the occurrence of a storm, is determined by fitting a GEVD through the h_S-storm maxima, i.e. the maximum of H_S

in each storm. The three parameter GEVD has the following CDF [7]:

$$F_X(x|c,\lambda,\delta) = \exp\left\{-\left[1+c\left(\frac{x-\lambda}{\delta}\right)\right]^{-1/c}\right\} \tag{5.4}$$

These parameters are estimated using least squares minimization in a Gumbel plot, which is shown in Figure 5.2. The parameter estimates are given in Figure 5.2 as well. Since $c > 0$, the extreme value distribution is of the Frechet-type.

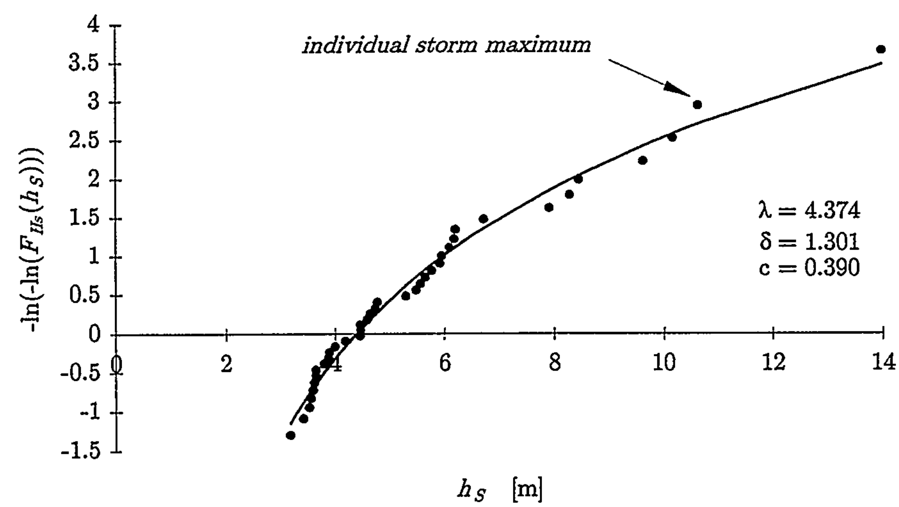

Figure 5.2: GEVD fitted to the H_S-storm maxima in a Gumbel-plot

The n-Year Return Period H_S-Values

The h_S-value corresponding to a return period of n years results from the combination of the occurrence rate and intensity distribution. Compounding the Poisson and the GEVD yields the CDF for the H_S-annual maxima:

$$F_{H_S}(h_S) = \exp\left\{-\nu\left(1-\exp\left\{-\left[1+c\left(\frac{h_S-\lambda}{\delta}\right)\right]^{-1/c}\right\}\right)\right\} \tag{5.5}$$

Return Period n [year]	h_S [m]
10	6.49
100	15.37
200	19.88

Table 5.2: Significant wave height h_S for different return periods

	C_1	C_2	C_3	C_4	C_5	C_6	C_7	C_8	C_9
a_i	56	84	88	34	0	-3	-3	-3	-3
b_i	585	123	207	-114	2	6	5	5	5

Table 5.3: Regression coefficients (multiplied by 1000)

The h_S-values corresponding to the three return periods of interest are given in Table 5.2.

5.4.3 Current Modeling

The top current velocity V_1 is plotted as a function of h_S in Figure 5.3. It can be concluded that, even though the average current velocity is almost invariant with respect to h_S, the variance of V_1 increases considerably with h_S. The same trend is observed for the other current velocities [38]. In order to stabilize the variance, the currents are divided by h_S. A linear regression between h_S and $\frac{v_i}{h_S}$ is made; the formula for the remaining "residual conditional current" C_i is:

$$c_i = \frac{v_i}{h_S} - (a_i\, h_S + b_i) \tag{5.6}$$

For all currents the values for the slope a_i and intercept b_i are determined from the over 1200 hourly current data and are listed in Table 5.3. The resulting model for every V_i is conditional upon the value of H_S. It can be seen from Figure 5.4 that the

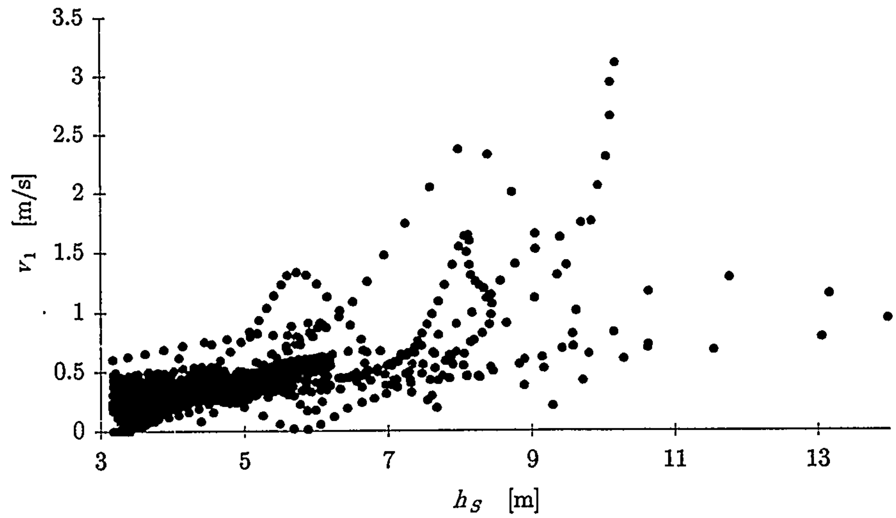

Figure 5.3: Top current velocity v_1 as a function of the significant wave height h_S

variance of C_1 is a lot more stable than for V_1. These "residual conditional current" C_i are now assumed to be zero mean jointly normal distributed random variables. The experimental CDF for the normalized marginal density of C_1 is shown in Figure 5.5 and compared with the standard normal CDF. The quality of the fit is satisfactory over the range $[-2, 2]$. The standard deviation σ, the skewness κ_1 and kurtosis κ_2 (second, third and fourth moment) for all marginal densities are listed in Table 5.4. If the distribution for the "residual conditional currents" C_i would be perfectly joint normal, the skewness and kurtosis would be 0 and 3 respectively for all marginal and partial joint distributions. Even though this is not the case, the result is found to be satisfactory, except for the tail region. The kurtosis-value, which is a measure for the "peakedness" of the distribution is too high, resulting in tails which are much longer than for the normal distribution.

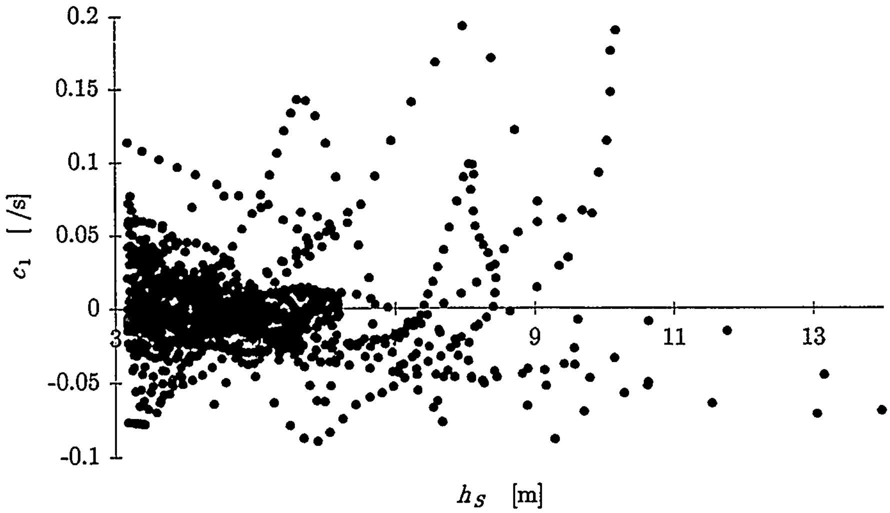

Figure 5.4: Top residual current c_1 as a function of the significant wave height h_S

	C_1	C_2	C_3	C_4	C_5	C_6	C_7	C_8	C_9
σ	0.034	0.031	0.028	0.022	0.007	0.002	0.002	0.002	0.002
κ_1	1.219	1.357	1.659	2.194	3.151	-1.42	-1.72	-1.73	-1.81
κ_2	7.788	7.330	4.151	10.60	42.46	9.859	11.03	11.13	12.39

Table 5.4: Standard deviation, skewness and kurtosis for the marginal current distributions

5.5 Reponse Modeling

In the present application, it is observed that peak responses are always associated with large storm events. In addition, the joint distribution of $\mathbf{C}$ does not depend on H_S, i.e. the residual currents distribution does not on depend on whether H_S is extreme or not. This justifies the choice of the joint point-in-time density for the

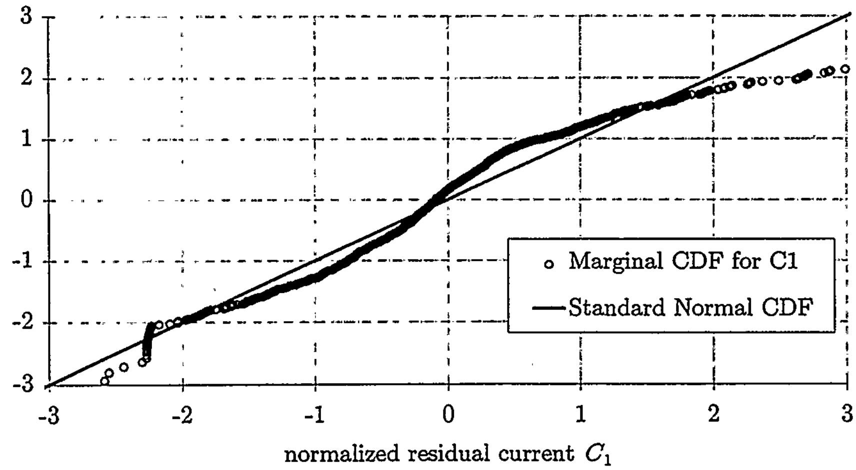

Figure 5.5: Experimental and Normal CDF for C_1 on standard normal scale

current velocities $\mathbf{V}$. The model is then as follows:

$$f_{H_S,\mathbf{V}}(h_S,\mathbf{v}) = f_{H_S}(h_S) f_{\mathbf{V}|H_S}(\mathbf{v},h_S) \tag{5.7}$$

The total log-likelihood function is then:

$$\ell_{H_S,\mathbf{V}}(h_S,\mathbf{v}) = \ell_{H_S}(h_S) + \ell_{\mathbf{V}|H_S}(\mathbf{v},h_S) \tag{5.8}$$

The log-likelihood for the annual H_S annual storm maxima can be obtained from (5.5) after differentiation:

$$\begin{aligned}\ell_{H_S}(h_S) = -\nu \left(1 - \exp\left\{-\left[1 + c\left(\tfrac{h_S-\lambda}{\delta}\right)\right]^{-1/c}\right\}\right) - \left[1 + c\left(\tfrac{h_S-\lambda}{\delta}\right)\right]^{-1/c} \\ - \left(\tfrac{1}{c} - 1\right)\ln\left[1 + c\left(\tfrac{h_S-\lambda}{\delta}\right)\right] + \text{ constants}\end{aligned} \tag{5.9}$$

Since the residual reduced currents $\mathbf{C}$ are assumed to be jointly normal with zero mean, their joint point-in-time density is given by:

$$f_{\mathbf{C}}(\mathbf{c}) = \frac{1}{(2\pi)^{9/2}\sqrt{\det \mathbf{\Sigma_{CC}}}} \exp\left\{-\tfrac{1}{2}\mathbf{c}^{\mathrm{T}}\,\mathbf{\Sigma}_{\mathbf{CC}}^{-1}\,\mathbf{c}\right\} \tag{5.10}$$

where $\mathbf{\Sigma_{CC}}$ denotes the 9×9 variance-covariance matrix of the residual reduced currents. After substitution of (5.6) in (5.10), the joint PDF of the current velocities $\mathbf{V}$ is obtained:

$$f_{\mathbf{V}|H_\mathrm{S}}(\mathbf{v}, h_S) = \frac{1}{(2\pi)^{9/2}\, h_S\,\sqrt{\det \mathbf{\Sigma_{CC}}}} \exp\left\{-\tfrac{1}{2h_S^2}\,(\mathbf{v}-\overline{\mathbf{v}})^{\mathrm{T}}\;\mathbf{\Sigma}_{\mathbf{CC}}^{-1}\;(\mathbf{v}-\overline{\mathbf{v}})\right\} \tag{5.11}$$

where $\overline{\mathbf{v}}$ is the column vector of the mean values for the current velocities:

$$\overline{\mathbf{v}} = \begin{bmatrix} \cdots \\ a_i\, h_S^2 + b_i\, h_S \\ \cdots \end{bmatrix} \tag{5.12}$$

From (5.11) the log-likelihood function is easily derived:

$$\ell_{\mathbf{V}|H_\mathrm{S}}(\mathbf{v}, h_S) = -\ln h_S - \tfrac{1}{2h_S^2}\,(\mathbf{v}-\overline{\mathbf{v}})^{\mathrm{T}}\;\mathbf{\Sigma}_{\mathbf{CC}}^{-1}\;(\mathbf{v}-\overline{\mathbf{v}}) + \text{ constants} \tag{5.13}$$

Substitution of (5.9) and (5.13) in (5.8) gives the total log-likelihood function.

5.6 RBDC Development

5.6.1 Inverse FORM

The different steps in the inverse FORM method are:

1. Determine the reliability index β for the different design risk levels, where $\beta = -\Phi^{-1}(q)$. The exceedance probabilities and corresponding reliability indices for the three return periods of interest are given in Table 5.5.

Return Period n [year]	Exceedance prob. q	Reliability index β
10	0.1	1.282
100	0.01	2.326
200	0.005	2.576

Table 5.5: Exceedance probabilities and reliability indices for the three return periods

2. Define a transformation $t : \mathbf{X} \rightarrow \mathbf{U}$, where $\mathbf{X}$ is the vector of the basic random variables, i.e. H_S and $\mathbf{V}$. The transformation used here is a Rosenblatt-transformation of the form (2.6):

$$\begin{cases} U_1 = \Phi^{-1}\left(F_{H_S}(H_S)\right) \\ U_i = \Phi^{-1}\left(F_{V_{i-1}|H_S}(V_{i-1}|H_S)\right) \text{ for } i = 2, ..., 10 \end{cases} \tag{5.14}$$

The transformation of the currents velocities $\mathbf{V}$ is greatly simplified here since the residual currents $\mathbf{C}$, are jointly normal with mean equal to $\mathbf{0}$. Since these residual currents are not independent however, they have to be transformed into independent, standard normal variates. Consider the symmetric variance-covariance matrix $\Sigma_{\mathbf{CC}}$:

$$\Sigma_{\mathbf{CC}} = \begin{bmatrix} \mathrm{Var}(C_1) & \mathrm{Covar}(C_1, C_2) & \cdots & \mathrm{Covar}(C_1, C_9) \\ \mathrm{Covar}(C_2, C_1) & & \ddots & \\ \vdots & & & \vdots \\ \mathrm{Covar}(C_9, C_1) & & \cdots & \mathrm{Var}(C_9) \end{bmatrix} \tag{5.15}$$

Clearly, a set of jointly normal random variables $\mathbf{Y}$ will be mutually independent if all covariances equal zero, i.e. if their variance-covariance matrix $\Sigma_{\mathbf{YY}}$ is a diagonal matrix. These independent normal variates $\mathbf{Y}$ can be obtained from a transformation [51]:

$$\mathbf{Y} = \mathbf{A}^{\mathrm{T}}\mathbf{C} \tag{5.16}$$

where $\mathbf{A}$ is an orthogonal matrix with column vectors equal to the orthonormal eigenvectors of $\Sigma_{\mathbf{CC}}$. By this transformation:

$$\Sigma_{\mathbf{YY}} = \begin{bmatrix} \mathrm{Var}(Y_1) & 0 & \cdots & 0 \\ 0 & & \ddots & \\ \vdots & & & \vdots \\ 0 & & \cdots & \mathrm{Var}(Y_9) \end{bmatrix} \tag{5.17}$$

where the non-zero diagonal elements in $\Sigma_{\mathbf{YY}}$ are given by the eigenvalues $\lambda_1, \ldots, \lambda_9$ of $\Sigma_{\mathbf{CC}}$. Dividing each of those independent normal variates Y_i by their standard deviation $\sqrt{\lambda_i}$ gives the corresponding standard normal variate U_{i+1} in the Rosenblatt-transformation (5.14).

3. After back-transformation to the original variable space, the solution $\mathbf{u}^*$ can be found from the constrained optimization problem:

$$\left\{ \begin{array}{l} \text{Find } \omega_q = \max \left[\dfrac{os(\mathbf{u}) + \displaystyle\int_0^L \left(\frac{\int_0^z \frac{1}{2}\rho_{\text{sea water}}\, c_d(\zeta)\, d(\zeta)\, v(\mathbf{u}(\zeta))\, |v(\mathbf{u}(\zeta))|\, d\varsigma}{t_{eff}(z)} \right) dz}{\displaystyle\int_0^L \frac{t_{eff}(0)}{t_{eff}(z)} dz} \right] \\ \text{subject to } \|\mathbf{u}\| = \beta \end{array} \right. \tag{5.18}$$

where os stands for the rescaled rig offset. This gives both the critical response ω_q and the RBDC $(h_S^*, \mathbf{v}^*)$. The results are given in Tables 5.6-5.8 for the three return periods of interest.

		Comb #1	Comb #2	Comb #3	Comb #4	Comb #5	Comb #6
β^*/β		1.00000	6.21832	2.77429	0.99997	2.43977	4.16279
First order β^*-value		1.28155	7.96910	3.55540	1.28151	3.12668	5.33482
Design values	Hs	7.05308	6.49100	7.05375	7.05296	7.01728	6.95944
	Current 1	0.69276	0.26244	0.00000	0.69274	0.99569	1.23413
	Current 2	0.50338	-0.13109	0.00000	0.50347	0.77765	0.99331
	Current 3	0.29254	-0.42562	0.00000	0.29278	0.54464	0.74323
	Current 4	0.08911	-0.41830	0.00000	0.08936	0.28274	0.43644
	Current 5	-0.00017	0.01206	0.00000	-0.00010	0.06417	0.11562
	Current 6	-0.01146	0.08362	0.00000	-0.01152	0.00635	0.02077
	Current 7	-0.01164	0.09022	0.00000	-0.01170	0.00615	0.02054
	Current 8	-0.01166	0.09033	0.00000	-0.01172	0.00614	0.02055
	Current 9	-0.01156	0.09131	0.00000	-0.01162	0.00639	0.02092
Exceedance probabilities	Hs*	0.08104	0.10007	0.08102	0.08104	0.08211	0.08387
	Current 1	0.50000	0.94485	0.99796	0.50000	0.09982	0.00995
	Current 2	0.50019	0.99747	0.98939	0.50000	0.09984	0.00996
	Current 3	0.50051	0.99984	0.92813	0.50000	0.09986	0.00996
	Current 4	0.50066	0.99975	0.72100	0.50000	0.09984	0.00996
	Current 5	0.50050	0.39738	0.49918	0.50000	0.09984	0.00996
	Current 6	0.49841	1.7E-13	0.20359	0.50000	0.09984	0.00996
	Current 7	0.49828	2.8E-15	0.19963	0.50000	0.09985	0.00996
	Current 8	0.49827	2.7E-15	0.19936	0.50000	0.09985	0.00996
	Current 9	0.49819	2.6E-15	0.20341	0.50000	0.09986	0.00996

Hs*	Exceedance probability on an annual basis
Combination #1:	PML, no values fixed
Combination #2:	Fix HS at the 10-year return level (HS=6.491m)
Combination #3:	Fix all currents at zero
Combination #4:	Fix all currents at their average value corresponding to HS
Combination #5:	Fix all currents at their 10% exceedance probability level
Combination #6:	Fix all currents at their 1% exceedance probability level

Table 5.6: Inverse FORM results for $n = 10$ year

		Comb #1	Comb #2	Comb #3	Comb #4	Comb #5	Comb #6
β^*/β		1.00000	1.04353	2.53927	1.00012	1.57533	2.43456
First order β^*-value		2.32634	2.42761	5.90721	2.32662	3.66476	5.66363
Design values	Hs	15.49910	15.37100	15.45218	15.50738	15.06386	14.82758
	Current 1	2.26178	2.26372	0.00000	2.26201	2.82055	3.28691
	Current 2	2.20332	2.17239	0.00000	2.20566	2.68515	3.09400
	Current 3	1.79726	1.74751	0.00000	1.80086	2.23898	2.61317
	Current 4	0.64041	0.59447	0.00000	0.64361	1.02034	1.32775
	Current 5	-0.00428	-0.01542	0.00000	-0.00358	0.13466	0.24335
	Current 6	-0.06671	-0.05063	0.00000	-0.06762	-0.02547	0.00660
	Current 7	-0.06564	-0.04809	0.00000	-0.06663	-0.02463	0.00736
	Current 8	-0.06584	-0.04826	0.00000	-0.06683	-0.02478	0.00724
	Current 9	-0.06415	-0.04614	0.00000	-0.06517	-0.02291	0.00931
Exceedance probabilities	Hs*	0.00978	0.01000	0.00986	0.00976	0.01056	0.01102
	Current 1	0.49872	0.47466	0.99999	0.50000	0.09982	0.00995
	Current 2	0.50008	0.49691	1.00000	0.50000	0.09984	0.00996
	Current 3	0.50136	0.51737	0.99998	0.50000	0.09986	0.00996
	Current 4	0.50288	0.54350	0.97192	0.50000	0.09984	0.00996
	Current 5	0.50255	0.54328	0.48720	0.50000	0.09984	0.00996
	Current 6	0.48910	0.30183	0.01375	0.50000	0.09984	0.00996
	Current 7	0.48798	0.28366	0.01482	0.50000	0.09985	0.00996
	Current 8	0.48797	0.28351	0.01465	0.50000	0.09985	0.00996
	Current 9	0.48768	0.27976	0.01757	0.50000	0.09986	0.00996

Hs*	Exceedance probability on an annual basis
Combination #1:	PML, no values fixed
Combination #2:	Fix HS at the 100-year return level (HS=15.371m)
Combination #3:	Fix all currents at zero
Combination #4:	Fix all currents at their average value corresponding to HS
Combination #5:	Fix all currents at their 10% exceedance probability level
Combination #6:	Fix all currents at their 1% exceedance probability level

Table 5.7: Inverse FORM results for $n = 100$ year

		Comb #1	Comb #2	Comb #3	Comb #4	Comb #5	Comb #6
β^*/β		1.00000	1.00276	2.90712	1.00029	1.48121	2.43078
First order β^*-value		2.57583	2.58295	7.48827	2.57658	3.81534	6.26130
Design values	Hs	19.95577	19.88400	19.80413	19.98726	19.02129	18.43888
	Current 1	3.41312	3.40964	0.00000	3.42011	3.98577	4.62020
	Current 2	3.58242	3.56064	0.00000	3.59322	4.02139	4.54821
	Current 3	3.10016	3.06986	0.00000	3.11138	3.49156	3.96805
	Current 4	1.12961	1.11323	0.00000	1.13491	1.54511	1.97781
	Current 5	-0.00717	-0.00272	0.00000	-0.00690	0.16811	0.33379
	Current 6	-0.11384	-0.10884	0.00000	-0.11605	-0.05646	-0.00421
	Current 7	-0.11149	-0.10603	0.00000	-0.11383	-0.05459	-0.00257
	Current 8	-0.11184	-0.10637	0.00000	-0.11418	-0.05487	-0.00279
	Current 9	-0.10869	-0.10320	0.00000	-0.11106	-0.05167	0.00061
Exceedance probabilities	Hs*	0.00495	0.00500	0.00505	0.00493	0.00563	0.00612
	Current 1	0.49887	0.48899	1.00000	0.50000	0.09982	0.00497
	Current 2	0.49992	0.49793	1.00000	0.50000	0.09984	0.00497
	Current 3	0.50055	0.50518	1.00000	0.50000	0.09986	0.00498
	Current 4	0.50127	0.50818	0.99528	0.50000	0.09984	0.00497
	Current 5	0.50083	0.48850	0.48099	0.50000	0.09984	0.00497
	Current 6	0.48146	0.43964	0.00177	0.50000	0.09984	0.00497
	Current 7	0.48003	0.43335	0.00209	0.50000	0.09985	0.00498
	Current 8	0.48002	0.43329	0.00204	0.50000	0.09985	0.00498
	Current 9	0.47980	0.43307	0.00282	0.50000	0.09986	0.00498

Hs*	Exceedance probability on an annual basis
Combination #1:	PML, no values fixed
Combination #2:	Fix HS at the 200-year exceedance level (HS=19.884m)
Combination #3:	Fix all currents at zero
Combination #4:	Fix all currents at their average value corresponding to HS
Combination #5:	Fix all currents at their 10% exceedance probability level
Combination #6:	Fix all currents at their 1% exceedance probability level

Table 5.8: Inverse FORM results for $n = 200$ year

5.6.2 MLL Method

Extreme Response

In this method the extreme response ω_q must be determined first. The time series for the response ω is generated from the time series for h_S and v. This involves the solution of the differential equation (5.2) using the integration scheme (5.3). Now, the critical responses corresponding to return periods of 10, 100 and 200 year are determined from an extreme value analysis on these time series using a similar procedure as for the significant wave height h_S. The occurrence rate of a storm is the same: $\nu = 0.427$ storms/year. The intensity distribution for the response storm maxima is a GEVD as before. The Gumbel-plot and the GEVD-parameters are shown in Figure 5.6. The n-year critical responses are listed in Table 5.9.

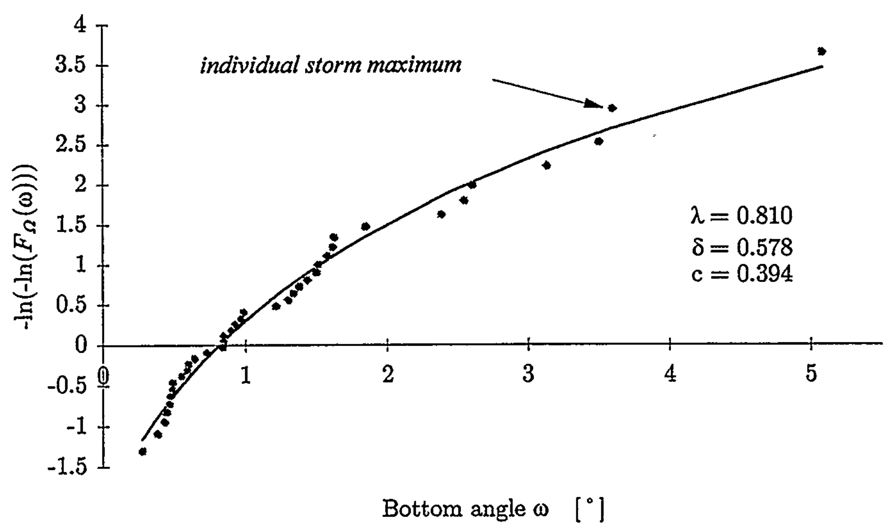

Figure 5.6: GEVD fitted to the ω-storm maxima in a Gumbel-plot

Return Period n [year]	Critical response ω [°]
10	1.7552
100	5.7458
200	7.7872

Table 5.9: Bottom angular response ω for different return periods

RBDC Development

When the MLL method is used to derive the RBDC, the calculations can be structured as follows:

1. The critical response level ω_q is known for the three return periods of interest and given in Table 5.9.

2. The log-likelihood function of the joint PDF of H_S and $\mathbf{V}$ is given in (5.8).

3. The RBDC are given as the solution $(h_S^*, \mathbf{v}^*)$ to the problem:

$$\begin{cases} \max \ell_{H_S,\mathbf{V}}(h_S, \mathbf{v}) = \ell_{H_S}(h_S) + \ell_{\mathbf{V}|H_S}(\mathbf{v}, h_S) \\ \text{subject to } \dfrac{os(h_S) + \displaystyle\int_0^L \frac{\int_0^z \frac{1}{2}\rho_{\text{sea water}}\, c_d(\zeta)\, d(\zeta)\, v(\zeta)\, |v(\zeta)|\, d\varsigma}{t_{eff}(z)} dz}{\displaystyle\int_0^L \frac{t_{eff}(0)}{t_{eff}(z)} dz} = \omega_q \end{cases} \tag{5.19}$$

where $os(h_S)$ is defined in (5.1).

The resulting RBDC are given for all three return periods in Tables 5.10-5.12. It may be concluded that, except for the 10-year return period, the results are practically identical. The difference between both methods for the 10-year return period, is entirely due to a difference in critical response ω_q. The structure of the solution is the same: h_S is the governing variable and the current velocities $\mathbf{v}$ are almost at their mean level. In the inverse FORM solution both ω_q and h_S^* correspond to a return period of 12.5 year, when determined from the respective GEVDs.

		Comb #1	Comb #2	Comb #3	Comb #4	Comb #5	Comb #6
Relative likelihood		1.00000	0.93317	0.00471	0.02160	0.01723	1.53E-06
˜ Log-likelihood		-4.01431	-4.08348	-9.37136	-7.84929	-8.07542	-17.40565
Design values	Hs	6.49554	6.49100	6.49667	6.49569	6.46721	6.41695
	Current1	0.61800	0.65380	0.00000	0.61761	0.89736	1.11790
	Current2	0.43347	0.45868	0.00000	0.43335	0.68670	0.88638
	Current3	0.23761	0.25177	0.00000	0.23770	0.47040	0.65430
	Current4	0.06980	0.07267	0.00000	0.06996	0.24832	0.39032
	Current5	0.00005	0.00005	0.00000	0.00000	0.05919	0.10662
	Current6	-0.00935	-0.00669	0.00000	-0.00944	0.00699	0.02025
	Current7	-0.00954	-0.00635	0.00000	-0.00964	0.00677	0.02001
	Current8	-0.00956	-0.00635	0.00000	-0.00966	0.00676	0.02002
	Current9	-0.00951	-0.00619	0.00000	-0.00961	0.00696	0.02032
Exceedance probabilities	Hs*	0.09990	0.10007	0.09985	0.09989	0.10100	0.10298
	Current1	0.49926	0.43416	0.99728	0.50000	0.10000	0.01000
	Current2	0.49973	0.44877	0.98436	0.50000	0.10000	0.01000
	Current3	0.50017	0.46864	0.90128	0.50000	0.10000	0.01000
	Current4	0.50043	0.49187	0.69076	0.50000	0.10000	0.01000
	Current5	0.49957	0.49957	0.49998	0.50000	0.10000	0.01000
	Current6	0.49719	0.41534	0.23037	0.50000	0.10000	0.01000
	Current7	0.49686	0.39864	0.22525	0.50000	0.10000	0.01000
	Current8	0.49685	0.39844	0.22503	0.50000	0.10000	0.01000
	Current9	0.49683	0.39584	0.22820	0.50000	0.10000	0.01000

Hs*	Exceedance probability on an annual basis
Combination #1:	PML, no values fixed
Combination #2:	Fix HS at the 10-year return level (HS=6.491m)
Combination #3:	Fix all currents at zero
Combination #4:	Fix all currents at their average value corresponding to HS
Combination #5:	Fix all currents at their 10% exceedance probability level
Combination #6:	Fix all currents at their 1% exceedance probability level

Table 5.10: MLL results for $n = 10$ year

		Comb #1	Comb #2	Comb #3	Comb #4	Comb #5	Comb #6
Relative likelihood		1.00000	0.81432	3.81E-07	0.99718	0.01936	1.79E-06
˜ Log-likelihood		-8.00460	-8.21001	-22.78565	-8.00742	-11.94912	-21.23635
Design values	Hs	15.50109	15.37100	15.46376	15.51917	15.07483	14.83821
	Current 1	2.26594	2.33651	0.00000	2.26476	2.82300	3.28919
	Current 2	2.20465	2.23254	0.00000	2.20887	2.68806	3.09676
	Current 3	1.79675	1.79804	0.00000	1.80385	2.24172	2.61581
	Current 4	0.64010	0.64102	0.00000	0.64472	1.02135	1.32871
	Current 5	-0.00240	0.01167	0.00000	-0.00358	0.13466	0.24334
	Current 6	-0.06579	-0.05158	0.00000	-0.06773	-0.02557	0.00650
	Current 7	-0.06461	-0.04884	0.00000	-0.06674	-0.02472	0.00727
	Current 8	-0.06481	-0.04899	0.00000	-0.06694	-0.02488	0.00715
	Current 9	-0.06313	-0.04715	0.00000	-0.06528	-0.02300	0.00923
Exceedance probabilities	Hs*	0.00977	0.01000	0.00984	0.00974	0.01054	0.01100
	Current 1	0.49594	0.41996	0.99999	0.50000	0.10000	0.01000
	Current 2	0.49942	0.44668	1.00000	0.50000	0.10000	0.01000
	Current 3	0.50228	0.47122	0.99998	0.50000	0.10000	0.01000
	Current 4	0.50347	0.48774	0.97204	0.50000	0.10000	0.01000
	Current 5	0.49578	0.44506	0.48718	0.50000	0.10000	0.01000
	Current 6	0.47676	0.31286	0.01368	0.50000	0.10000	0.01000
	Current 7	0.47432	0.29205	0.01476	0.50000	0.10000	0.01000
	Current 8	0.47430	0.29180	0.01458	0.50000	0.10000	0.01000
	Current 9	0.47421	0.29097	0.01750	0.50000	0.10000	0.01000

Hs*	Exceedance probability on an annual basis
Combination #1:	PML, no values fixed
Combination #2:	Fix HS at the 100-year return level (HS=15.371m)
Combination #3:	Fix all currents at zero
Combination #4:	Fix all currents at their average value corresponding to HS
Combination #5:	Fix all currents at their 10% exceedance probability level
Combination #6:	Fix all currents at their 1% exceedance probability level

Table 5.11: MLL results for $n = 100$ year

		Comb #1	Comb #2	Comb #3	Comb #4	Comb #5	Comb #6
Relative likelihood		1.00000	0.82630	9.13E-12	0.99133	0.02132	2.08E-06
˜ Log-likelihood		-9.25389	-9.44469	-34.67318	-9.26260	-13.10200	-22.33729
Design values	Hs	20.17101	19.88440	20.05093	20.24506	19.24167	18.73153
	Current1	3.48551	3.50837	0.00000	3.49363	4.05516	4.56322
	Current2	3.65983	3.61796	0.00000	3.68330	4.10296	4.52045
	Current3	3.16873	3.09647	0.00000	3.19758	3.56899	3.94581
	Current4	1.15412	1.12094	0.00000	1.16735	1.57710	1.92606
	Current5	-0.00241	0.01219	0.00000	-0.00712	0.16983	0.30533
	Current6	-0.11420	-0.09395	0.00000	-0.11923	-0.05851	-0.01532
	Current7	-0.11155	-0.08939	0.00000	-0.11692	-0.05658	-0.01358
	Current8	-0.11190	-0.08970	0.00000	-0.11729	-0.05686	-0.01382
	Current9	-0.10868	-0.08631	0.00000	-0.11407	-0.05358	-0.01039
Exceedance probabilities	Hs*	0.00481	0.00500	0.00489	0.00477	0.00546	0.00587
	Current1	0.49244	0.43149	1.00000	0.50000	0.10000	0.01000
	Current2	0.49839	0.46096	1.00000	0.50000	0.10000	0.01000
	Current3	0.50277	0.48647	1.00000	0.50000	0.10000	0.01000
	Current4	0.50353	0.50107	0.99579	0.50000	0.10000	0.01000
	Current5	0.48715	0.44678	0.48064	0.50000	0.10000	0.01000
	Current6	0.45877	0.29735	0.00155	0.50000	0.10000	0.01000
	Current7	0.45503	0.27651	0.00184	0.50000	0.10000	0.01000
	Current8	0.45499	0.27627	0.00180	0.50000	0.10000	0.01000
	Current9	0.45515	0.27551	0.00251	0.50000	0.10000	0.01000

Hs*	Exceedance probability on an annual basis
Combination #1:	PML, no values fixed
Combination #2:	Fix HS at the 200-year exceedance level (HS=19.884m)
Combination #3:	Fix all currents at zero
Combination #4:	Fix all currents at their average value corresponding to HS
Combination #5:	Fix all currents at their 10% exceedance probability level
Combination #6:	Fix all currents at their 1% exceedance probability level

Table 5.12: MLL results for $n = 200$ year

5.7 Alternative RBDC

5.7.1 General

In this section, other than "most likely" design combinations are determined. For practical design purposes, one may wish to fix one or more environmental design parameters. The objective is to determine the most likely combination of the remaining environmental parameters, when these fixed values and ω_q are given. For both methods and the three return periods of interest, several alternative design combinations are determined. They can be divided into three categories:

1. Fix H_S at the n-year return level
2. Fix $\mathbf{V}$ at $\mathbf{0}$
3. Fix $\mathbf{V}$ at a chosen marginal exceedance probability level

In the following, the procedure is outlined for both RBDC methods. The results are given in Tables 5.6-5.8 and Tables 5.10-5.12 for the inverse FORM and the MLL method respectively.

5.7.2 Procedure For Forward FORM

When forward FORM is used the most likely design combinations when j parameters are fixed is the solution of the optimization:

$$\begin{cases} \min\left(\|\mathbf{u}\| \mid \mathbf{U}_j = \mathbf{u}_j\right) \\ \text{subject to } \dfrac{os(h_S(\mathbf{u})) + \displaystyle\int_0^L \frac{\int_0^z \frac{1}{2}\rho_{\text{sea water}}\, c_d(\zeta)\, d(\zeta)\, v(\mathbf{u}(\zeta))\, |v(\mathbf{u}(\zeta))|\, d\varsigma}{t_{eff}(z)} dz}{\displaystyle\int_0^L \frac{t_{eff}(0)}{t_{eff}(z)} dz} = \omega_q \end{cases} \tag{5.20}$$

The procedure for the three types of problems is as follows:

1. When H_S is fixed at the n-year return level, the standard normal variate u_1 is easily determined from the GEVD for H_S (5.5) and (5.14a). The optimization (5.20) problem is now reduced to 9 dimensions.

2. When the current velocities $\mathbf{V}$ are fixed at zero, the residual currents $\mathbf{C}$ are determined from (5.6):

$$\mathbf{C} = -\left(\mathbf{a}\, H_S + \mathbf{b}\right) \tag{5.21}$$

   The mutually independent normal variates $\mathbf{Y}$ are found from the transformation (5.16). After scaling of the components of $\mathbf{Y}$ by their standard deviations, given in (5.17), the standard normal $u_i, i = 2, ..., 10$ are obtained. Consequently, the vector equation (5.21) actually adds 9 equations to the optimization problem (5.20) which is formally reduced to a constrained optimization in 1 dimension.

3. When the current velocities $\mathbf{V}$ are fixed at a chosen marginal exceedance probability p, the residual currents c_i are:

$$c_i{=}\Phi^{-1}(p)\, \sigma_{C_i} \tag{5.22}$$

   where σ_{C_i} is the standard deviation of the residual current C_i, and listed in Table 5.4. The actual current velocity v_i is determined from (5.6). Inversion of (5.16) gives y_i from where u_i is easily determined through scaling by the standard deviation $\sigma_{Y_i} = \sqrt{\lambda_i}$ (5.17). Inversion of $\mathbf{A}$ (5.16) is readily obtained since the matrix $\mathbf{A}$ is orthonormal. Consequently, the optimization problem (5.20) is reduced to a constrained optimization in 1 dimension only.

5.7.3 Procedure For The MLL Method

When the MLL method is used, the most likely design combinations when j parameters are fixed is the solution of the constrained optimization problem:

$$\begin{cases} \max \ell_{H_S,\mathbf{V}}\left(h_S, \mathbf{v} \mid \mathbf{X}_j = \mathbf{x}_j\right) \\ \text{subject to } \dfrac{os(h_S) + \displaystyle\int_0^L \frac{\int_0^z \frac{1}{2}\rho_{\text{sea water}}\, c_d(\zeta)\, d(\zeta)\, v(\zeta)\, |v(\zeta)|\, d\varsigma}{t_{eff}(z)} dz}{\displaystyle\int_0^L \frac{t_{eff}(0)}{t_{eff}(z)} dz} = \omega_q \end{cases} \tag{5.23}$$

where $\mathbf{X}_j$ stands for those original variables H_S or V_i which are fixed. Re-arrangement of the equations is avoided. In the MLL method, the dimension of the optimization is directly reduced.

1. The H_S-value corresponding to the n-year return level is readily available from the GEVD (5.5). The dimension of the optimization (5.23) is reduced to 9.

2. When the current velocities $\mathbf{V}$ are fixed at zero, the residual currents $\mathbf{C}$ are determined from (5.21). The optimization is directly reduced to a 1-dimensional problem.

3. When the current velocities $\mathbf{V}$ are fixed at a chosen marginal exceedance probability p, the residual currents c_i are:

$$c_i = \Phi^{-1}(p)\, \sigma_{C_i} \tag{5.24}$$

   where σ_{C_i} is the standard deviation of the residual current C_i, and listed in Table 5.4. The actual current velocity v_i is immediately determined from (5.6). Consequently, the optimization problem (5.23) is reduced to a constrained optimization in 1 dimension only.

5.7.4 Discussion

The MLL method avoids the transformation of the original basic variables to the standard normal space. This results in a more direct algorithm when other than most likely design combinations have to be determined.

Even though the 9 residual currents are assumed jointly normal in the original variable domain, the transformation into mutually independent standard normal variates requires the determination of the eigenvalues and eigenvectors. It must be stressed that this is numerically difficult in this particular application. The condition of the matrix Σ_{CC} is given as the ratio of the largest to the smallest eigenvalue. In this application $\lambda_{\max}/\lambda_{\min} \simeq 32 \times 10^6$, which indicates that 7 digits may be lost in the calculations. When the MLL method is used a matrix inversion is required, which is also prone to round-off error.

As outlined in Chapter 2, the value for β_{n-j} can be interpreted as a measure for the relative occurrence likelihood of the design combination with some fixed parameters compared with the occurrence of the most likely design combination. All design combinations result in the same response level ω_q, with exceedance probability q, however.

When the MLL method is used for this purpose, a relative likelihood of both design combinations is obtained at once. This is a relative probability density, rather than a relative probability.

5.8 Conclusions

Since the current velocities $\mathbf{V}$ are very small over the bottom part of the riser, the significant wave height H_S is the governing variable in this drilling riser application. This results for almost all analyzed cases in a PML (or minimal distance point when inverse FORM is used) where the H_S-exceedance probability level is very close to the one selected for the response angle Ω. The currents are then very close to their mean value.

Only for the 10-year return period, the h_S^*-value obtained from inverse FORM does not correspond to the 10 year return level for H_S. This results in a critical response $\omega_{0.1,InvFORM}$ which is significantly larger than the more accurate value which is obtained directly from an extreme value analysis on the generated time series for Ω. When H_S is fixed at the 10 year return level, the relative likelihood of the design combination yielding this $\omega_{0.1,InvFORM}$ is very small (see Table 5.6). The bottom currents need to be extremely high (marginal exceedance probability almost zero) to compensate for too small an h_S-value in this case.

On the other hand, fixing the currents at their mean level, yields almost the same design combination as at the PML, i.e. for the full optimization problem. This results in relative likelihoods very close to 1.

When the currents are fixed at their 10% level the relative likelihood of this design combination drop to about 1% compared with the PML. If the current velocities are fixed at the 1% exceedance level, this results in relative likelihoods of about 10^{-7}.

5.9 Summary

In this chapter, the performance of the RBDC methods is analyzed for a practical application where data records are available for the basic variables rather than a joint distribution. In this particular application, the LSF is known in algorithmic form only.

When inverse FORM is the used basic variables must be transformed into the standard normal **U**-space. Even though the residual currents **C** are assumed to be jointly normal, the transformation to mutually independent, standard normal variables is delicate. It requires to determine the eigenvalues of the variance-covariance matrix Σ_{CC}. Since the Σ_{CC} is ill-conditioned, this is not possible without numerical difficulty.

When the MML method is used, the actual RBDC development is uncoupled from the determination of the critical response level ω_q. This opens the possibility to determine this response ω_q directly from an extreme value analysis of the generated time series for the response Ω.

For this application, other than most likely design combinations, which result in the same critical response ω_q, are determined as well. Both a FORM and MLL approach to this problem are given and the results are compared. A solution using the MLL method is computationally attractive since the transformation of the basic variables into the standard normal space is avoided.

The relative likelihood of joint occurrences of extreme currents and significant wave height is very low. This indicates that for this application associating the environmental design parameters with the recurrence interval of the response is more appropriate than an extreme event philosophy: there is no need to combine extreme sea states with extreme currents. This is in agreement with results reported by Prince-Wright for combined wave and current loading in TLP design [47].

Chapter 6

Conclusions

6.1 Summary and Conclusions

Chapter 2 describes two, conceptually different methods to develop RBDC. The inverse FORM method maximizes the response along a β-contour surface, i.e. all combinations of input variables with exceedance probability q. These contours are response-independent. The MLL method searches for the most likely point (PML) on the iso-response curve for the response y_q.

The inverse FORM method is exact only for linear limit state functions $g_u(\mathbf{u})$. Additionally, the basic random variables must be transformed into the standard normal space. The MLL method is more versatile, but the critical response level y_q must be determined from a separate analysis.

Chapter 2 also presents approximate, second moment formulations which account for model uncertainty. Use of these techniques avoids the explicit introduction of additional random variables, which would increase the dimension of the problem, to describe them.

The methods are applied and compared in Chapters 3, 4 and 5. In these applications the computational complexity is gradually increased. Only joint normal distributions are used in the moving load problem in Chapter 3. In Chapter 4, a two-dimensional application of practical interest is made. A two-dimensional Rosenblatt-transformation is required for the inverse FORM formulation. Even though the conditional distribution of the currents is joint normal, this transformation becomes computationally involving in the riser application presented in Chapter 5. On the other hand, the critical response level y_q, which is required for the MLL method, can be determined straightaway from an extreme value analysis. The MLL method avoids this computationally expensive Rosenblatt-transformation.

The performance of both the inverse FORM and MLL method for RBDC development in the three applications presented in this thesis is generally satisfactory. Based on the experience gained from the applications, some general conclusions concerning the performance of each method can be drawn:

- The approximation error in the FORM method is mainly due to the linearization $g_L(\mathbf{u})$ of the LSF $g_u(\mathbf{u})$. A first-order approximation $g_L(\mathbf{u})$ of the limit state function $g_u(\mathbf{u})$ may be inaccurate. An example is given in the moving load application (Figure 3.9). Because of the transformation to the standard normal $\mathbf{U}$-space, the degree of non-linearity will usually increase when the original basic variables are non-normally distributed. A first-order approximation of the LSF may then result in an inaccurate estimate for q. However, for RBDC development purposes the error on the critical response y_q is of interest rather than the error on the actual exceedance probability q. It is shown that the error Δy_q is proportional to the error $\Delta \ln q$ rather than Δq. When the slope $L'(y_q)$ (3.33) of the log-exceedance function L at y_q is not too small, a first order estimate of the true exceedance probability may be sufficiently accurate even for a non-linear LSF.

- In the MLL method the actual RBDC development is independent of the method used to compute the critical response level y_q. Consequently, a vast range of more performant methods is available to determine the response level y_q. In the most general case, this level is to be obtained iteratively as the solution of:

$$\int_{g(\mathbf{x},y_q)\leq 0} f_{\mathbf{X}}(\mathbf{x})d\mathbf{x} = q \qquad (6.1)$$

Since y_q is located in the tail of the distribution for the response Y, this equation is best solved in the (L, y)-domain. The MLL method is theoretically exact, but the iterative solution of (6.1) may be computationally expensive.

As a result, the following practical recommendation can be made:

- The inverse FORM method is computationally efficient. An easy way to check its accuracy consists of calculating the RBDC for two different risk levels q_1 and q_2 and plotting the log-exceedance function L. The slope L' is then a measure for the error on the RBDC.

- In some particular applications, however, the critical response level can easily be determined from an extreme value analysis. In this case, the MLL method is a valuable alternative, since the transformation of the basic variables to the standard normal space is avoided.

When modeling uncertainty must be considered in the RBDC development, a second moment formulation is justifiable as long as this model uncertainty does not govern the response.

- Both statistical uncertainty and actual model inexactness can be handled in this way. The second moment formulation provides a convenient format to account for the discrepancies between experimental evidence and model predictions as well. In this way a clear and formal incentive is provided towards designers and code developers to use more accurate models.

- If the inverse FORM method is used an inflated contour level β^* is determined from estimated omission sensitivity factors (2.24). In this method the target reliability index is modified such that the reduced model, which does not account for model uncertainty, yields the correct response.

- Ignorance factors on the other hand change the limit state function such that the reduced model yields the correct target reliability.

- The applications show that both approaches are equally accurate. An ignorance factor is conceptually more appealing since only information from the reduced analysis is required. On the other hand, the omission factors in the standard normal U-space are easier to incorporate in the inverse FORM method.

6.2 Recommendations For Future Research

The applications presented in this thesis clearly show the power of the RBDC. Since the usefulness of this methodology is now established, extensions of this inverse reliability technique to different fields of application are desirable. In addition, more efficient and/or accurate algorithms need to be developed:

RBDC Development For Time-Dependent Problems

The methods used so far are restricted to time-invariant reliability problems, which can be formulated in terms of basic random variables. In a lot of practical applications, the combined effect of several time-dependent load processes can not accurately be described using time-invariant methods.

Consequently, there is a need for an extension of these inverse reliability techniques to time-dependent applications.

RBDC Development In The Original Domain

The performance of the inverse FORM method in the applications considered in this thesis suggests that first-order reliability techniques may be more accurate in their "inverse" than in "forward" direction.

Unfortunately, the transformation to the U-space may become difficult and numerically ill-conditioned when the basic variables are no longer independent. This justifies the development of asymptotic approximations for the evaluation of the probability integral in the original variable domain [5], [18].

Their format should be modified to allow for "inverse" reliability application.

RBDC Development For Structural Systems

In this thesis it is assumed that failure occurs due to violation of one limit state function (LSF) only. This assumption essentially limits the applicability of the methods to structural components. An extension to multiple limit state problems is required to develop RBDC in terms of overall system reliability rather than on the component reliability level.

Efficient Algorithms

In the applications presented here, general purpose optimization routines are used. More efficient algorithms taking advantage from the particular structure of the mathematical inverse reliability program (2.13) are necessary when the problem complexity increases. Two examples for inverse FORM may be found in [14] and [58].

For non-linear LSF the inverse FORM method may be inaccurate. To overcome this limitation a mixed inverse FORM/SORM algorithm is tentatively suggested. SORM is not suited for an inverse reliability formulation since the failure probability estimate does not only depend on the reliability index β but also on the curvature at $\mathbf{u}^*$. The mixed algorithm works as follows:

1. Perform an Inverse FORM computation to find $\mathbf{u}^*_{FORM}$
2. Calculate the main curvatures and find the required correction on the failure probability due to the non-linearity of the LSF $g_u(\mathbf{u})$. Determine the corrected reliability index β^*
3. Find a better estimate for $\mathbf{u}^*$ from an inverse FORM using β^*

The underlying idea is that the main curvatures at the new design point $\mathbf{u}^*$ will not be too much different from the ones at the first order design point $\mathbf{u}^*_{FORM}$. If desired, iteration on steps 2-3 is possible. It is believed, however, that this will not be necessary. As a matter of fact, the idea to correct the reliability index based on a comparison of the first-order probability approximation and a more accurate estimate is not restricted to SORM only. A further generalization includes the use of any method in step 2.

Multiple PML problems can tentatively be handled in the same way, even though there is only a heuristic justification in this case. For multiple PML problems the only method which guarantees to find the exact response level is crude MCS. Combination with the MLL method then results in the RBDC.

Bibliography

[1] API, *Recommended Practice for Planning, Designing and Constructing Tension Leg Platforms (RP2T)*, tech. report, American Petroleum Institute, 1987.

[2] D. Boos, *Using Extreme Value Theory to Estimate Large Percentiles*, Technometrics, 26 (1984), pp. 33–39.

[3] P. Bratley, B. Fox, and L. Schrage, *A Guide to Simulation*, Springer-Verlag, New York, NY, 1983.

[4] K. Breitung, *Asymptotic Approximations for Multinormal Integrals*, ASCE Journal of the Engineering Mechanics Division, 110 (1984), pp. 357–366.

[5] ——, *Probability Approximations By Log-Likelihood Approximation*, ASCE Journal of Engineering Mechanics, 117 (1991), pp. 457–477.

[6] ——, *Asymptotic Approximations for Probability Integrals*, vol. 1592 of Lecture Notes in Mathematics, Springer-Verlag, 1994.

[7] E. Castillo, *Extreme Value Theory in Engineering*, Statistical Modeling and Decision Science, Academic Press, Boston, MA, 1988.

[8] P. Chalk and R. Corotis, *Probability Model for Design Live Loads*, ASCE Journal of the Structural Division, 106 (1980), pp. 2017–2033.

[9] CIRIA Underwater Engineering Group, *Dynamics of Marine Structures: Methods of Calculating the Dynamic Response of Fixed Structures Subject to Wave and Current Action*, Atkins Research and Development, London, UK, second ed., 1978.

[10] K. Conner, D. Szabo, D. Garrett, and G. Gu, *First Order Operability Study for Exploration Drilling at Tranche 6.* File 469-72, Dallas E&P Engineering, Mobil RDC, Dallas, TX, 1994.

[11] M. DeGroot, *Optimal Statistical Decisions*, McGraw-Hill, New York, NY, 1970.

[12] Department of Energy, *Offshore Installations: Guidance on Design, Construction and Certification*, tech. report, UK, 1990.

[13] A. Der Kiureghian, *Measures of Structural Safety under Imperfect States of Knowledge*, ASCE Journal of Structural Engineering, 115 (1989), pp. 1119–1140.

[14] A. Der Kiureghian, Y. Zhang, and C.-C. Li, *Inverse Reliability Problem*, ASCE Journal of Engineering Mechanics, 120 (1994), pp. 1154–1159.

[15] O. Ditlevsen, *Model Uncertainty in Structural Reliability*, Structural Safety, 1 (1982), pp. 73–86.

[16] H. Faÿ, *Dynamic Positioning Systems: Principles, Design and Applications*, Éditions Technip, Paris, 1990.

[17] D. Garrett, *Riser Development - Characterization of Current Loads on a Drilling Riser.* File 054-10.1993.TN1, Dallas E&P Engineering, Mobil RDC, Dallas, TX, 1993.

[18] P. Geyskens, *Optimization and Quadrature Algorithms for Structural Reliability Analysis in the Original Variable Domain*, PhD thesis, Katholieke Universiteit te Leuven, Heverlee, Belgium, December 1993.

[19] A. Ghali and A. Neville, *Structural Analysis: A Unified Classical and Matrix Approach*, Chapman and Hall, London, UK, third ed., 1989.

[20] GUMSHOE, *Gulf of Mexico Storm Hindcast of Oceanographic Extremes.* Oceanweather Report, August 1990.

[21] S. HAVER, *On the Prediction of Extreme Waves from Wave Hindcast of the Most Severe Storms*, in Advances in Underwater Technology, Ocean Science and Offshore Engineering. Vol.12: Modelling The Offshore Environment, London, UK, 1987, Society for Underwater Technology, Graham Trotman, pp. 31–44.

[22] S. HAVER AND K. NYHUS, *A Wave Climate Description For Long Term Response Calculations*, in Fifth International Symposium on Offshore Mechanics and Arctic Engineering, Vol. 4, Tokyo, Japan, 1986, OMAE, pp. 27–34.

[23] R. HOGG AND A. CRAIG, *Introduction to Mathematical Statistics*, Macmillan Publishing Co., fourth ed., 1978.

[24] M. HOHENBICHLER AND R. RACKWITZ, *Non-Normal Dependent Vectors In Structural Safety*, Journal of the Engineering Mechanics Division, Proceedings of the ASCE, 107 (1981), pp. 1227–1238.

[25] L. HUYSE, M. MAES, G. GU, AND R. JOHNSON, *Response Based Design Criteria For Marine Risers*, in 15th International Conference on Offshore Mechanics and Arctic Engineering, Vol. 2, Copenhagen, DK, June 1995, OMAE, pp. 317–339.

[26] L. HUYSE, M. SINGH, AND M. MAES, *A Static Drilling Riser Model Using Free Boundary Conditions*, In preparation, (1995).

[27] H. JAHNS AND J. WHEELER, *Long-Term Wave Probabilities Based on Hindcasting of Severe Storms*, in 4th Annual Offshore Technology Conference, OTC 1590, Houston, TX, 1972, pp. I739–I758.

[28] N. Johnson and S. Kotz, *Distributions in Statistics. Continuous Univariate Distributions-1*, Probability and Mathematical Statistics, John Wiley & Sons, New York, NY, 1970.

[29] N. Johnson and S. Kotz, *Distributions in Statistics. Continuous Multivariate Distributions*, Probability and Mathematical Statistics, John Wiley & Sons, New York, NY, 1972.

[30] J. Kleijnen, *Statistical Techniques in Simulation - Part 1*, vol. 9 of Statistics: Textbooks and Monographs, Marcel Dekker, New York, NY, 1974.

[31] R. Larrabee and C. Cornell, *Upcrossing Rate Solution for Load Combinations*, ASCE Journal of the Structural Division, 105 (1979), pp. 125–132.

[32] ——, *Combination of Various Load Processes*, ASCE Journal of the Structural Division, 107 (1981), pp. 223–239.

[33] H. Madsen, *Omission Sensitivity Factors*, Structural Safety, 5 (1988), pp. 35–45.

[34] H. Madsen and T. Egeland, *Structural Reliability - Models and Applications*, International Statistical Review, 57 (1989), pp. 185–203.

[35] H. Madsen, S. Krenk, and N. Lind, *Methods of Structural Safety*, Prentice-Hall, Englewood Cliffs, NJ, 1986.

[36] M. Maes, *Ignorance Factors Using Model Expansion*, Submitted to the ASCE Journal of Engineering Mechanics, (1994).

[37] M. Maes, K. Breitung, and D. Dupuis, *Asymptotic Importance Sampling*, Structural Safety, 12 (1993), pp. 167–186.

[38] M. Maes and L. Huyse, *Techniques for Formulating Response Based Design Criteria.* submitted to Mobil RDC, Dallas E&P Engineering, Dallas, TX, December 1994.

[39] M. Maes, Ph. Geyskens, and K. Breitung, *MAIS - Monte Carlo Asymptotic Importance Sampling for Reliability Analysis.* March 1993.

[40] G. Marsh, E. Denison, and S. Pekera, *Marine Riser System for 7,500-Ft Water Depth*, in 16th Annual Offshore Technology Conference, OTC 4750, Houston, TX, 1984, pp. 337–344.

[41] R. Melchers, *Structural Reliability: Analysis and Prediction*, Ellis Horwood Series in Civil Engineering, Ellis Horwood, 1987.

[42] J. Myers, C. Holm, and R. McAllister, *Handbook of Ocean and Underwater Engineering*, McGraw-Hill, New York, NY, 1969. Prepared under the auspices of North American Rockwell Corporation.

[43] H. Niederreiter, *Random Number Generation and Quasi-Monte Carlo Methods*, vol. 63 of CBMS-NSF Regional Conference Series in Applied Mathematics, SIAM, Philadelphia, PA, 1992.

[44] A. Papoulis, *Probability, Random Variables, and Stochastic Processes*, McGraw-Hill Series in Electrical Engineering, McGraw-Hill, New York, NY, third ed., 1991.

[45] M. Patel, *Dynamics of Offshore Structures*, Butterworths, London, UK, 1989.

[46] H. Pearce and Y. Wen, *Stochastic Combination of Load Effects*, ASCE Journal of Structural Engineering, 110 (1983), pp. 1613–1629.

[47] R. PRINCE-WRIGHT, *Maximum Likelihood Models of Joint Environmental Data for TLP Design*, in 15th International Conference on Offshore Mechanics and Arctic Engineering, Vol. 2, Copenhagen, DK, June 1995, OMAE, pp. 535–545.

[48] R. RUBINSTEIN, *Simulation and the Monte Carlo Method*, Probability and Mathematical Statistics, John Wiley & Sons, New York, NY, 1981.

[49] T. SARPKAYA AND M. ISAACSON, *Mechanics of Wave Forces on Structures*, Van Nostrand Reinhold, New York, NY, 1981.

[50] G. SMITH, *Probability and Statistics in Civil Engineering*, Nichols Publishing Company, 1986.

[51] P. THOFT-CHRISTENSEN AND M. BAKER, *Structural Reliability Theory and Its Applications*, Springer-Verlag, Berlin, 1982.

[52] C. TURKSTRA, *Theory of Structural Safety*, tech. report, Solid Mechanics Division, University of Waterloo, Waterloo, ON, 1970. SM Study No. 2.

[53] C. TURKSTRA AND H. MADSEN, *Load Combinations in Codified Structural Design*, ASCE Journal of the Structural Division, 106 (1980), pp. 2527–2543.

[54] A. VROUWENVELDER AND J. VRIJLING, *Probabilistisch Ontwerpen*, TU Delft, The Netherlands, 1987.

[55] Y. WEN, *Reliability-Based Design Under Multiple Loads*, Structural Safety, 13 (1993), pp. 3–19.

[56] S. WINTERSTEIN, T. UDE, C. CORNELL, P. BJERAGER, AND S. HAVER, *Environmental Parameters for Extreme Response: Inverse FORM with Omission Factors*, in Structural Safety & Reliability, Schuëller, Shinozuka, and Yao, eds., 1994, pp. 551–557.

[57] S. Yakowitz, *Computational Probability and Simulation*, Applied Mathematics and Computation, Addison-Wesley, Reading, MA, 1977.

[58] Y. Zhang and A. Der Kiureghian, *Two Improved Algorithms for Reliability Analysis*, in Sixth IFIP Working Conference on Reliability and Optimization of Structural Systems, R. Rackwitz, G. Augusti, and A. Borri, eds., London, UK, 1995, IFIP, Chapman & Hall, pp. 297–304.